Predicting the cutting rate of a diamond wire

Application to wreck removal

L.P.F. Pierik

February 2023

TU Delft

Boskalis

Predicting the cutting rate of a diamond wire

Application to wreck removal

by

L.P.F. Pierik

to obtain the degree of
Master of Science
in Mechanical Engineering
at the Delft University of Technology,
to be defended publicly on Tuesday February 14, 2023 at 10:00 AM.

Student number:	4560493	
MSc track:	Multi-Machine Engineering	
Report number:	2023.MME.8759	
Thesis committee:	Dr. C. Walters,	TU Delft, daily supervisor
	Ir. M. Biesheuvel,	Boskalis
	Ir. N. Scheffer,	Boskalis
	Dr. J. Jovanova,	TU Delft
	Dr. ir. H. Polinder,	TU Delft
Date:	February, 2023	

This thesis is confidential and cannot be made public until February 14, 2023.

TU Delft

Abstract

The process of salvaging wrecks can be costly and time-consuming, making it crucial for salvagers to select the appropriate technique(s) and accurately estimate the total costs to minimize expenses and optimize efficiency. Salvagers typically use their expertise, experience, and data from previous projects to make these estimates. Diamond wire cutting is a material-cutting technique with much potential for use in wreck salvaging. However, a previously conducted literature review revealed a lack of sufficient information in the existing literature to determine the cutting rates of diamond wire used in wreck removal, indicating a gap in current knowledge. A deeper understanding of the technique is needed to evaluate salvagers' capability of cutting diamond wire in wreck removal. Therefore, the primary focus of this paper is to provide a method to estimate the cutting rate of diamond wire when used in wreck removal. The effect of wire speed, normal load on the workpiece, various materials encountered in wreck cutting, different geometries, and environments on cutting rate have been investigated. Filling this knowledge gap is of particular interest to Boskalis, as they currently have limited knowledge and experience with diamond wire cutting, making it challenging to estimate costs. Additionally, research into wreck removal techniques is socially significant, as the ability to remove wrecks efficiently and with minimal environmental impact is crucial. Therefore, this thesis aims to provide a deeper understanding of diamond wire cutting in its application in wreck removal.

Main factors determining the potential of a technique for removal include the total duration of removal, the required assets, and the associated risks. The primary focus of this thesis is to develop a method to estimate the cutting rate of diamond wire when used in wreck removal. The cutting rate will be predicted using the Archard wear equation, which requires an unknown coefficient (K) that can be determined through experiments. A real-world set-up with diamond wire was used to obtain data.

The results show that for the steels and cast iron in this survey, Archard's assumption that the wear volume is inversely proportional to hardness is not supported. Consistent with Archard's equations, the wear volume has been found to be proportional to normal load, sliding distance but independent of speed within the range of tested conditions. As such, the Archard wear equation can be applied to the materials tested, but its applicability to materials that differ significantly from those tested is uncertain. Furthermore, results show that cooling significantly impacts both wire life and cutting rate. Specifically, fully submerging the workpiece resulted in a 25% improvement in the cutting rate as compared to spraying with coolant. It should be noted that these results were obtained under controlled conditions where normal load, wire speed, and cutting angle were kept constant, and proper cooling was possible. These operational parameters may vary in real-world scenarios, such as cutting through a shipwreck, leading to deviation from the predicted cutting rates.

Acknowledgements

First of all, I would like to extend my gratitude to Mark Biesheuvel and Niels Scheffer, who provided invaluable guidance as my daily supervisors from Boskalis. Their expertise and problem-solving approach taught me a lot, they were closely involved in the study and were always ready to answer my questions.

I also would like to thank Theo Prins for his support and dedication during the testing days.

My gratitude also goes out to Carey Walters, he closely followed the research as my daily supervisor from TU Delft. Invaluable critical input was provided in this research by his thorough, helpful, and honest feedback at any time of day, which significantly helped me and allowed me to learn a lot.

Lastly, I am grateful to Henk Polinder and Jovana Jovanova for serving on my committee, and to Henk, in particular, for serving as the chair.

Laurens Pierik
February 14, 2023

Contents

Abstract iii

Acknowledgements v

1 Introduction 1
- 1.1 Situation outline and problem statement . . . 1
- 1.2 Research objective and relevance . . . 2
- 1.3 Structure . . . 3

2 Theory 5
- 2.1 Working principle . . . 5
  - 2.1.1 Wire types . . . 5
  - 2.1.2 Chip formation . . . 8
  - 2.1.3 Wire wear . . . 10
  - 2.1.4 Reasons for cooling the diamond wire . . . 11
  - 2.1.5 Additonal information . . . 11
- 2.2 Materials encountered on a ship . . . 12
- 2.3 Modelling cutting rate . . . 14
  - 2.3.1 Analytical Modelling . . . 14
  - 2.3.2 Finite Element Modelling . . . 18
  - 2.3.3 Discussion . . . 18
- 2.4 Test set-ups encountered in literature . . . 19
- 2.5 Summary . . . 21

3 Methodology 23
- 3.1 Test set-up . . . 23
- 3.2 Test plan . . . 28
- 3.3 Test procedure . . . 30
- 3.4 Measurement . . . 30
- 3.5 Processing data . . . 34

4 Results and Discussion 37
- 4.1 Wire wear . . . 37
- 4.2 Influence of wire speed on K . . . 39
- 4.3 Influence of normal load on K . . . 40
- 4.4 Influence of hardness on K . . . 41
- 4.5 Production . . . 44
- 4.6 Test piece temperature . . . 46
  - 4.6.1 Submerged in salt water . . . 47
- 4.7 Chip accommodation space . . . 49
- 4.8 Power consumption . . . 50
- 4.9 Optimal cutting parameters . . . 53
- 4.10 Additional observations . . . 53
  - 4.10.1 Data comparison . . . 54

5 Conclusions and Recommendations 55
- 5.1 Conclusions . . . 55
- 5.2 Recommendations . . . 58
  - 5.2.1 Further research . . . 58
  - 5.2.2 Improve the certainty of the current results . . . 58
  - 5.2.3 Improve the testing setup . . . 59

A Appendix **61**
A.1 Scientific paper 61

B Appendix **63**
B.1 Accuracies 63
B.2 Detailed test procedure 66
B.3 Data gaps 67
B.4 Data Hilti and Husqvarna. 68
B.5 Steel discolouration temperatures 69

C Appendix: Raw data **71**

List of Figures

2.1 Diamond wire . . . 6
2.2 **(a)** Subsea cutting of a pipe with a diamond wire saw (Ashtead Technology, 2022) **(b)** Subsea cutting of the AIS Giorgis II with diamond wire (Cutting Undewater Technologies, 2019) . . . 6
2.3 Schematic side view of the diamond wire (Tönshoff and Hillmann-Apmann, 2002) . . . 6
2.4 **(a)** Schematic cut trough of the diamond wire (Tönshoff and Hillmann-Apmann, 2002) **(b)** Exploded view of the diamond wire (Tönshoff and Hillmann-Apmann, 2002) . . . 7
2.5 Bead types . . . 7
2.6 Comparison of the general stress-strain curve of a ductile and brittle material . . . 8
2.7 FEM representation of brittle chip formation (Tu and Shi, 2019) . . . 9
2.8 Cutting mechanism during grinding of a metal material (Tönshoff and Hillmann-Apmann, 2002) . . . 9
2.9 Schematic cross-section of the Baltic ace on the seabed . . . 13
2.10 Comparision of yield strength reduction factors (Qiang et al., 2012) . . . 14
2.11 Steel discolouration caused by heat (Cotoco et al., 2017) . . . 14
2.12 **(a)** Schematic representation of abrasive indentation **(b)** Cutting volume on a workpiece over single path of wire (right) according to Kim et al. (2016) . . . 15
2.13 2D representation of the wear caused by compressing and shearing an asperity under normal load F_n and displacement s, based on the 3D model . . . 16
2.14 3D representation of the wear caused by compressing and shearing an asperity under normal load F_n at speed v (Hu et al., 2018) . . . 16
2.15 Schematic representation of the wear test set-up for abrasive materials . . . 18
2.16 Schematic representation of wire saw set-up with static workpiece and constant feed speed (Huang and Xu, 2013) . . . 20
2.17 Single diamond wire sawing setup (Xu et al., 2022) . . . 20
2.18 Schematic representation of constant feed force set-up (Huang and Xu, 2013) . . . 20
2.19 Modified tribometer (Zhang et al., 2021) . . . 21

3.1 Schematic representation of the test set-up . . . 23
3.2 Test set-up: **(1)**:DSW 1510-CA sawing machine from Hilti **(2)**:Tachometer **(3)**:Steel container **(4)**:Diamond wire **(5)**:Hand hoist **(6)**:Load cell **(7)**:(variable) test weight . . . 24
3.3 **(a)** Inside Hilti machine (facing side on Figure 3.2) **(b)** Inside Hilti machine (non-facing side on Figure 3.2) . . . 24
3.4 Assembly of Hilti's Single-Pair Pulleys, the frame and the guided trolley with a test piece (cooling positions of test days 1 and 2 are indicated by numbers 1 and 2 accordingly, 3 indicates the video camera) . . . 25
3.5 Hilti's Single-Pair Pulley (Hilti, 2022) . . . 25
3.6 **(a)** Neutral position workpiece **(b)** Work piece position loaded with testweight . . . 26
3.7 Geometry of the test pieces . . . 27
3.8 Welded tube with loose round pieces inside . . . 27
3.9 Schematic representation of the cutting direction . . . 27
3.10 Schematic representation of the forces on the trolley assembly **(a)** without balance with **(b)** with balance weigth . . . 28
3.11 **(a)** Weighing set-up testpiece **(b)** Weighing set-up density . . . 31
3.12 **(a)** Schematic representation of the pneumatic cylinder **(b)** Positioning of the pulley set 32
3.13 **(a)** Testpiece with thermocouple inserted **(b)** Schematic representation of thermocouple set-up . . . 33
3.14 Induction motor power factor as a function of full-loadamperage (Natural Resources Canada, 2004) . . . 33

3.15 Measurements a plate of S255 (40x200x100mm) under nominal test conditions 34
3.16 Measurements of solid round piece of 42CrMo4 (d: 120mm, h: 100mm) under nominal test conditions 35
3.17 A subset of measurements of an S235 solid block (150x150x100mm) under nominal test conditions, with the exception of a wire speed of 6 m/s (a part of the full measurement is displayed) 36

4.1 Results of wear tests diamond wire (Wear coefficient K is obtained under identical test conditions, except the cooling of test day 1 compared to test day 2) 37
4.2 Microscopic pictures of: **(a)** new wire **(b)** wire after test day 1 **(c)** wire after test day 2. Because the images depicted are of different wires, they do not depict the same sections. 38
4.3 K-factor wear tests after correction of wire wear 38
4.4 Corrected K^* factor vs varying wire speeds (S235 (150x150x100mm) with all other parameters remaining constant) 39
4.5 Corrected K^* factor vs varying loads (S235 (150x150x100mm) with all other parameters remaining constant) 40
4.6 Corrected K^* factor vs varying surface hardnesses (other parameters are kept constant, except the geometry of 42CrMo4 is round d:120mm instead of a square of 150x150mm) 41
4.7 Chips produced during cutting 42
4.8 Corrected K^* factor vs varying width of the testpieces S235 (weight difference is corrected, other test parameters are constant) 43
4.9 K^* vs hardness, the asterisk indicates tests that are corrected with the assumed relationship on the width of test pieces 44
4.10 Corrected production vs varying wire speed (other parameters are kept constant) 45
4.11 Corrected production vs varying normal load (other parameters are kept constant) . . . 45
4.12 Corrected production vs varying surface hardness (other parameters are kept constant) 45
4.13 Thermocouple measurement test 15 46
4.14 Under nominal test conditions, but with improper cooling, discolouration of the cutting surface was observed on a round S235 test piece (d: 120mm, h: 100mm) 47
4.15 Corrected K-factor vs wire speed obtained submerged in salt water (other parameters are kept constant) 47
4.16 Corrected K-factor vs normal load obtained submerged in salt water (other parameters are kept constant) 48
4.17 Corrected K-factor vs hardness obtained submerged in salt water (other parameters are kept constant) 48
4.18 Representation of smearing the bead with steel 49
4.19 Schematic representation of the chip accommodation space (Chuang et al., 2003) . . . 49
4.20 Schematic representation of chip accommodation space 50
4.21 Shaft power at varying wire speeds (other parameters are kept constant unless otherwise indicated in the figure) 51
4.22 Shaft power at varying loads (other parameters are kept constant unless otherwise indicated in the figure) 51
4.23 Shaft power vs wear corrected cutting rate (other parameters are kept constant unless otherwise indicated in the figure) 52
4.24 Cut test piece consisting of a tube (120x120x100mm, thickness 16mm) containing loose round pieces 54

C.1 Raw data test 1 71
C.2 Raw data test 2 72
C.3 Raw data test 3 73
C.4 Raw data test 4 74
C.5 Raw data test 5 75
C.6 Raw data test 6 76
C.7 Raw data test 7 77
C.8 Raw data test 8 78
C.9 Raw data test 9 79

C.10 Raw data test 10 80
C.11 Raw data test 11 81
C.12 Raw data test 12 82
C.13 Raw data test 13 83
C.14 Raw data test 14 84
C.15 Raw data test 15 85
C.16 Raw data test 16 86
C.17 Raw data test 17 87
C.18 Raw data test 18 88
C.19 Raw data test 19 89
C.20 Raw data test 20 90
C.21 Raw data test 21 91

List of Tables

2.1 Typical materials encountered in ships (Bureau Veritas, 2021) 13

3.1 Types of test pieces 26
3.2 Variation per parameter 28
3.3 Test matrix 29
3.4 Accuracies measured parameters 30

4.1 Calculation parameters accommodation space 50
4.2 Data comparison 54

5.1 K factors 56

B.1 Life time and speed prediction for wet cutting of solid steel metal of standard steel grade (J. Vos, personal communication, August 8) 68
B.2 Wire life time and cutting rate predictions from Husqvarna (D. Demey, personal communication, June 23) 68
B.3 Lifetime estimation test day 1 and 2 69
B.4 Steel colouring due to temperature (Cotoco et al., 2017) 69

1 Introduction

1.1. Situation outline and problem statement

The transportation of goods via water is critical to global trade, as more than 80% of the volume of international trade is shipped by sea. In recent years, there have been significant improvements in ships' safety and operational safety. However, it is not possible to completely eliminate accidents involving vessels. In many cases, these accidents require the assistance of marine salvors (United Nations, 2021; Muller, 2020).

Three recent examples of ship accidents that required salvage efforts include the Ever Given, the Costa Concordia, and the Baltic Ace. The Ever Given is a 400-meter-long container ship that became stranded on the banks of the Suez Canal due to high winds blocking the canal. The ship was eventually freed after seven days with the help of the salvage company Smit Salvage (BBC News, 2021). The Costa Concordia was a cruise ship that collided with a rock on January 13, 2012, resulting in a ripped hull and the ship sinking in shallow water. After being refloated by salvors, the vessel was towed to a port for dismantling (Tikannen, 2017). Finally, the Baltic Ace was a car transport ship that sank to a depth of 35 meters off the coast of Goeree-Overflakkee on December 5, 2012, after colliding with a container ship. To remove the wreckage from the seabed, the ship was first cut into pieces, after which the loose parts were collected from the seabed and transported away (Kulbiej and Wołejsza, 2016).

Accurate cost estimation is essential for salvagers like Smit (the salvage division of Boskalis) to offer competitive and profitable prices for salvage projects. By accurately predicting the costs of salvage projects, salvagers can offer attractive prices to potential clients and maintain profitability. Salvagers typically base their estimates on their expertise, experience, and data from previous projects. They have various techniques available for salvaging or removing a wreck, and the choice of a technique or combination of techniques depends on the specific circumstances of the wreck. The salvager is responsible for identifying the most cost-effective and compliant methods for removing the wreckage, considering constraints such as time limits and environmental regulations. This thesis focuses on techniques that can be used for wrecks that cannot be removed as a whole, such as the Baltic Ace, and is being carried out on behalf of Boskalis' salvage division.

To understand the techniques that salvage companies can utilize, the available literature was reviewed to identify the various techniques available in the market. This included researching common salvage techniques and techniques commonly used to cut steel structures into pieces that could also be used to cut up a wreck. This research identified 14 techniques that could potentially be used to remove a wreck that cannot be removed as a whole.

These techniques were divided into those involving diving activities and those requiring little or no diving. As the deployment of divers is often very costly, and the workability of divers is limited because their safety during work needs to be guaranteed. Further research was conducted on techniques requiring little or no diving: chain cutting, the guillotine, the grab, the Smit sawing wire, and diamond wire cutting.

To determine the potential of a specific technique (or combination of several techniques) for the removal of a wreck, it is essential to understand the capabilities and limitations of a certain technique.

If historical data is not readily available, a model that can predict the cutting/production rate based on the type of wreck could help provide a more accurate estimate of the feasibility of deploying a particular technique. Such a model can aid in evaluating a technique's potential and facilitate its application in various situations. Factors that are important in this context include:

- The duration of removal, which is influenced by factors such as the speed and efficiency as well as the robustness and workability of a technique.
- Required assets, including the mobility, accessibility and cost of the required assets.
- Risks of a technique, including the potential for downtime and its impact on costs and schedule.
- The cost of a technique, including daily operating costs, consumables, and mobilization expenses.

To the best of the author's knowledge, the previous literature review revealed a lack of available methods/models to predict the cutting rate/production of the selected techniques applied to wreck removal, indicating a gap in current knowledge.

Due to time constraints, working on all five selected techniques during this thesis will not be feasible. As a result, another selection was made among the five techniques considered. Based on the relevance to Boskalis and the previous literature review, the decision was made to focus on diamond wire cutting as Boskalis has limited knowledge and data on its use compared to the other techniques. In addition, several potential advantages of diamond wire cutting over the other four techniques became apparent from the literature review. These include precision in the targeted cutting of specific areas of the wreckage without causing excessive damage to salvaged material, the guarantee of a complete cut once the wire has fully passed trough the wreckage, minimal waste production whick makes it an environmentally favourable option, and reduced forces exerted on the wreckage, potentially resulting in lower energy consumption.

Within the topic of diamond wire cutting, the focus will be on the cutting process. An ideal model for estimating the costs and time needed for wreck removal would consider all factors that impact the project, including the cutting rate of the wire, forces involved, power requirements, wear on the wire, potential risks, workability of the diamond wire, and optimal cutting parameters. It would also consider the costs associated with installing and mobilizing the system at the system level. While it will not be possible to incorporate all of these factors within the available time frame, a first start will be made with a focus on estimating the diamond wire's cutting rate.

1.2. Research objective and relevance

The primary focus of this thesis is to provide a method that Boskalis can use to estimate the cutting rate of diamond wire. As such, the research question being addressed is:

What are the achievable cutting rates for a known diamond wire when cutting a wreck under specific conditions, and how can these rates be applied in a practical setting?

To address the main research question, several sub-questions have been identified:

1. What impact does the wire speed have on the cutting rate?
2. What impact does the normal load on the workpiece have on the cutting rate?
3. How is the cutting rate affected by various materials encountered in wreck cutting?
4. How do different geometries affect the cutting rate?
5. How does the cutting rate vary in different environments encountered in wreck cutting?
6. What impact do operational parameters have on power consumption?

This research is of commercial relevance to Boskalis as it will enable them to estimate the cutting rate better and gain a deeper understanding of the practical aspects of diamond wire cutting. Furthermore, from a scientific perspective, this study aims to fill the gap in knowledge about estimating diamond wire-cutting rates during wreck removal and assess the usefulness of the Archard wear equation for this purpose. The social significance of this research is that it investigates a technique that produces minimal waste compared to other options and exerts relatively low forces on a wreck, potentially consuming less power, making it a more environmental friendly choice for removal, compared to the other techniques.

1.3. Structure

This thesis aims to provide new insights into the cutting rate of diamond wire in the context of wreck removal. First Chapter 2 provides theory and modelling methods relevant to diamond wire cutting. Then, the methodology used in this thesis is described in Chapter 3. The results of the experiments conducted are presented and discussed in Chapter 4. Finally, the thesis concludes with Chapter 5, which includes conclusions about the research, recommendations for improving current research, and suggestions for future research.

2

Theory

In this chapter, Section 2.1 first describes the working principle of diamond wire and the different types of diamond wire. After that, Section 2.2 addresses materials typically encountered during wreck removal. Followed by Section 2.3 describing models to be used as potential starting points for modelling the diamond wire cutting rate. Section 2.4 addresses test set-up encountered in literature. And finally, the approach will be explained in Section 2.5.

2.1. Working principle

Diamond wire cutting is a method for cutting through stone, steel, and other hard materials using a wire to which beads coated with synthetic diamonds are strung. Figure 2.1 depicts an example of the wire, typically made of high-strength steel or synthetic material. The method was developed in Italian quarries in the 1960s when marble blocks were cut with a diamond wire, and it is still commonly used in the stone industry today. In quarries, they pass the wire around a stone block; the wire is then fed through a wire saw utilising a set of pulleys and guides. Finally, the wire is joined together to create an endless loop. The wire saw contains a motor that drives the wire at high speed to move in one direction along the stone block; the speed can vary from 5 to 30 m/s. As the wire is moved at high speed under tension along the stone block, the synthetic diamonds on the wire abrade against the stone. The hardness of the diamonds and the normal force applied to the rock by the beads enables the wire to cut through the stone. To effectively cut through the material, it is essential to maintain enough tension on the wire to create the normal force for the abrasive cutting action. To ensure even wear on the wire, it is typically twisted 1.5 to 2 times per running meter before being joined to form an endless loop. The wire is pre-twisted, so it rotates on its axis during the cutting process, evenly wearing the diamond beads. Additionally, cooling the wire during the cutting process can help to reduce wear on the wire and facilitate the pickup and removal of wear debris.

The diamond wire saw is frequently used in subsea applications to cut pipes and cables, as illustrated in Figure 2.2 (a). It can also be used to cut through wrecks, as shown in 2.2 (b). It is essential to properly guide the wire during the cutting process to make sure the wire does not get stuck, cuts straight and to ensure the accuracy of the cut. To ensure proper guidance of the wire, a frame with pulleys can be used, as depicted in Figure 2.2 (b). Both Hilti and Husqvarna recommend this method. The wire can then be used to cut through the vessel from either the top down or the bottom up, depending on the specific requirements of the project (Cao et al., 2006a; Cutting Undewater Technologies, 2019)

2.1.1. Wire types

The diamond wire is made up of several components. As discussed earlier, the base is often steel cable or synthetic wire. Beads with synthetic diamonds are strung around this base. These beads are made of a steel sleeve around which synthetic diamonds are attached using bonding. The different methods of bonding the diamonds to the sleeve, and hence the different types of beads, are discussed further below. The beads are held in place using springs, as shown in Figures 2.3 and 2.4. Finally, the whole wire, except for the diamonds, is covered in a rubber coating. The rubber coating prevents wire corrosion, wear, and bead displacement. The coating is very wear-resistant as long as it is kept below a

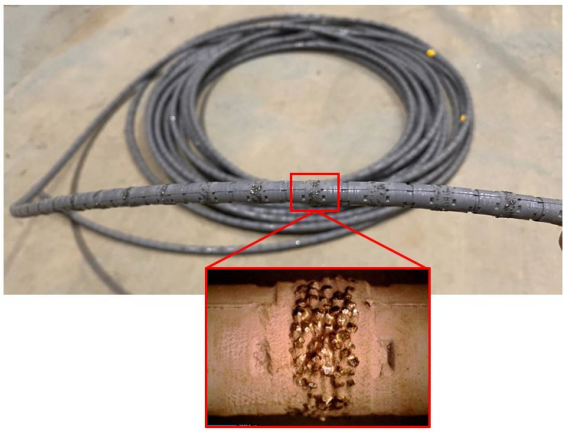

Figure 2.1: Diamond wire

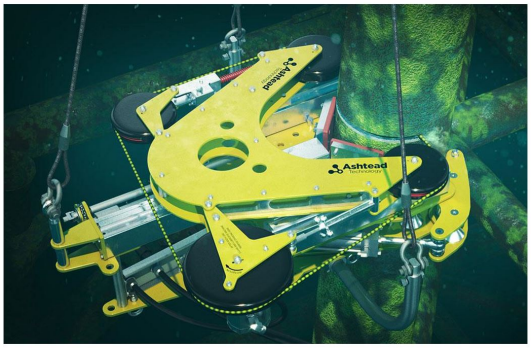

(a)

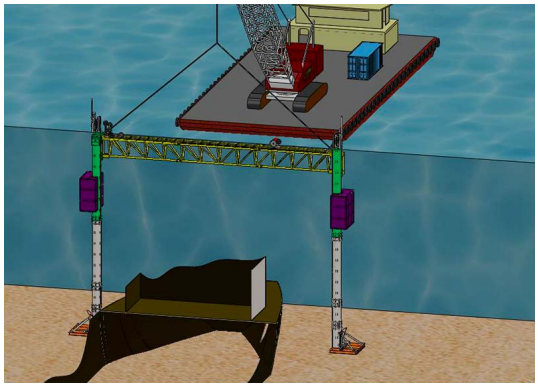

(b)

Figure 2.2: **(a)** Subsea cutting of a pipe with a diamond wire saw (Ashtead Technology, 2022) **(b)** Subsea cutting of the AIS Giorgis II with diamond wire (Cutting Undewater Technologies, 2019)

certain temperature threshold to avoid burning. If the temperature of the rubber rises above this threshold for an extended period, the wire may become unusable. The threshold number for Husqvarna's wire sits at 147 degrees Celsius (D. Demey, personal communication, June 23)

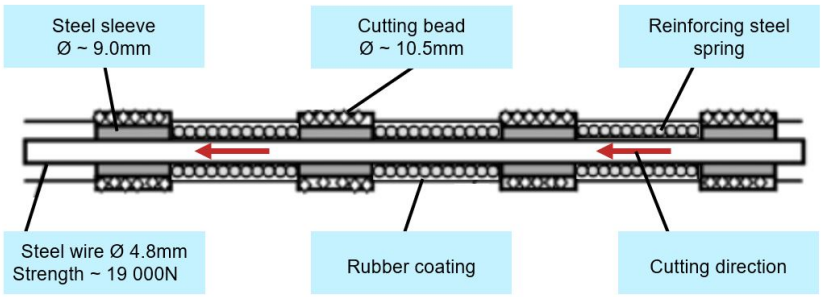

Figure 2.3: Schematic side view of the diamond wire (Tönshoff and Hillmann-Apmann, 2002)

The overall structure of diamond wires is generally consistent across different manufacturers, but there may be variations in the type and number of beads per meter. These variations can include differences in the shape (conical or non-conical) and size (diameter and length) of the beads and the method used to bond the diamonds to the steel sleeve. Currently, three bonding methods are commonly used: sintered, vacuum brazed, and electroplated, as shown in Figure 2.5.

There are two ways to join a wire to form a continuous loop: 'open' or 'spliced'. An 'open' wire is

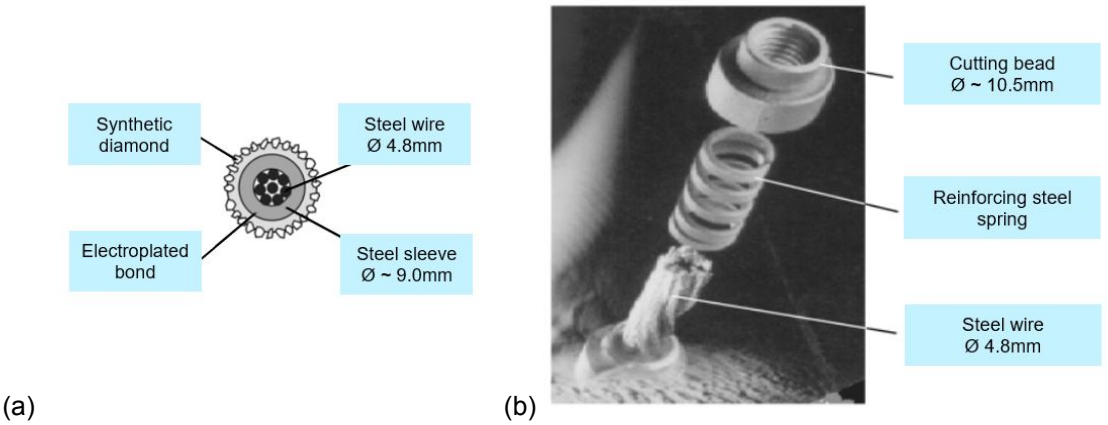

Figure 2.4: **(a)** Schematic cut trough of the diamond wire (Tönshoff and Hillmann-Apmann, 2002) **(b)** Exploded view of the diamond wire (Tönshoff and Hillmann-Apmann, 2002)

joined together using a connector. This method carries the risk of failure of the connector and, thus, the wire becoming loose if too much tension is applied. Therefore, it is recommended not to put more than $3500N$ of tension on the wire to prevent the connector from breaking. One of the benefits of an open wire is that it can be cut to the desired length on-site and can be easily manoeuvred under a wreck and connected on-site, such that the wreck is located in the middle of the looped wire. Another possibility is that a ”split” wire is woven together at the factory so that no connector creates a weak point in the cable, making the wire equally strong everywhere. As a result, the maximum strength until the cable breaks is determined by the strength of the steel cable. Since a spliced wire is already made into a continuous run in the factory, it cannot be cut to length on-site. Therefore, it is necessary to determine the desired wire length in advance. Additionally, positioning the wire in the same way as an open wire during cutting from bottom to top is not feasible. However, there are techniques where a spliced wire along with a frame can also be used to cut from bottom to top, but it involves more effort.

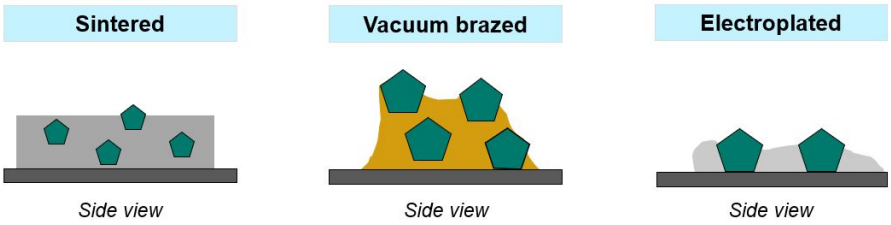

Figure 2.5: Bead types

Sintered

Sintered segments are created by mixing metal powder and diamonds, pressing the mixture into a mould, and then subjecting it to high pressure and temperature (700-1000 °C) in a process called sintering. This results in a segment with multiple layers of diamonds.

Diamond segments made using sintering technology typically have a longer lifespan than other manufacturing methods. During the cutting process, the outer diameter decreases as diamonds and bonding material wear away. They are available in a wide range of bond types, diamond qualities, and grit sizes to suit different cutting needs. Sintered segments are suitable for cutting concrete, reinforced concrete and cast iron and can be used for wet and dry cutting. However, they are not ideal for cutting steel due to their inability to withstand the high temperatures and pressures involved in the cutting process. Therefore, using a different diamond segment is recommended for steel-cutting applications.

The purpose of the student association Pandora is to expand the perspectives of Multi-machine Engineering students and establish connections between students and the industry. My role within Pandora involved managing partnerships with existing companies and attracting new ones.

Vacuum brazed

Vacuum-brazed segments are created by joining two pieces together using a third molten metal called braze alloy. This process, called brazing, relies on a chemical reaction to bond the diamond to a metal substrate. Vacuum-brazed segments typically have two layers of diamonds and the diamonds are generally larger than those found in other types of segments. This method of manufacturing diamond segments allows for a strong and durable bond between the diamonds and the metal substrate, resulting in a long-lasting cutting tool.

Vacuum brazed wire is made using premium quality, large-size diamonds, making it ideal for cutting highly reinforced concrete, pure steel, heat-treated steel, and metal alloys. Its high resistance and durability allow for a long lifespan when used in the proper application and with the appropriate settings. During the cutting process, the outer diameter decreases as diamonds and bonding material wear away. Vacuum brazed wire can be utilized for both dry and wet cutting of steel and concrete, but it is essential to carefully control the temperature, especially when cutting dry steel. Otherwise, the wire will degrade much faster, shortening its lifetime.

Electroplated

Electroplating is a process that uses an electric current to reduce dissolved metal ions and deposit them onto an electrode (bead) in the form of a thin, coherent metal coating. This process binds diamonds to the metal substrate in manufacturing the diamond segments. Electroplated segments have only one layer of diamonds, as the electroplating process is unsuitable for adding multiple layers.

The electroplated wire is suitable for cutting many materials, including concrete, reinforced concrete, steel, and metal alloys. However, it has a shorter lifespan compared to sintered or vacuum-brazed wire due to its single layer of diamonds. An advantage of electroplated wire is that the outer bead diameter remains constant over the life of the wire, which can be beneficial if it is expected that the cut cannot be completed with one wire. This is due to the consistent diameter of both the used and new wire, allowing for the continuation of cuts with a new wire. The cutting rate of the wire will gradually decrease as it wears down until it is no longer usable. Electroplated wire can be used for wet and dry cutting in concrete, and it is recommended for wet cutting in steel to reduce heat generation.

2.1.2. Chip formation

In diamond wire cutting, the type of chip formed can depend on whether the material is undergoing brittle or ductile fracture. A brittle fracture occurs when a material breaks without significant deformation. This type of fracture is typically associated with materials with low ductility and results in small, granular chips with minimal material deformation. Brittle materials can be more prone to cracking or breaking during cutting, resulting in additional fracture mechanisms. As stated by (Williams (1999)), with brittle materials, the breakage can occur not only due to plastic flow but also through other mechanisms such as intergranular or intragranular fracture.

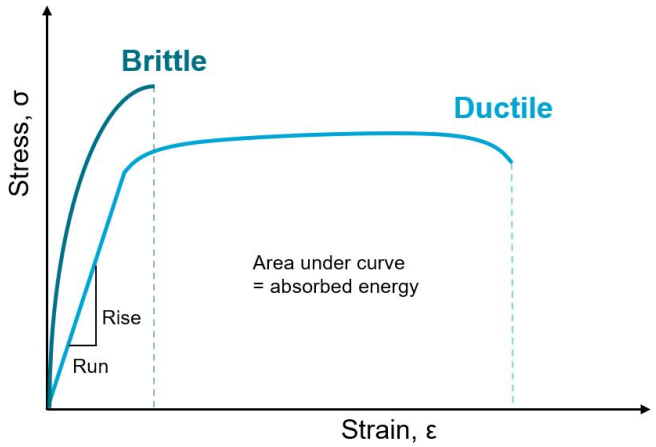

Figure 2.6: Comparison of the general stress-strain curve of a ductile and brittle material

On the other hand, during ductile fracture, the material can experience significant deformation before breaking, resulting in larger, more elongated chips (ribbon chips). Ductile fracture is typically associated with materials that have high ductility, such as metals. During ductile fracture, the material generally can handle higher loads before breaking, which means that the material can withstand higher stresses and strains before failure. This is because ductile materials generally have a higher ability to absorb energy through deformation before reaching their breaking point, compared to brittle materials, which generally have a lower ability to absorb energy before breaking. Figure 2.6 displays general stress-strain curves of brittle and ductile material. Both types of chips mentioned, ductile and brittle, are at the extremes of the spectrum, and chip formation can vary from granular to ribbon and everything in between (Atkins, 2009; Zhang et al., 2021).

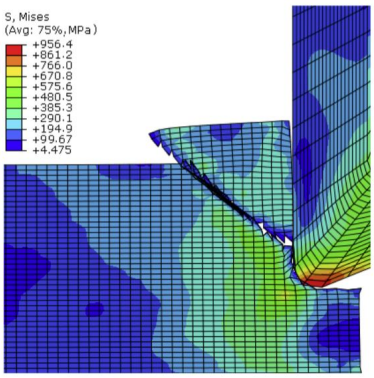

Figure 2.7: FEM representation of brittle chip formation (Tu and Shi, 2019)

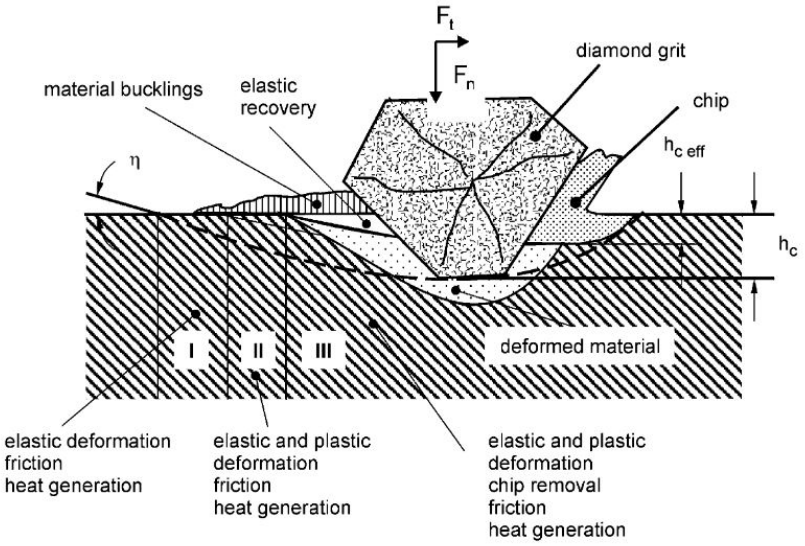

Figure 2.8: Cutting mechanism during grinding of a metal material (Tönshoff and Hillmann-Apmann, 2002)

For both ductile and brittle fractures, the process is initially the same. When the material comes into contact with a diamond abrasive, it experiences compression until a specific compression limit is reached. At this point, the material begins to separate from the workpiece in the shear plane. The primary shear force causes deformation in the shear plane, which extends upwards in front of the diamond wire. When the shear angle is large, the cutting force is high, and the shear path is short, resulting in thicker chips. On the other hand, a smaller shear angle leads to a lower cutting force and a longer shear path, resulting in thinner chips. Brittle materials have a higher compression limit than ductile materials,

which affects how the chip is formed. The chip is formed through fracture following increasing compression on the material in brittle materials, as depicted in Figure 2.7. While in ductile materials, the material deforms plastically to create the chip; this process is represented in 2.8. In zone I, the material deforms elastically, then the friction between the workpiece and the abrasive increases, and plastic deformation occurs in zone II. Accompanied by an increase in the temperature of the material. Finally, as pressure and temperature rise, a chip forms in zone III, causing plastic displacement of the material by shearing, which eventually breaks away from the workpiece (Tönshoff and Hillmann-Apmann, 2002).

2.1.3. Wire wear

Tool wear of the grains and wire can be divided into microscopic and macroscopic wear, as described in further detail below (Tönshoff and Hillmann-Apmann, 2002).

Microscopic wear

Microscopic wear occurs due to mechanical and thermal stress on the diamonds and bonding material during the cutting process. The diamonds on the beads wear due to the stress they are subjected to during the cutting process, leading to grain and bond wear. Wear on the diamond grits may result in them being active or inactive (Ertingshausen, 1985; Heuer, 1992).

Active diamond grits:

- New grits: new diamonds can provide good cutting performances with no damage to the grain, making them beneficial for the cutting process.
- Fractured grits: thermal stresses and rapid cooling, along with mechanical stress during the cutting process, can cause parts of the grit to chip off. This wear process eventually makes the tool unusable, but it also creates new sharp cutting edges that contribute to the cutting process. Therefore, balanced wear is desirable, where new cutting edges are formed when the old ones have become dull to extend the lifespan of the wire.

Non-active diamond grits:

- Broken grits: thermal stresses and rapid cooling, as well as mechanical stress during the cutting process, can put excessive strain on the diamond. If this stress becomes too great, it can cause a fragment of the diamond to shatter and a significant portion of the diamond to break off. This can result in the loss of its cutting capacity and hinder its ability to contribute to the cutting process.
- Pull-out of grits: excessive friction between the diamond and the workpiece can cause the diamond to break loose completely. This effect can be aggravated by a bonding system that is too soft, as the bond's grain retention forces are insufficient. Most of the time, this is due to excessive wear in multilayer bonding systems. Even so, if the cutting bead has multiple diamond layers, it can retain its cutting power. This is not the case with an electroplated bead, which consists of one layer of diamonds.
- Polished grits: due to mechanical wear caused by friction, the grit is continuously worn away and forms rounded or flattened cutting edges. These rounded or flattened edges do not contribute to cutting and cause high friction.

Macroscopic wear

Besides microscopic wear, the wire can also experience wear at the macroscopic level.

- Macroscopic wear includes reduction of the tool diameter and forming a conical shape of the cutting bead. The abrasive action of the chip material removes the binding material. Consequently, bond wear will affect the ability to hold the grains in the bond. Radial wear of wire saw tools is crucial for wire saws with multilayer beads because wear allows a new layer of diamond to come into contact with the workpiece, improving the cutting process. This is not the case with electroplated beads, as the bead consists of only one layer (Tönshoff and Hillmann-Apmann, 2002).
- If the diamond wire becomes too hot, the rubber coating protecting it may burn, potentially damaging or rendering the wire unusable. The threshold temperature for a Husqvarna diamond wire

2.1.4. Reasons for cooling the diamond wire

In diamond wire cutting, the use of water cooling is a crucial method for maintaining the wire's integrity and enhancing the cutting process. Though dry cutting is an option, monitoring the wire's temperature and implementing alternative cooling measures as required is important to ensure optimal performance.

There are several reasons why cooling can help to reduce wire wear in the wire sawing process:

- Keeping the diamond wire cooled prevents the rubber coating that holds it together from burning and potentially damaging or rendering the wire unusable. Maintaining proper cooling can preserve the integrity and functionality of the wire (Qiu, 2022).
- During the cutting process, the heat generated can cause the bonding material that connected the diamond to the bead to relax, leading to a permanent reduction or complete loss of the cutting ability of the wire. This is because the diamonds may align themselves in the direction of the wire, preventing new sharp edges from coming into contact with the material surface. This process is irreversible (Molfino and Zoppi, 2012).
- During the cutting process, coolant can act as a lubricant to reduce friction between the abrasives and the workpiece by decreasing the contact length between the chip and the diamond. This reduces the stress on the diamond and helps to keep the diamonds securely in place and prevent them from breaking off. However, it is essential to maintain enough pressure on the diamonds to avoid polishing them, rendering them ineffective and making the cable unusable (Denkena et al., 2022).

Cooling the wire during the cutting process can help improve performance for several reasons:

- Coolant facilitates the pick-up and removal of chips and small abrasive particles from the work area, preventing the chip accommodation space from filling up and disrupting the diamonds' contact with the workpiece. This allows the diamond grains to continue cutting into new material, maintaining the cutting capability of the beads. If this does not happen, the diamond wire's cutting rate may decrease (Deshpande and Deshpande, 2019).
- If the material being cut becomes too hot, it may start to stick to the diamond bead and cover the diamonds, reducing the cutting ability of the wire. This is because the diamonds lose their cutting power, and there is no more space for chip collection. However, this process is reversible and can be mitigated by subsequently cutting material that does not stick to the bead, such as material that has been adequately cooled. In this case, the pieces of material covering the diamonds will wear off, restoring the cutting power of the diamonds (Deshpande and Deshpande, 2019).

2.1.5. Additonal information

Interviews and communication with Hiliti and Husqvarna revealed additional information on the potential risks associated with the use of diamond wire, as well as tables indicating rough estimates of cutting rates and wire lifetime under nominal conditions (D. Demey, personal communication, June 23; J. Vos, personal communication, September 19). This information will be discussed further below.

Potential risks

-
-
-

Cutting rate and lifetime
Hilti and Husqvarna have provided tables (see Appendix B.4) that offer rough estimates of the cutting rates and wire lifetime that can be achieved using diamond wire. On the other hand, Husqvarna's table provides information that is specific to the material but does not specify the type of wire used nor provide wire-specific values, nor if the wire used to obtain the data was kept constant. They did recommend using different types of wire depending on the material being cut and suggested using a vacuum-brazed wire when cutting through a wreck due to its longer lifespan.

It should be noted that the data provided is only a theoretical prediction under standard conditions and actual results may vary based on several factors such as wire speed, normal force, and type of cooling.

2.2. Materials encountered on a ship

The materials used in the construction of ships may vary. Table 2.1 shows some materials commonly encounter on a ship.

The thickness of a ship's hull varies based on the areas where it needs to absorb a large amount of force, as well as the size of the ship. The hull thickness of a large container ship is typically between 16 and 25 mm but may be as thick as 80 mm in specific locations. On smaller vessels, the hull thickness is usually between 9 and 12 mm (Bureau Veritas, 2021).

As stated before in Section 2.1.2, a material's response to mechanical loading can be classified as either ductile or brittle. Ductile materials tend to deform plastically under stress and can withstand more deformation before breaking. On the other hand, brittle materials break or fracture without much

Table 2.1: Typical materials encountered in ships (Bureau Veritas, 2021)

Part	Material
Hull	Steel (Grade A (similar to S235))
Inner structure	Steel (AH32, AH36, DH36, EH36)
Shaft	
Engine	Grey cast iron
Interior	Cables, pipes, cargo, etc.

deformation. In the case of brittle materials, the breakage can occur not only due to plastic flow but also through other mechanisms such as intergranular or intragranular fracture. Most of the metals depicted in Table 2.1 exhibit ductile behaviour under nominal conditions, except for cast iron, which is a brittle material (Williams, 1999).

Figure 2.9 illustrates a schematic representation of a shipwreck cut into sections using the Smit sawing wire, specifically the Baltic Ace. The figure shows that the shipwreck consists of a hull and an internal structure. Table 2.1 provides information on the materials likely encountered during cutting. Depending on the location of the cut, the propeller shaft or engine block may also be encountered. Additionally, in the case of the Baltic Ace, it was filled with cars, so those could also be encountered during cutting.

Figure 2.9: Schematic cross-section of the Baltic ace on the seabed

Heating of metals

As stated in Section 2.1.2, the diamond wire-cutting process leads to the heating of the material being cut. This heating can have several consequences, two of which will be discussed below.

Firstly, increasing the temperature of metals can greatly impact their mechanical properties, as shown in Figure 6 which illustrates the decrease in yield strength under the influence of temperature. As the temperature of metal rises, its mechanical properties will change to the point where the material will even melt (Qiang et al, 2012).

In addition to affecting the mechanical properties of steel, heat can cause the formation of an oxide layer on its surface. This oxide layer can be used to determine the temperature of the steel as its thickness increases with the temperature. While iron oxide is usually not transparent, the thin layer that forms on the surface of the steel can allow light to pass through and be reflected off both the top and bottom surfaces. The oxide layer on steel starts as light yellow and changes to brown, purple, blue, and finally, light green/grey as the layer thickens (see Figure 2.11). These visible colour changes occur at specific temperatures, providing an accurate indicator of the steel's temperature. Up to 427°C, the

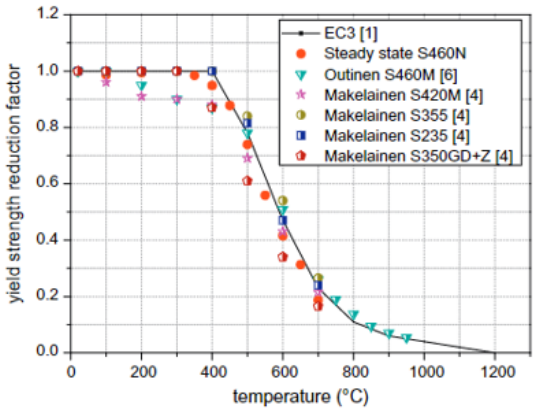

Figure 2.10: Comparision of yield strength reduction factors (Qiang et al., 2012)

colouration is caused by oxidation of the surface. Above that temperature, the colouration is caused by high thermal energy, resulting in glowing colours (Cotoco et al., 2017).

Figure 2.11: Steel discolouration caused by heat (Cotoco et al., 2017)

2.3. Modelling cutting rate

This section will present various models identified through the previously conducted literature study as potential starting points for analyzing and predicting the diamond wire cutting rate. First, Section 2.3.1 will address analytical models, followed by numerical models in Section 2.3.2. And finally, Section 2.3.3 will conclude which model will be used during this thesis.

The diamond wire-cutting process can be analyzed at different levels, namely micro, meso, macro and system level. The microscale approach involves analyzing the interactions between the diamond abrasives and the material being cut at the atomic and molecular levels. The mesoscale approach focuses on the cutting rate and forces involved in a single abrasive particle and how it affects the microstructure and properties of the material being cut.

On the other hand, the macroscale approach looks at the cutting process at the level of multiple abrasives (one bead) or even multiple beads set with diamonds working together. It involves analyzing the overall cutting rate and forces of the process at the wire level and is particularly useful in understanding the efficiency and productivity of the wire as a whole.

And finally, at the system level, which looks at the implementation of diamond wire on a large scale, such as when cutting through a wreck. This approach is particularly useful in understanding the whole process, including the equipment and the personnel involved and how they interact with the diamond wire and the material being cut. This approach requires a comprehensive understanding of the wire-level mechanics, so at macrolevel. Some analytical and numerical encountered in literature methods will be explained below.

2.3.1. Analytical Modelling

The model presented by Kim et al. (2016) aims to predict the theoretical sawing speed (Δh [μm/min]) of a monocrystalline workpiece that is cut with a thin wire saw, so at the meso level. The wire saw has abrasives attached directly to the wire along its entire length. The model combines equations 2.1 and

2.2 and is illustrated in Figure 2.12. The model takes into consideration factors such as the indentation depth of a single spherical abrasive (δ), the average force acting on it (f), the total number of abrasives in contact with the workpiece ($N = nw$), and the width of the workpiece (w). Additionally, the model includes a proportional constant (k) that depends on various process conditions, such as environmental conditions and the coolant. It is important to note that the proportional constant is situation-dependent and depends on many factors. Thus, it must be determined through testing in an environment that closely matches the actual situation. The model assumes that the abrasives have the shape of a sphere, but it is also possible to model the abrasives as spherical cones, polygonal pyramids or more precisely as tetrakaidecahedrons, as proposed by Lan et al. (2020).

Applying Kim's model to the wire-cutting scenario described in Section 2.1.1 is challenging as the model requires several parameters that are difficult to determine and measure in a real-world setting, such as the concentration of abrasives on the wire, the indentation ratio, and the cross-sectional cutting area. Additionally, the model assumes a thin wire with synthetic diamonds attached directly, which does not align with the wire described in Section 2.1.1, where beads with synthetic diamonds are strung around a wire. This difference in wire structure leads to a different interaction between the wire and the material being cut, making it difficult to predict, particularly with varying speeds, loads and geometries. The mesolevel nature of the model also makes it difficult to accurately determine the parameters for the wire in a scenario that closely mimics reality at full speed and load.

$$\Delta h = \frac{\Delta V}{\pi R w} \tag{2.1}$$

$$\Delta V = (kA_h)(nl)(w) \tag{2.2}$$

$$A_h = r^2\left(cos^{-1}(1-\rho) - (1-\rho)\sqrt{2\rho-\rho^2}\right) \tag{2.3}$$

with $\rho = \delta/r$ (the indentation ratio).

$$\delta = r - \sqrt{r^2 - \frac{2F}{\pi n w \sigma_y}} \tag{2.4}$$

with normal force F, n the concentration of abrasives in a unit length based on a projection view, w the width of the test piece and σ_y the hardness of the workpiece.

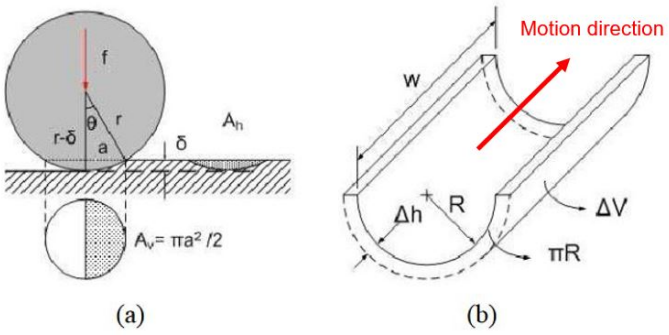

Figure 2.12: (a) Schematic representation of abrasive indentation **(b)** Cutting volume on a workpiece over single path of wire (right) according to Kim et al. (2016)

The cutting rate can also be considered directly at the macro level and predicted with the help of the wear rate formula of Archard (1953), shown in Equation 2.10. Williams (1999) and Tönshoff and Hillmann-Apmann (2002) state that processes of abrasive machining, such as diamond wire cutting, can be thought of as being analogous to abrasive wear, and Williams (1999) opted to use the Archard

equation to model abrasive wear. And according to Tönshoff and Hillmann-Apmann (2002) the Archard equation is the starting point when considering macro-scale wear.

The Archard wear equation describes the relationship between the steady-state wear loss of a material, the normal load applied to it, and the hardness of the softest material. It is based on asperity contact theory, which investigates the behaviour of a single asperity (a small, raised area) in contact with a harder material. The equation can be used to estimate material wear loss and is consistent with experimental observations made by Archard (1953). It should be noted that the Archard wear equation is an empirical equation derived from several wear test data sets, and the values of the constants can vary depending on the material and tribological system under consideration, the factors and relationships that affect friction and wear. It is particularly useful for understanding abrasive wear, in which hard abrasive particles or asperities wear away the surface of a softer material. In this case, the hardness of the material, in combination with the load, controls the penetration depth of the abrasive particles, and the wear loss can be accurately predicted using the Archard wear equation (Archard, 1953; Williams, 1999).

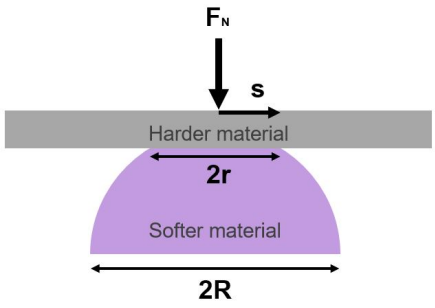

Figure 2.13: 2D representation of the wear caused by compressing and shearing an asperity under normal load F_n and displacement s, based on the 3D model

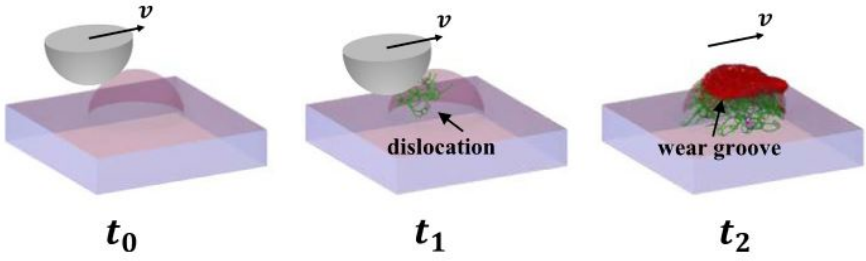

Figure 2.14: 3D representation of the wear caused by compressing and shearing an asperity under normal load F_n at speed v (Hu et al., 2018)

The Archard wear law is derived using the flattened asperity model, where a normal load (F_n) creates a contact radius (r) by flattening the asperity plastically, shown schematically in Figure 2.13 and in 3D in Figure 2.14. The normal load can be calculated using Equation 2.5. The wear volume is proportional to the volume of a hemisphere of radius r, represented by Equation 2.6, in which γ is a proportionality parameter. The wear volume of a single asperity per unit sliding distance can be calculated using Equation 2.7, by taking a sliding distance (ds) of $2r$. Combining Equation 2.7 and 2.5 gives Equation 2.8, where K is the wear coefficient. The total wear volume of the macroscopic surface is represented by Equation 2.9, which takes the sum of the material wear of all asperities (Archard, 1953; Hu et al., 2018).

$$F_N = \pi * r^2 * H \tag{2.5}$$

$$dW = \gamma * \frac{2}{3}\pi r^3 \tag{2.6}$$

$$\frac{dW}{ds} = \frac{\gamma * \frac{2}{3}\pi r^3}{2r} = \frac{\gamma}{3} * \pi r^2 \tag{2.7}$$

$$\frac{\gamma}{3} * \frac{F_N}{H} = K\frac{F_N}{H} \tag{2.8}$$

$$\frac{dW}{ds} = K\frac{\sum F_N}{H} = K\frac{P}{H} \tag{2.9}$$

Finally, resulting in Equation 2.10, the Archard wear equation that will be considered during the thesis.

$$W = K\frac{Ps}{H} \tag{2.10}$$

W: wear/cutaway volume $[mm^3]$
K: dimensionless wear coefficient $\left[\frac{mm^3 * N/mm^2}{mm * N}\right]$
P: normal load on the contact $[N]$
s: sliding distance $[mm]$
H: surface hardness of the softest surface $[N/mm^2]$

The following points regarding the Archard equation should be noted:

- It assumes that the wear volume is independent of the apparent contact area.
- It states that the wear rate (total wear per unit sliding distance) is independent of the sliding speed
- No assumptions regarding the surface topography are made.

(Archard, 1953; Williams, 1999; Tönshoff and Hillmann-Apmann, 2002)

A search for dimensionless wear coefficients K for cutting metals with diamond wire revealed a lack of available values. To the best of the author's knowledge, this represents a gap in current literature. However, Williams (1999) gives a typical K value of $7 * 10^{-3}$ for mild steel sliding against tool steel in dry, unlubricated pin-on-disc tests in air. Furthermore, according to Thompson and Thompson (2006), a typical wear coefficient by abrasive wear, the process to which diamond wire cutting can be compared, is in the order of 10^{-2} to 10^{-1}. The K-factor for diamond wire cutting is expected to be higher than Williams' value and in the range indicated by Thompson and Thompson.

The dimensionless wear coefficient K varies based on various parameters such as the environment or lubricant, temperature, and the combination of materials. Therefore, this constant must be determined through experiments under conditions as close as possible to the actual situation, which will require designing a test set-up that differs from the method regularly used to compute K and depicted in Figure 2.15. The K-factor in both the models of Kim and Archard refers to a proportional constant that is dependent on the process conditions, but it may not be the same. Although the K-factor in the two models may be related, they are calculated from different parameters and factors, and therefore will not be identical.

The set-up depicted in Figure 2.15 is commonly used to determine the value of K. In this set-up, a pin is pressed against a rotating disk with a known load of P. The sliding distance is determined based on the disk's rotation speed, the time the disk has rotated, and its radius. Furthermore, the mass difference determines the pin's amount of wear to calculate the constant K (Archard, 1953; Williams, 1999).

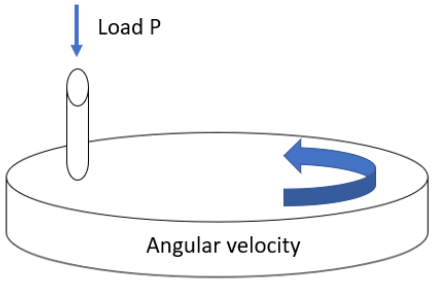

Figure 2.15: Schematic representation of the wear test set-up for abrasive materials

2.3.2. Finite Element Modelling

Zhang et al. (2021) uses a numerical model to predict the cutting force required for machine cutting of steel, considering a single diamond grit, focusing on interactions at the meso scale level. This was done using finite element analysis (FEA) and response surface methods. They examined the effect of different parameters on chip formation, including the cutting speed, coefficient of friction, and cutting speed of a single grain. It is important to note that the coefficient of friction is an input parameter that should be known to model the cutting process accurately.

Lan et al. (2020) found that the cutting speed, depth of cut, and density of the diamond grains all influence chip formation and are important parameters to consider when modelling the cutting process. However, scaling up models from the meso scale to the macro scale is very difficult due to the meso level's strong nonlinearities and surface uncertainties. Nevertheless, attempts have been made to do so, but so far, with little success (R. van Ostayen, personal interview, June 8, 2022).

In addition, models to describe the grinding process of a grinding wheel have been encountered in literature. Although a grinding wheel and a diamond wire saw are different, the processes are essentially the same. Both meso scale and macro scale models can be found in the literature.

Liu et al. (2002) performed an FEA study on grinding and lapping of silicon wafers, focusing on the effect of different geometric and process parameters on the cutting of 0.8 mm thin wafers. This model focuses on a process that takes place at the meso scale.

Furthermore, Chuang et al. (2003) examine the interaction between the grinding wheel and the workpiece. They model the grinding forces, associated stress, and deformation field generated while grinding a ceramic workpiece. They develop a 2D finite element model where the input variables consist of the mechanical properties of the workpiece and the grinding parameters. This model also focuses on the meso scale.

2.3.3. Discussion

Zhang et al. (2021) used a numerical model to predict the cutting force required for diamond wire cutting at the meso scale. Liu et al. (2002) presented a study on grinding and lapping of 0.8 mm thick silicon wafers, which also focuses on a process at the meso scale. Scaling up models from the meso scale to the macro-scale is difficult due to the strong nonlinearities encountered at the meso scale. Therefore, creating a model at the micro or meso scale is not recommended and then trying to scale it up.

Chuang et al. (2003) developed a 2D finite element model where the input variables consist of the mechanical properties of the workpiece and the grinding parameters. It is essential to conduct full-scale tests to obtain the necessary input parameters for numerical models, such as the coefficient of friction between the workpiece and the wire, and to validate the prepared model. While validated finite element models can be helpful because they allow for the simulation of many different tests without physical experimentation, creating and verifying the model can be time-consuming. It may not be feasible within a given time frame.

Two analytical models to predict the amount of cut or worn-away material in diamond wire cutting have been discussed, Archard (1953) en Kim et al. (2016). Both models include a factor of K for

unknown process conditions, such as the environment.

Kim's model considers the cross-sectional cutting area of a single asperity and reflects the relationship between the force on that asperity and the hardness of the cut material. The cross-sectional area is then multiplied by the relative sliding length, a factor K, and the total volume of abrasives that have been in contact with the workpiece.

Archard's model calculates the total volume of abraded material based on the total normal load, the sliding distance, the hardness of the softer material, and the K-factor. Like Kim's model, Archard's model is derived at the asperity level and approaches the asperities as hemispheres, making the two models quite similar.

Since the surface is continuously worn away during the process of diamond wire cutting, it will be difficult to predict what the cross-sectional area of a single asperity will be after some time. Furthermore, it will be challenging to translate from a single asperity to the entire bead. Conducting experiments at an accurate scale in an environment similar to reality could be helpful. For Archard's model, it will also be necessary to conduct large-scale tests as close to reality as possible to reduce uncertainties.

Both Archard's and Kim's models appear to be suitable for predicting the amount of material worn away during cutting. However, the two models may vary in terms of the accuracy of their predictions and the ease of measuring the required input parameters. Kim's model considers the cross-sectional cutting area of an individual asperity and reflects the relationship between the force on that asperity and the hardness of the material being cut. These input parameters may be more difficult to measure in a high-speed cutting process. However, focusing on the asperity level makes the model more precise than Archard's. On the other hand, Archard's model is more general, and the required input parameters (total normal load, sliding distance, hardness of the softer material, and cut-away volume) may be easier to measure in a real-world scenario. However, the model may also be less accurate due to its more general nature.

For all models, an accurate prediction will require adapting the model to the specific wreck being removed and the operational conditions used, as each removal operation is unique. For the model to be useful for Boskalis, it must be relatively easy to understand. Furthermore, it is crucial that the model's parameters can be accurately measured in real-world applications, is suitable to implement at the macro level (wire size), and can be developed within the given timeframe of the thesis. Therefore, Archard's wear equation will be used as a starting point for describing the cutting rate of diamond wire for the removal of wrecks.

2.4. Test set-ups encountered in literature

This section will outline various diamond wire sawing set-ups encountered in literature, used to measure sawing parameters, such as cutting rate, sawing force and feed force among other parameters. One of the main differences between the set-ups is whether a long wire or a continuous loop wire is used. The continuous loop is typically 10-12mm in diameter and is used for cutting through metals. It is driven by 1-2 drive pulleys and tensioned by a tensioning pulley (as shown in Figure 2.16).

The long wire, used for slicing wafers, is usually 30-40μm in diameter and is moved back and forth by using two guide rollers (as shown in Figure 2.17).

Other distinctions between the setups will be discussed further below, such as movable vs. stationary workbed/workpiece, feed force vs. feed speed regulation, wire cooling, and parameter measuring. And finally, an entirely different setup will be discussed.

Turchetta et al. (2017) and Molfino and Zoppi (2012) use a set-up where the workpiece stays in place, and the diamond wire moves towards the work piece (an schematic example is shown in Figure 2.16). This set-up presents difficulties on a large scale due to the required size of the moving parts. But the advantage is that the measuring equipment, often a dynamometer that is directly connected to the workpiece, remains stationary, reducing measurement disturbance from dynamic effects due to moving measuring equipment (a dynamometer measures the forces acting on a workpiece in three planes (x, y, and z) by utilizing properly arranged load cells. However, dynamometers are costlier and less durable compared to standard load cells).

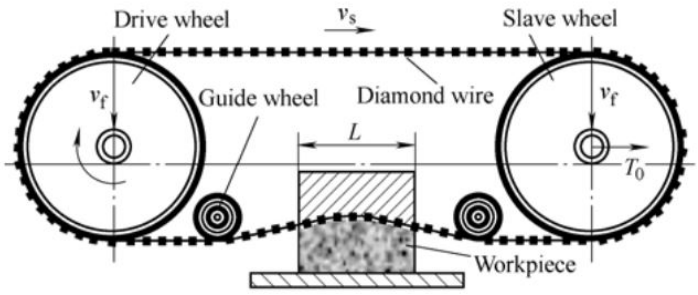

Figure 2.16: Schematic representation of wire saw set-up with static workpiece and constant feed speed (Huang and Xu, 2013)

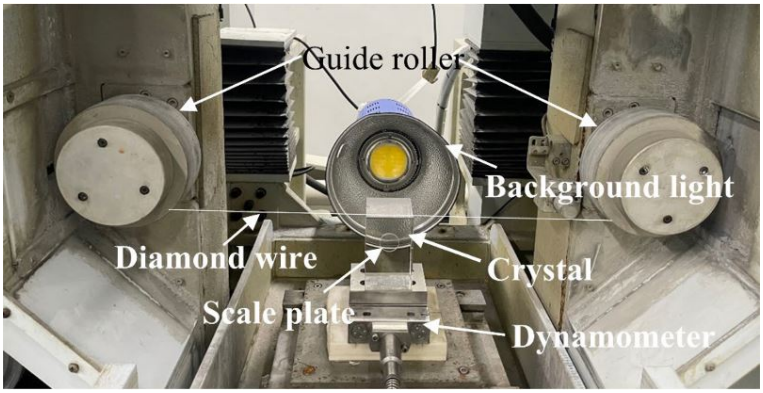

Figure 2.17: Single diamond wire sawing setup (Xu et al., 2022)

Kim et al. (2016) and Huang and Xu (2013) use a set-up where a test block is pressed against the diamond wire with constant feed force instead of feed speed by using dead weight. A schematic representation of Huang and Xu (2013) set-up is shown in Figure 2.18. Xu et al. (2022) and Qiu (2022) also use a movable workbed with a stationary wire, but instead of a constant load, a constant feed speed is applied.

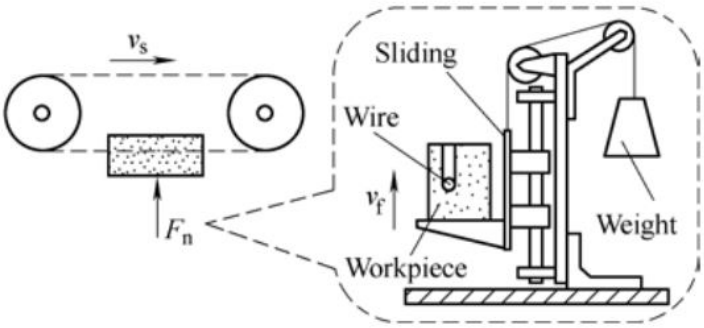

Figure 2.18: Schematic representation of constant feed force set-up (Huang and Xu, 2013)

In terms of cooling, Molfino and Zoppi (2012) and Qiu (2022) vary by also using bath cooling in addition to jet or no cooling. Molfino and Zoppi (2012) submerges the entire set-up in a tank while Qiu (2022) used as small bath to submerge only the workpiece, to compare the impact of bath vs. jet cooling on cutting force and vibration. Yao et al. (2020) used two cooling methods, pouring liquid supply and electrostatic spraying liquid supply, to examine the effect of electrostatic spraying liquid supply on the surface roughness and thickness of K9 optical glass cuts. However, this cooling method is not applicable for large-scale diamond cutting in wreck removal given the scale and application.

For measuring the cutting parameters several set-ups use dynamometer, as described above (Huang and Xu, 2013; Turchetta et al., 2017; Xu et al., 2022; Qiu, 2022). Kim et al. (2016) alternatively measures only the feedforce and wire tension using two separate load cells.

A set-up that is completely different, is the set-up of Lan et al. (2020) and Zhang et al. (2021), shown in Figure 2.19. Lan et al. (2020) and Zhang et al. (2021) use a modified SFT-2 M pin-disc friction and wear tester to investigate the influence of cutting parameters on chip shape and residual stress of a single diamond grit. The cutting speed can be adjusted by adjusting the rotational speed and offset distance of the grain, with the maximum cutting speed being determined by the maximum radius and maximum achievable rotation speed.

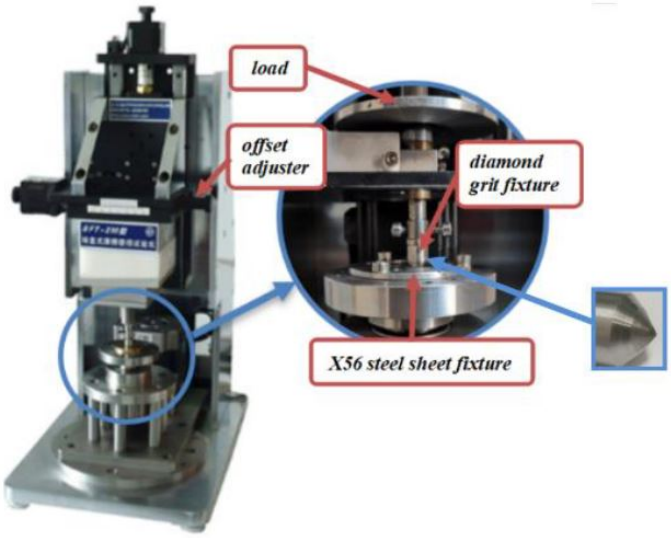

Figure 2.19: Modified tribometer (Zhang et al., 2021)

When considering the parameters in the Archard Equation, a desirable set-up must be able to apply a constant load, allow for various geometries and materials of test pieces, and simulate real-world conditions by testing under different environmental conditions and with varying speeds and loads. The set-up used will be further described in Section 3.1.

2.5. Summary

As a starting point, the Archard wear equation will be used. To apply this equation to diamond wire cutting of a wreck, the specific K-factors for using a diamond saw on a wreck must be determined, as these values are not currently available in the literature. To ensure that these values are relevant to the real-world situation of cutting through a wreck, the speed and load values must be comparable to those experienced in an actual scenario, and the environment in which the wreck is located must be considered. The commonly used set-up for determining the K described in Section 2.3.1 deviates too much from the actual situation, making it very difficult to determine whether the values obtained are applicable in an actual situation. Thus, a new set-up must be designed to determine the K-factor as close as possible to the real situation, considering budget and time constraints. The design should incorporate the capability to apply a constant force, test different shapes and materials of specimens, and simulate realistic scenarios through tests under varying conditions such as speed, load, and environment.

Based on the data obtained, the validity of Archard's equation will have to be critically examined. In addition, the performance of the diamond wire, power consumption, and practicality of diamond wire cutting will be evaluated based on the tests.

3

Methodology

In this chapter, Section 3.1 describes the set-up first, followed by Section 3.2 which details the test plan that was performed. Section 3.3 explains the test procedure, Section 3.4 discusses the sensors involved and their (in)accuracy, and Section 3.5 describes how the data was processed.

3.1. Test set-up

Figure 3.1 shows a schematic representation and Figure 3.2 shows the test setup in real life. The test setup essentially consists of the following elements:

- DSW 1510-CA sawing machine from Hilti
- 15-metre electroplated diamond wire from Hilti
- Frame
- Guide trolley (to which the test pieces are attached)
- Test pieces
- Steel container

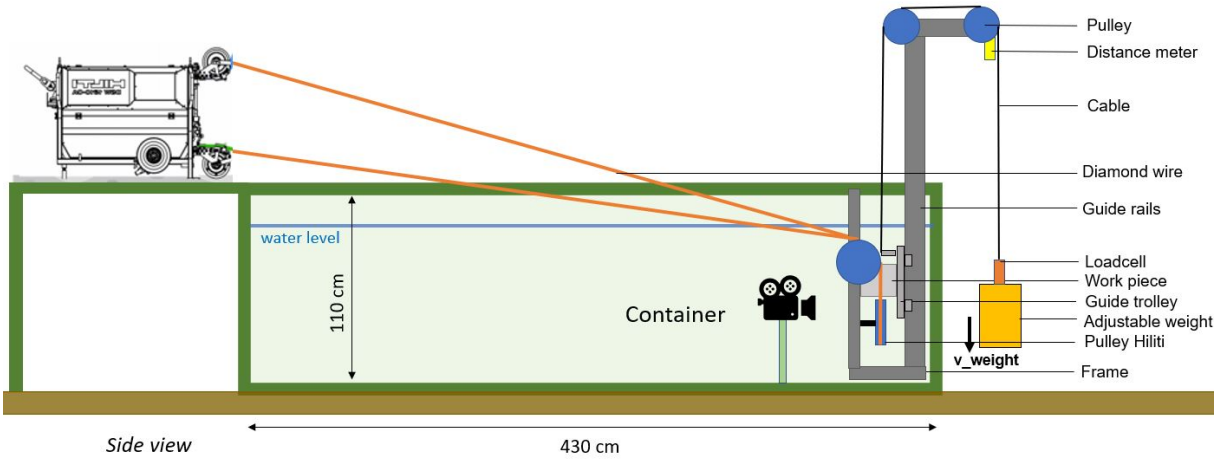

Figure 3.1: Schematic representation of the test set-up

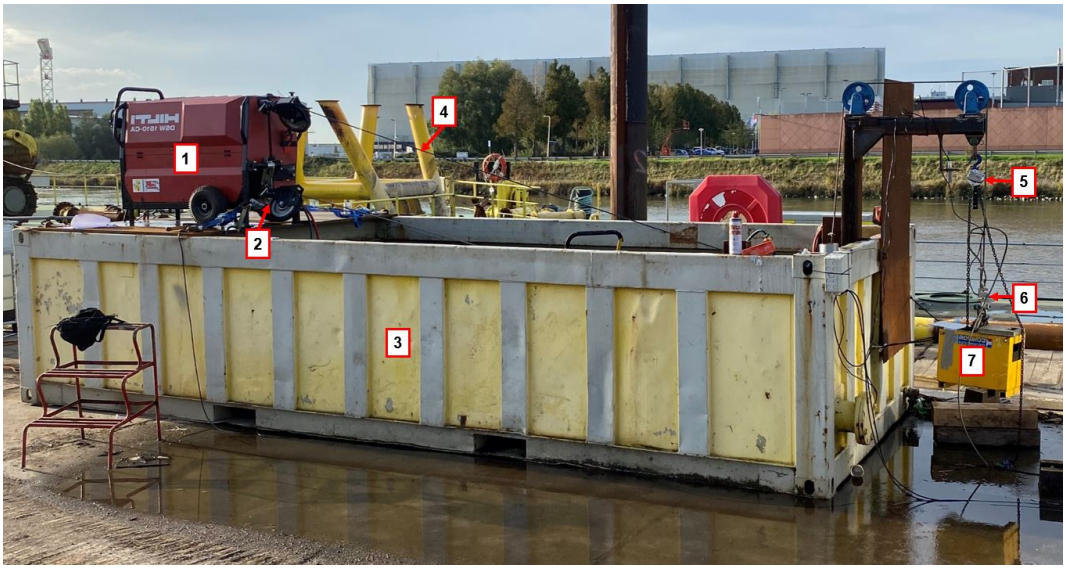

Figure 3.2: Test set-up: **(1)**:DSW 1510-CA sawing machine from Hilti **(2)**:Tachometer **(3)**:Steel container **(4)**:Diamond wire **(5)**:Hand hoist **(6)**:Load cell **(7)**:(variable) test weight

Sawing machine

The wire speed and wire tension can be adjusted via the sawing machine. The wire can be brought to tension using an air cylinder (see Figure 3.3 (b)) which is connected to a set of movable pulleys depicted in Figure 3.3 (a). The speed can be set on a remote controller, after which two 8kW motors drive the wire via two drive pulleys, as shown in Figure 3.3 (b). Furthermore, two nozzles are connected to the machine that provides cooling water.

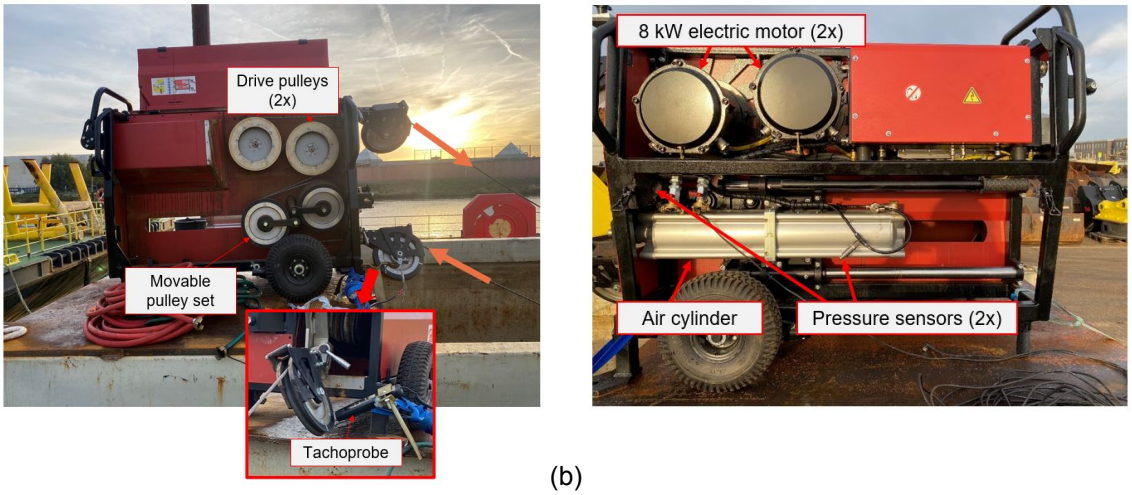

(a) (b)

Figure 3.3: (a) Inside Hilti machine (facing side on Figure 3.2) **(b)** Inside Hilti machine (non-facing side on Figure 3.2)

Diamond wire

The vacuum-brazed diamond wire (as depicted in Figure 2.1) was advised by Hilti and used for testing. This wire is recommended because the outer diameter remains constant during the cutting process, allowing the wire to be reinserted into the same cut if necessary in the event of breakage during wreck removal. Additionally, the wire is suitable for cutting pure steel, heat-treated steel, metal alloys, and cast iron. Refer to Section 2.1 for a more detailed description. The wire's composition is depicted in Figure 2.3, with beads of an outer diameter of 10.5 mm spaced 44 beads per meter along the wire.

Frame

The frame is made of a steel U-shaped section welded into the steel container (shown in Figure 3.4 and

has two mounting points for Hilti's Single-Pair Pulleys, displayed in Figure 3.5. Hilti's Single-Pair Pulleys guide the diamond wire from the sawing machine to the test piece. The pulleys can be positioned such that the wire is positioned horizontally above the test piece; see left image in Figure 3.6. Furthermore, a tube with two guide rails for the trolley, to which the test piece is mounted, is attached to the U-shape and a crossbeam is connected to the top of the tube, to which two (blue) pulleys are attached (see Figure 3.2). The pulleys direct the movement of a steel cable connected to the guided trolley and the desired test weight. A hand hoist can be used to lift and position the test weight. Lowering the test weight then pushes the test piece up against the diamond wire (see Figure 3.6 (b)), providing a constant load on the workpiece, and allowing it to be cut.

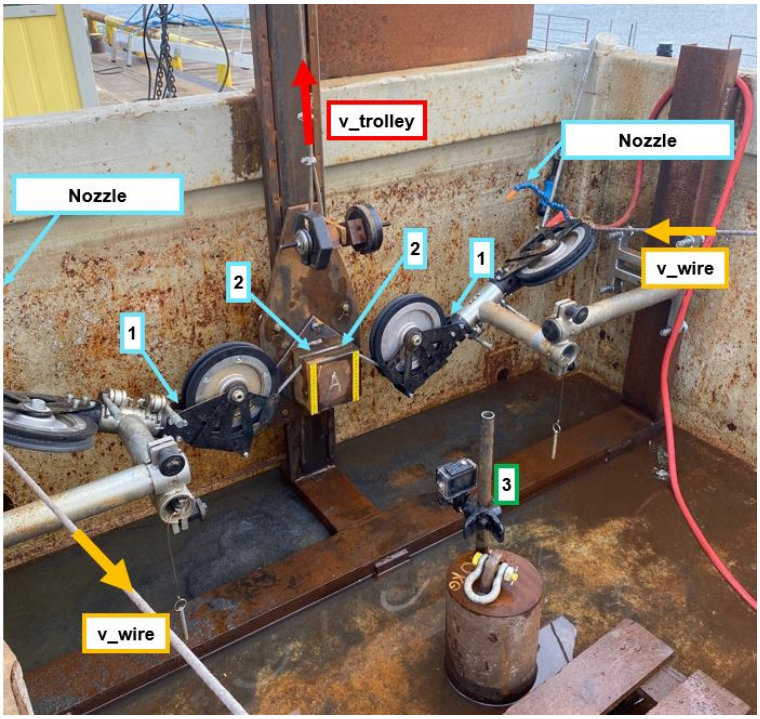

Figure 3.4: Assembly of Hilti's Single-Pair Pulleys, the frame and the guided trolley with a test piece (cooling positions of test days 1 and 2 are indicated by numbers 1 and 2 accordingly, 3 indicates the video camera)

Figure 3.5: Hilti's Single-Pair Pulley (Hilti, 2022)

(a) 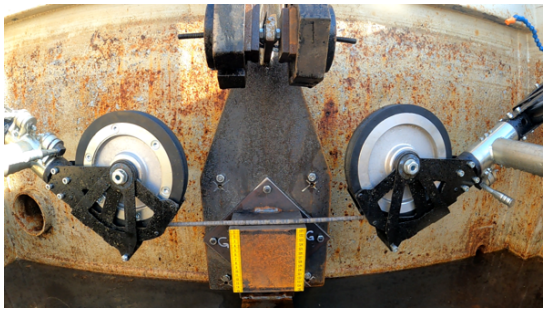 (b) 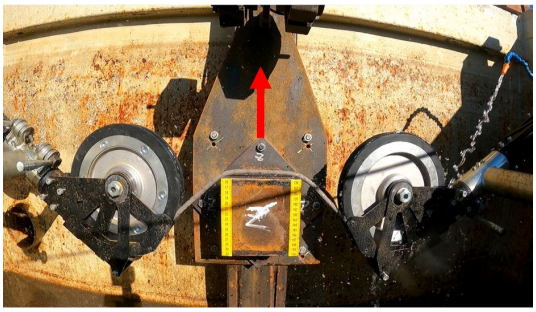

Figure 3.6: **(a)** Neutral position workpiece **(b)** Work piece position loaded with testweight

Guide trolley

The guided trolley consists of a base plate, four wheels and a pulling strip. On the base plate of the trolley, the test pieces can be secured using four bolts. The trolley wheels connect closely to the guide rails that guide the trolley up and down. It is also possible to add balance weights to the test strip to balance out the assembly of the guided trolley and test piece, and to reduce friction (see Section: balancing below). The entire assembly is depicted in Figure 3.4 below.

Test pieces

The test pieces used in the experiments are listed in Tabel 3.1 and consist of three materials: S235, cast iron, and 42CrMo4. These materials represent the hull, an engine block, and a ship's propeller shaft, respectively. The test pieces have different geometries, including standard-size blocks of 150x150x100mm. They were chosen because they are large enough for precise measurement of the removed material volume but still manageable. There are also test pieces with different geometries to study the effect of geometry on the cutting rate. A special test piece also includes individual round tube pieces inserted into a square tube to evaluate how the diamond wire performs when cutting loose parts. Figure 3.7 shows the various geometries, and Figure 3.8 shows the square tube with the round loose pieces inside.

Table 3.1: Types of test pieces

Material	**Shape**	**Size (l x w x h)**
S235	Solid	150x150x100mm
S235	Solid (round)	d: 120mm, h: 100mm
S235	Plate	20x200x100mm
S235	Plate	40x200x100mm
S235	Tube with loose pieces	200x200x100mm, t: 16mm
CGI	Solid	150x150x100mm
42CrMo4	Solid (round)	d: 120mm, h: 100mm

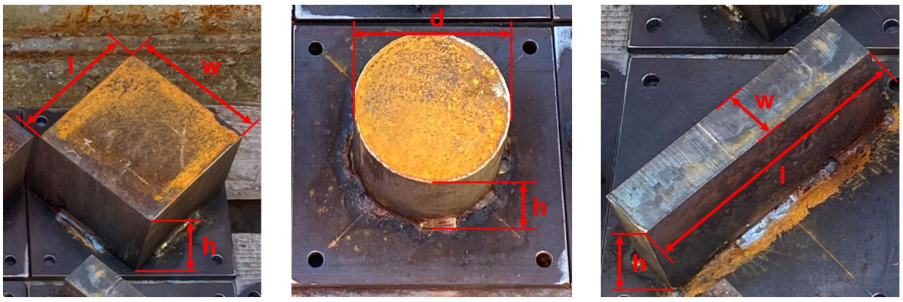

Figure 3.7: Geometry of the test pieces

Figure 3.8: Welded tube with loose round pieces inside

All test pieces are fixed to a steel bottom plate. These steel bottom plates fit precisely on the four bolts of the guided trolley's base so that the test pieces can be fastened to the guided trolley and easily replaced. The 'height' of test pieces is 100mm, so two cuts can be made per test piece (see Figure 3.9).

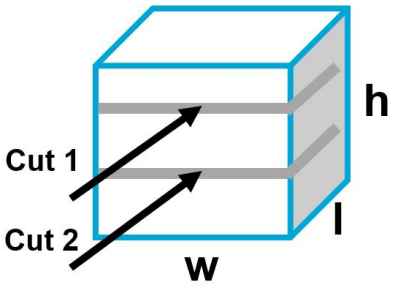

Figure 3.9: Schematic representation of the cutting direction

Steel container

The installation is partly placed in a steel container (number 1 depicted in Figure 3.2). This container can be filled with water for submerged testing.

Balancing

The interplay of forces visible in Figures 3.10 (a) and (b) must be aligned to ensure that the load attached to the trolley fully translates into a normal force on the test piece. To this end, weight can be added to the trolley. A slot is made in the pulling strip of the trolley so that weight can be added here. By varying the added balance weight and the positioning of the weight in the slot, it can be ensured that forces are aligned. As the diamond wire will cut the test pieces at two different heights, two pulling holes have been added to the strip. As a result, the steel wire that pulls the trolley upward can also vary in height.

Furthermore, the pulley directly above the trolley is adjustable so that the pulley can be aligned with the pulling hole, aligning the diamond wire and steel pulling wire.

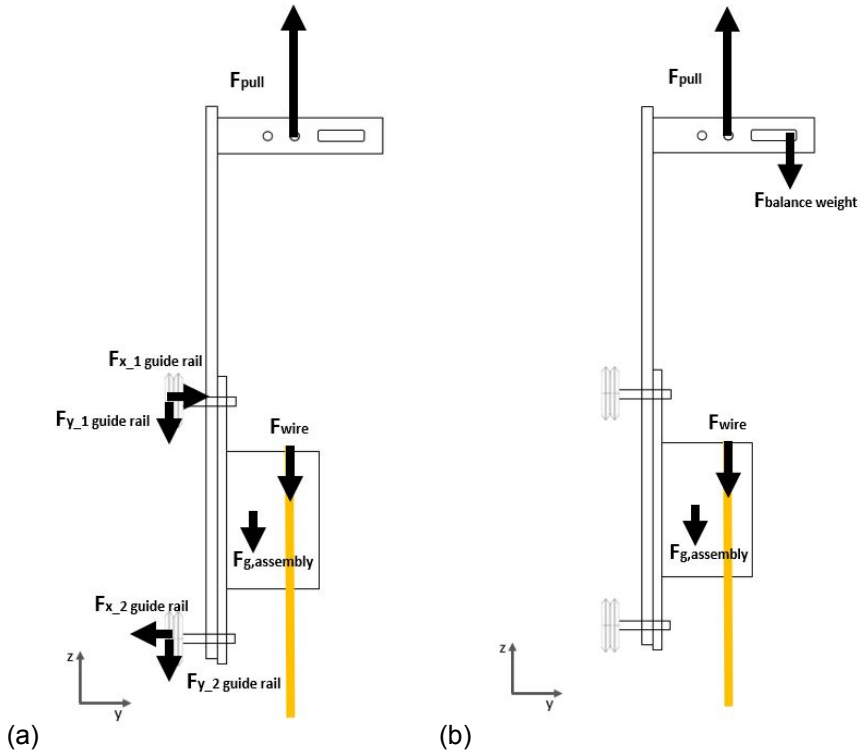

Figure 3.10: Schematic representation of the forces on the trolley assembly **(a)** without balance with **(b)** with balance weigth

3.2. Test plan

The test plan was compiled to establish a usable local cutting model of the diamond wire (considering wreck removal) based on the Archard wear equation. The wire speed, normal load, hardness, environment and geometry were varied (see Table 3.2). Table 3.3 shows the complete test matrix.

Table 3.2: Variation per parameter

Parameters	**Variation 1**	**Variation 2**	**Variation 3**	**Variation 4**
Wire speed				
Test weight				
Material	S235	Cast Iron	42CrMo4	
Environment*	Jet cooling (nozzles)	Submerged (salt water)		
Geometry	Solid (150x150x100mm)	Solid (20x200x100mm)	Solid (40x200x100mm)	Round (d:120mm h:100mm)

*Wrecks are usually partially or completely submerged and often located at sea. The cutting performance will be evaluated both underwater and above the waterline to account for the variations in environmental conditions. When cutting above the waterline, nozzle cooling is recommended and will be implemented during the testing process.

The cooling water will be sourced from a spur of the IJssel River, which is adjacent to the testing site and delivered through two nozzles with a flow rate of 7.5 l/min. The fully submerged conditions are simulated by dissolving NaCl in the freshwater sourced from the IJssel River until it reaches a density of 1025 kg/m^3, similar to the density of seawater at 20 °C.

Because the sawing machine cannot start up at too high a load when combined with sharp workpiece

corners, the test pieces are first pre-cut at a lower load until the cut is fully developed. These pre-cut test pieces are then subjected to typical load testing.

Table 3.3: Test matrix

	Test	Test piece	Material	Geometry (width x length x 100mm)	Environment	Wire speed [m/s]	Normal load [kg]	Setting*	Note
Day 1	1	B	S235	Solid(150x150mm)	Nozzles			1	wear test **
	2	C	S235	Solid(150x150mm)	Nozzles			1	
	3	E	Gray cast iron	Solid(150x150mm)	Nozzles			1	
	4	F	42CrMo4	Solid (shaft D: 120 mm)	Nozzles			1	
	5	Z	S235	Solid(150x150mm)	Nozzles			1	
	6	G	S235	Solid(150x150mm)	Nozzles			1	wear test **
	7	H	S235	Loose pieces in tube	Nozzles			1	
	8	D	S235	Solid (shaft D: 120 mm)	Nozzles			1	
Day 2	9	R	S235	Solid(150x150mm)	Nozzles			1	wear test **
	10	S	S235	Solid(150x150mm)	Nozzles			1	
	11	A	S235	Solid(150x150mm)	Nozzles			2	
	12	B	S235	Solid(150x150mm)	Nozzles			2	wear test **
	13	C	S235	Solid(150x150mm)	Nozzles			2	
	14	Z	S235	Solid(150x150mm)	Nozzles			2	
	15	BZN	S235	Solid(150x150mm)	Nozzles			2	wear test**
	16	F	42CrMo4	Solid (shaft D: 120 mm)	Nozzles			2	
	17	E	Gray cast iron	Solid(150x150mm)	Nozzles			2	
	18	J	S235	Plate (20x200mm)	Nozzles			2	
	19	K	S235	Plate (40x200mm)	Nozzles			2	
	20	R	S235	Solid(150x150mm)	Nozzles			2	wear test**
	21	G	S235	Solid(150x150mm)	Submerged			2	

*Two cuts are made per test piece, resulting in two distinct settings. The variations in the settings arise from the alignment of Hilit's pulleys, pull cable, and compensation weight

**In order to examine the wear of the cable, wear tests are conducted under identical conditions. If the wire does not exhibit signs of wear, the outcomes of the wear tests should be consistent. The deviation in cutting rate from the expected outcome provides insight into the level of wear experienced by the cable

During the first test day, a strong influence of wire wear was observed, which overshadowed the results obtained. So it was decided to monitor wire wear more closely during the second test day. Because the Hilti machine was only available for two days, the decision was made to compromise on repeatability and opt for a larger variety of tested parameters to obtain as much information as possible.

3.3. Test procedure

The same test procedure was maintained for each test to ensure the continuity of all tests. In doing so, a fixed preload of about 1000N on the wire has been held for each test. The procedure will be briefly described below; see Appendix B.2 for a detailed description.

1. Pre-cut the test pieces (until the cut is fully developed)
2. Weighing of the test pieces
3. Setting the correct parameters
    - Wire speed
    - Normal load
    - Environment
4. Cutting the test piece (up to about 3-5 cm from the end)
5. During the test, the sensors measure the required data
6. Weighing the cut test piece to determine the volume cutaway

3.4. Measurement

This section explains the sensors and methods used to obtain the data. Table 3.4 below lists the sensors used and their accuracy.

Table 3.4: Accuracies measured parameters

Parameter	Device	Unit	Range estimate	Accuracy*
Wear/cut volume	Submerged weighing	mm^3	30 000 - 150 000	± 1.79 % OR
Weight	Loadcell Keli 30 kg	N	50-250	± 0.03 % FS
Normal load	Load cell SCAIME 250kg	N	50 - 1000	± 0.03 % FS
Speed wire	Tachoprobe A2108	m/s	5 - 25	± 0.5 % OR
Hardness	Streuer Durascan 70	N/mm^2	125 - 260	± 30-70 OR
Distance	Ultra sonics sensor Honeywell	mm	400-1000	± 5 mm
Pressure	Electronic pressure sensor	bar	0-10	± 0.5 % OR
Temperature	Infrared laser	$^{\circ}C$	10 - 500	± 1 % OR
	Thermocouple	$^{\circ}C$	10 - 500	± 1 % OR
Water density	Hydrometer	g/ml	995-1025	± 0.002

*See Appendix B.1 for the exact accuracies of all measurements and further explanations.

Wear volume

To determine the cutaway/wear volume, a necessary parameter for calculating the K factor, the test pieces were weighed before and after cutting. To accurately measure the weight of a test piece, the test piece must be completely dry to avoid including the weight of any water still attached to the piece. However, allowing the specimen to dry completely can take a significant amount of time, which is why the setup in Figure 3.11 (a) was used. This setup allowed for submerged weighing of the test pieces, eliminating the need to be completely dry before weighing. The final wear volume was then calculated using Equation 3.1, and the density of the water and the test pieces was determined using a hydrometer. The density of the test pieces was determined by weighing smaller pieces, wet and dry, and using Equation 3.2 and the set-up depicted in Figure 3.11 (b).

$$W = \frac{F_{pre-cut} - F_{final}}{9.81 * (\rho_{testpiece} - \rho_{water})} \tag{3.1}$$

$$\rho_{testpiece} = \frac{w_{dry}}{w_{dry} - w_{wet}} * \rho_{water} \tag{3.2}$$

(a) 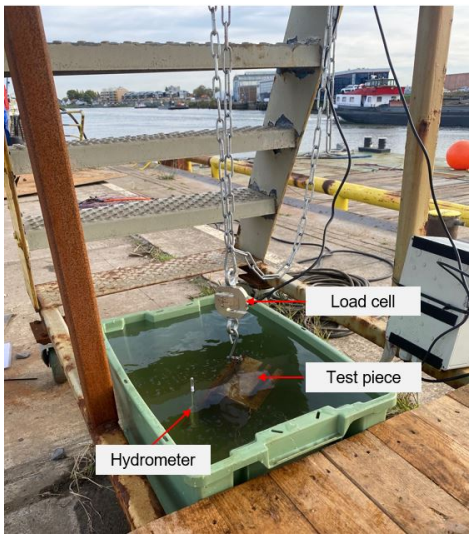

(b) 

Figure 3.11: (a) Weighing set-up testpiece **(b)** Weighing set-up density

Normal load

The normal load on the test piece is a required parameter to determine the K factor and is determined using a load cell between the test weight and the steel wire rope (number 6 in Figure 3.2). To arrive at the normal load from the measured weight, Equation 3.3 is used.

$$F_{normal} = F_{measured} - F_{trolley} - F_{testpiece} - F_{balanceweights} - F_{friction} \tag{3.3}$$

$F_{measured}$: Measured load before the cutting started $[N]$
$F_{trolley}$: Weight of the guided trolley $[N]$
$F_{testpiece}$: Weight of the test piece $[N]$
$F_{balanceweights}$: Weight of the balance weights $[N]$
$F_{friction}$: Load lost to friction in the set-up $[N]$

Where $F_{friction}$ is the load measured during the upward movement of the trolley without the test weight attached, minus the sum of loads of the trolley, test piece and balance weights. It is assumed that the weight of the steel cable is more or less evenly distributed on both sides of the pulleys on top and, therefore, self-cancelling in the equation.

Wire-speed

The sliding distance can be determined based on the wire speed, making the wire speed essential for determining the K-factor. The wire speed is measured via a tachometer directed at the lower pulley, where the wire enters the sawing machine. The measured pulley is a guide pulley, so slip between the wire and pulley will be minimal. The measured signal is in revolutions per minute and is converted via Equation 3.4 into the wire speed, with v_{wire} $[m/s]$, revolutions per minute (RPM) and r_{pitch} $[mm]$.

$$v_{wire} = RPM * \frac{2\pi}{60} * r_{pitch} \tag{3.4}$$

Hardness

The hardness of a test piece is a required parameter for determining the K factor and is measured using Struers' Hardness tester DuraScan 70 according to standards EN ISO 6507, ASTM E384.

Distance

The measured distance is the distance between the adjustable weight and the distance meter (as depicted in Figure 3.1). What is of interest is the relative distance difference at the end of the test compared to when cutting is started, as it represents the cut distance in the workpiece. The distance is not needed to determine the K-factor but was applied as a supporting measurement. Nevertheless, it gave a reference during cutting by giving a first indication of the cutting progress and the influence of changing parameters during testing. In addition, it can be used to retrospectively analyse the feed rate of the wire.

Pressure

The pressure was measured using two pressure sensors to measure p_1 and p_2 depicted in Figure 3.12 (a). Based on these two measured pressures and the angle (depicted in Figure 3.12 (b)) at which the wire is tensioned, Equations 3.5 and 3.6 are used to determining the tension (F_{span}) in the wire. During the experiments, the angle (α) at which the wire was tensioned was more or less constant and equal to 15 degrees.

The wire tension is not necessary for determining the K-factor. However, it is essential for the consistency of the experiments that the tension remains constant during the tests. Hence it is monitored.

$$F_{cylinder} = \frac{\pi}{4}(p_1 * d_1^2 - p_2 * d_2^2) * cos(\alpha) \tag{3.5}$$

$$F_{wiretension} = F_{cylinder}/4 \tag{3.6}$$

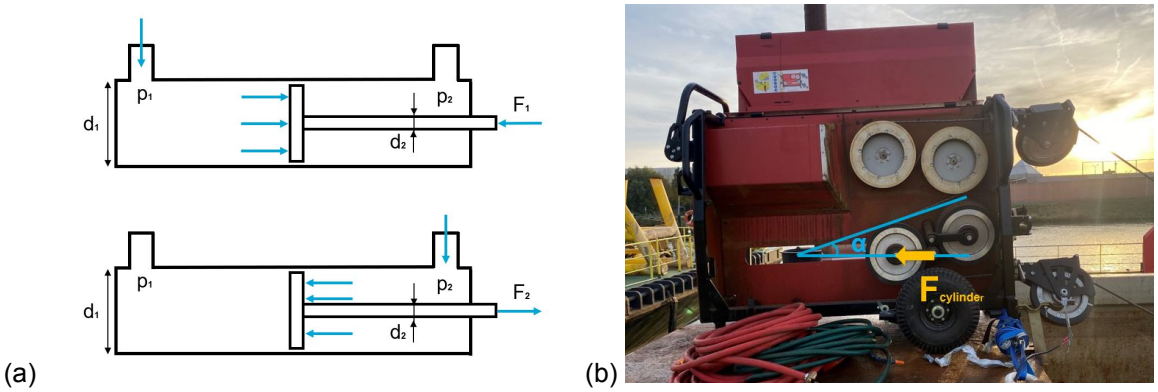

(a) (b)

Figure 3.12: (a) Schematic representation of the pneumatic cylinder **(b)** Positioning of the pulley set

Temperature workpiece (only during test day 2)

The temperature of the workpieces was determined using an infrared laser and a thermocouple, with the thermocouple serving as a check for the laser. The temperature of the workpiece just above the cable was measured with the laser once the sawing machine was stopped, and it was safe to approach. To fit the thermocouple, holes were drilled in the workpiece, as shown in Figure 3.13 (a). A thermocouple was placed during tests 20, 24 and 26. As Figure 3.13 (b) shows, The thermocouple was inserted as close as possible to the cut, at a distance t of 1-5 mm, to prevent damaging the thermocouple.

Water density

The density of the water in which the test pieces were weighed was measured with the help of a hydrometer.

Data acquisition

The data from the various sensors were logged using a National Instruments NI USB-6211 and Labview. A sampling time of 0.1 seconds was used.

Power consumption

Equation 3.7 provides an estimate of the total power on the drive shaft of the drive pulleys (P_{shaft} [W]).

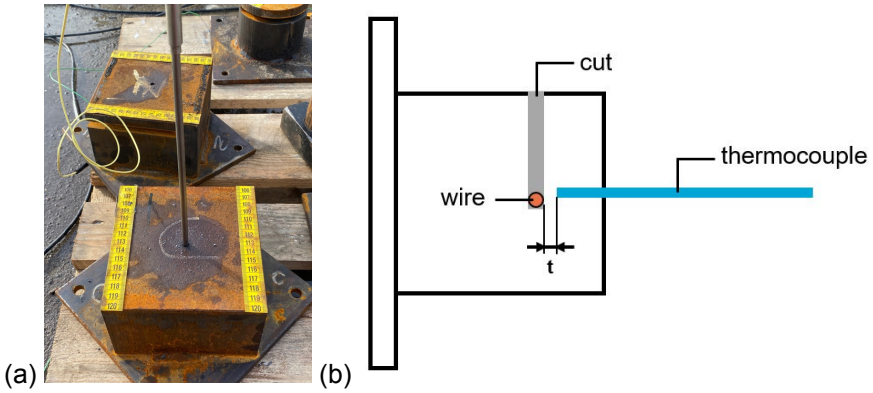

Figure 3.13: (a) Testpiece with thermocouple inserted **(b)** Schematic representation of thermocouple set-up

The power consumption (I [A]) of the sawing machine is measured using an ampere clamp (FLUKE i310s), measuring the amperage consumed by the sawing machine during cutting. The sawing machine measured and displayed the Line-to-Line Voltage (V_{L-L} [V]), which was approximately constant at 390V throughout the measurements. The power factor of the motor (PF_{motor}) under nominal load is equal to 0.89. The exact power factor varies depending on the load, as shown in Figure 3.14. However, it can also be seen that the power factor above a load amperage of 50% is generally more or less equal to the power factor at full load for an induction motor. While cutting the test pieces, the machine operated at the top of its capabilities, indicated by the fact that the sawing machine regularly stopped working due to an overload error. Therefore, it is assumed that the induction motors operated continuously above 55 % of the full load, and strong linearities occur below that; hence, a constant power factor of 0.89 will be used to estimate the power consumed. For a correct power calculation, the power factor of the transformer will also have to be considered. The power factor of a transformer ($PF_{transformer}$) is dependent on the load as well and can negatively impact efficiency when the load has a poor lagging power factor, as seen in induction machines. The exact power consumption value is uncertain due to the variable and unknown power factors. For estimation purposes, the power factor of the transformer is assumed to be constant as well since it is operated above 55% of the load. based on the literature, a constant factor of 0.97 is used (Amoiralis et al., 2007). Therefore a total efficiency of 0.86 is used.

$$P_{shaft} = \sqrt{3} * PF_{motor} * I * V_{L-L} * PF_{transformer} \tag{3.7}$$

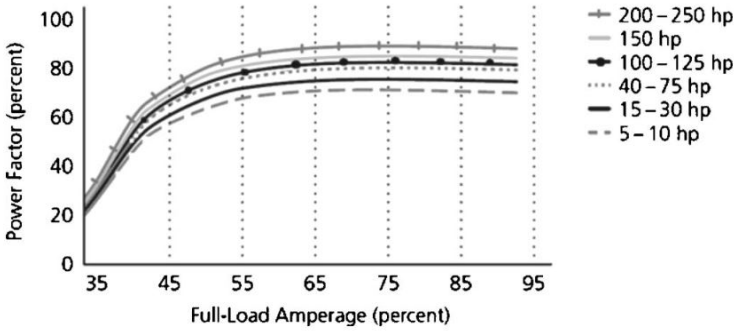

Figure 3.14: Induction motor power factor as a function of full-loadamperage (Natural Resources Canada, 2004)

Other obtained information

In addition to the data obtained from the sensors, the following information was also obtained:

- Chips collected (only during test day 1)
- Photographs of the wire using a microscope

- The amount of power used during the experiments (according to the display of the remote controller of the sawing machine)
- Video footage of the tests

3.5. Processing data

The data logged from the sensors were stored in Excel using Labview. Then the obtained data were plotted against time in graphs using Python. An example is shown in Figure 3.15 below.

Figure 3.15: Measurements a plate of S255 (40x200x100mm) under nominal test conditions

Below, the measurements from Test 19 displayed in Figure 3.15 will be reviewed from top to bottom:

- The load signal starts just above N and oscillates around N during the sawing process due to vibrations in the setup during cutting. After that, it ends again at N after the sawing is finished. Therefore, the measured value of the load used to obtain the K factor, in this case, is equal to N
- The wire speed is logged throughout the sawing process. The speed increases from 0 to about m/s at the same time as the load disturbance starts and then drops back to 0 when the load disturbance is over again.
- The data regarding the wire tension shows that the tension on the wire remained nearly constant during the whole cutting process, as it shows a horizontal line.
- Finally, it can be seen that the distance data starts horizontally (no displacement), then rises with a linear trend and ends horizontally again. The wire moves through the test piece during the rise, causing the weight to drop. When the sawing stops, the displacement also stops. Hence the distance measurement is horizontal again. The movement of the weight can explain the disturbance seen in the measurement signal by the wind

Figure 3.16: Measurements of solid round piece of 42CrMo4 (d: 120mm, h: 100mm) under nominal test conditions

Figure 3.16 shows 4, with similar measurements compared to Test 19.

- The load begins at about N, oscillates around that number and then returns to
- The distance is horizontal before cutting, increases throughout cutting, and then ends again horizontally.
- The wire tension remains constant during the test.
-

Figure 3.17: A subset of measurements of an S235 solid block (150x150x100mm) under nominal test conditions, with the exception of a wire speed of 6 m/s (a part of the full measurement is displayed)

The data of test 14 are comparable to those of tests 19 and 4 in Figures 3.15 and 3.16. However, the vibrations in the load signal indicate that the cutting process pauses at 2300 samples and resumes around 3000 samples this time. This is because the sawing machine repeatedly stopped throughout the measurements owing to a machine overload error or jamming of the wire. Therefore, to determine the sliding distance needed to determine the K-factor with the missing data, the wire speed must be estimated during these data gaps, like in test 4 (see Appendix B.3 for more details).

Sliding distance

The sliding distance for each measurement was calculated using the trapezoidal method, taking into account the wire speed. However, there were several instances when the tachometer failed to record the wire speed, resulting in gaps in the data. To account for this, the complete measurements were used to determine the overall trend of the speed decrease, which was then applied to estimate the sliding distance for the incomplete measurements.

- Original data used when present
- Missing data extrapolated with the trend line from data measured during the experiment
- Method is verified to different data sets with full data, and the accuracy of the method is determined

The estimated error for the sliding distance consists of the sum of the tachometer error and the error due to filling in the data gaps. The error caused by filling in the data gaps varies depending on the number of stops/starts made during the measurement and is scaled by the proportion of the data that has been completed (see Appendix B.1 for a more detailed explanation).

4

Results and Discussion

This section will display and discuss the test results obtained.

4.1. Wire wear

During the first day of testing, two tests (Test 1 and 6) were conducted to assess the wear of the diamond wire. The conditions for both tests were identical, including the environment, normal load, wire speed, material, and geometry of the test piece. If there was no wear on the diamond wire between Test 1 and 6, both tests should give the same K value and produce a horizontal trendline concerning K. However, as seen in Figure 4.1, the K-factor, or the non-dimensional wear rate, decreased by almost % between Test 1 and 6, indicating diamond wire wear. Figure 4.2 depicts the cable's wear over the two test days. The appearance of a new cable is shown in Figure 4.2 (a). Figures 4.2 (b) and (c) depict segments of the cable after being used for an entire test day. In both cases, a new cable was installed on the machine at the beginning of each day. The cable in Figure 4.2 (b) was used on the first day of testing and shows visible signs of wear, including fractures on the diamonds and some diamonds being torn away from the bonding material. The cable in Figure 4.2 (c) was used on the second day and also shows wear, but appears to be in better condition than the first-day cable, with fewer diamonds torn loose.

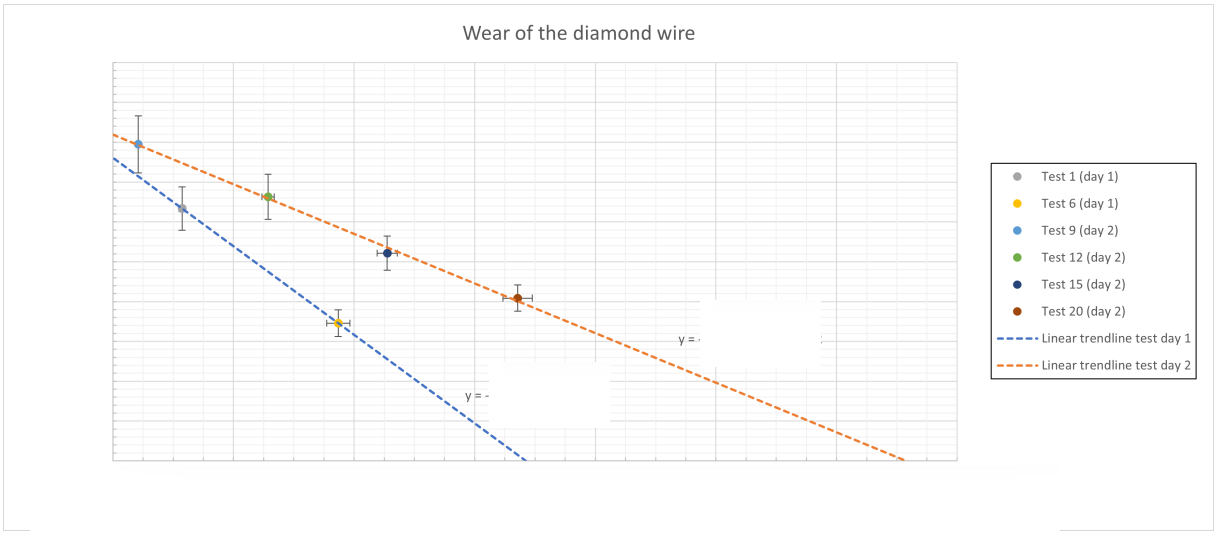

Figure 4.1: Results of wear tests diamond wire (Wear coefficient K is obtained under identical test conditions, except the cooling of test day 1 compared to test day 2)

Since the course of the wear between two points cannot be determined, four tests were conducted

on the second day of testing to capture the wire wear adequately. The results of these tests are shown in Figure 4.1.

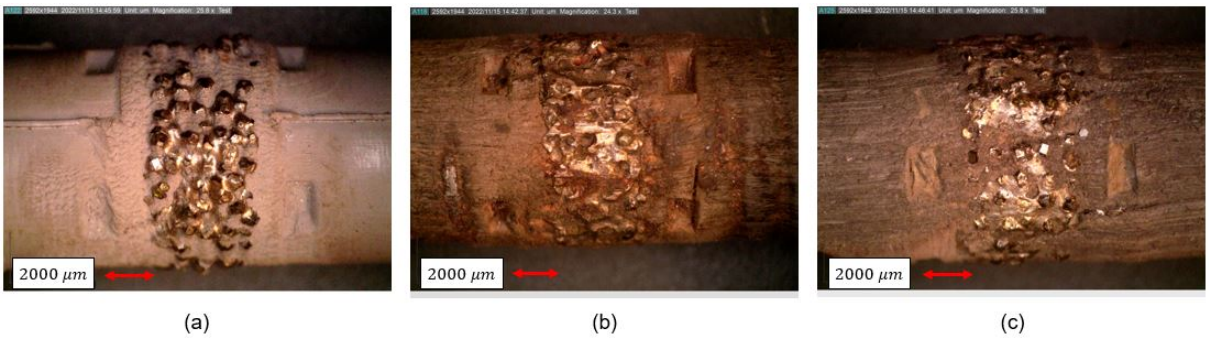

Figure 4.2: Microscopic pictures of: **(a)** new wire **(b)** wire after test day 1 **(c)** wire after test day 2. Because the images depicted are of different wires, they do not depict the same sections.

The second day's testing results show a linear relationship between decreasing wear coefficient (K) and increasing sliding distance (s). A linear trend is also assumed for day 1, but this relationship cannot be established with certainty based on two points. As a result, only interpolation using these data will be performed.

The linear relationship between wear and sliding distance suggests that the wear observed within the tested parameters seems to depend only on the sliding distance and not on other variables, such as different speeds, loads, or materials. But this is probably because the tests between wear tests often included tests performed both above and under nominal conditions, which may have resulted in an averaging of wear when considering the times at which the wear tests were conducted.

The influence of wire wear on the K-factor dominates the test results, so the results will be adjusted to account for wear to enable comparison. Ideally, a new wire would have been used for each test to keep the wire constant, but this was not feasible. Therefore, the results for both test days are corrected by multiplying the directional coefficient of the trendlines from Figure 4.2 by the total distance travelled and adding this difference in absolute form (K) to the K-factor obtained from the different tests, according to Equation 4.1. The effect of wire wear on the K-factor is omitted after correction, as shown in Figure 4.3.

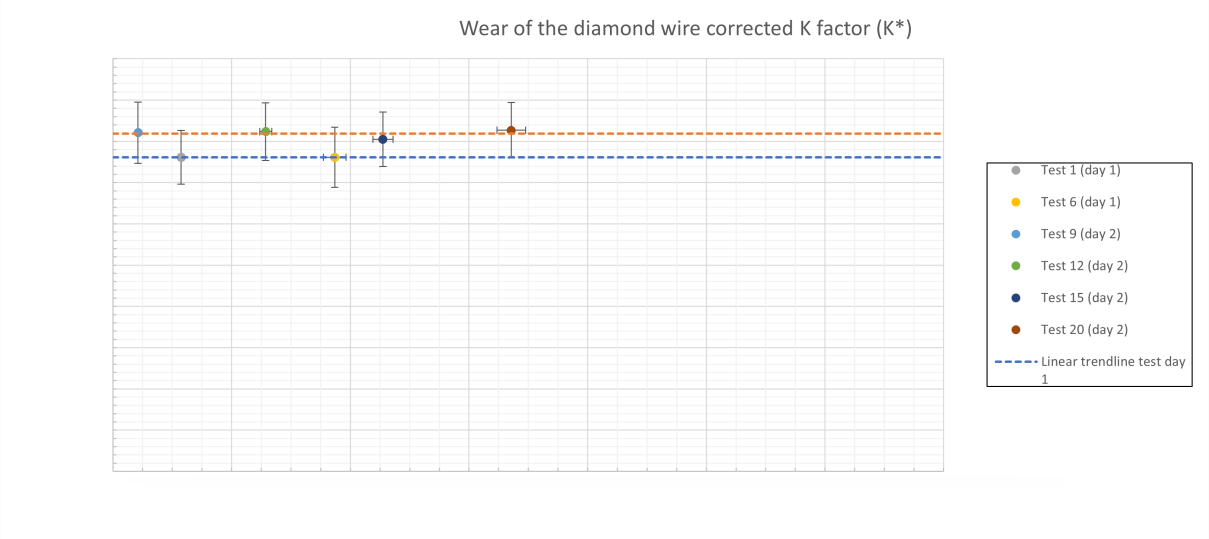

Figure 4.3: K-factor wear tests after correction of wire wear

$$K^* = K + \Delta K \tag{4.1}$$

The variations in wire wear observed during test days 1 and 2 can be attributed to differences in cooling; see Figure 3.4. On the first day, the nozzles were positioned in a way that resulted in water flowing along the diamond wire but not being directed directly into the cut. On the second day, the nozzles were repositioned to cool the entire test piece and direct water directly into the cut and onto the wire. The data shows a strong correlation between cooling the wire and the workpiece and the wear of the wire. As discussed in Section 2.1.4, cooling positively impacts wire lifetime and the cutting process by facilitating the removal of chips and small abrasive particles from the work area. The importance of chip removal will be further examined in Section 4.7.

4.2. Influence of wire speed on K

As explained in Section 2.3.1, according to Archard's wear equation, the worn/cutaway volume is independent of the cutting speed (not to be confused with feed speed). This implies that the K-factor is not influenced by wire speed. As a result, tests conducted under similar conditions but with different cutting speeds should also exhibit a similar K-factor. The figure shows the results of these tests, in which a standard S235 test piece (150x150x100mm) was cut, and all test conditions except for speed were kept constant.

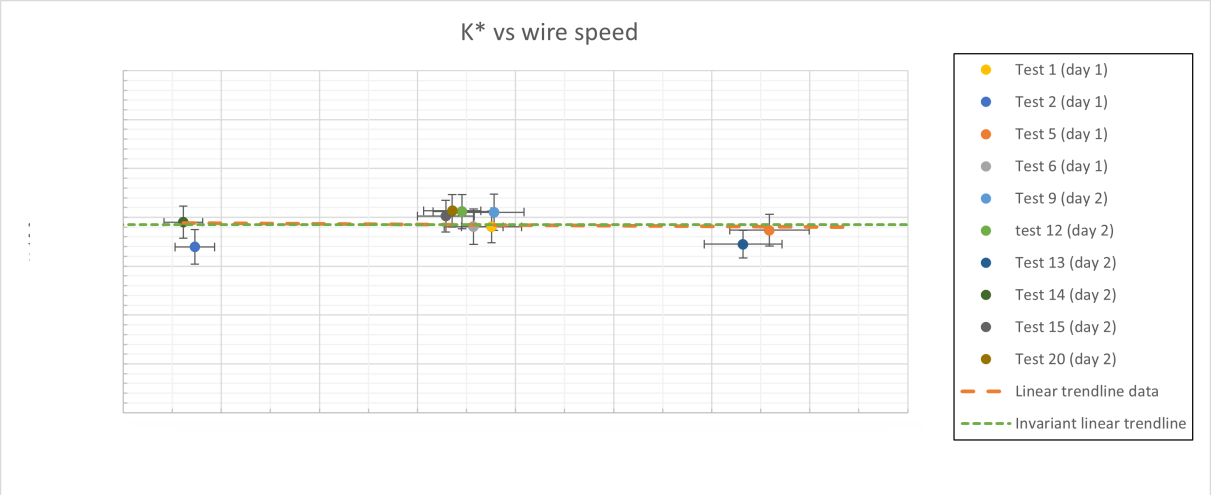

Figure 4.4: Corrected K^* factor vs varying wire speeds (S235 (150x150x100mm) with all other parameters remaining constant)

Figure 4.4 shows that the K-factor remains relatively constant with varying speeds. While efforts were made to maintain consistent test conditions, it is not always possible to perfectly control all variables in practice, which may account for the slight variations in speed and K-factors.

The more or less constant K-factor may be explained as the penetration depth of the abrasives remaining the same under the constant load at different speeds. The cutting rate will double for a constant penetration depth if an abrasive is pulled over the material at twice the speed. This means that the cutting rate is proportional to the sliding distance and independent of the K-factor. To compare this finding to another machining method, the research conducted by Wei et al., 2016 was considered, which examines the impact of drilling parameters on the performance of drilling on stacks made of carbon fibre-reinforced plastic and titanium alloy. This study's results indicate that the drill's torque and thrust force, or normal load, is not influenced by the cutting speed when drilling a titanium alloy, which aligns with the finding explained above.

It is important to ensure sufficient cooling is applied, as higher speeds can generate more heat and increase the temperature of the workpiece. This can change the material's mechanical properties, such as decreasing the yield strength of steel, which can increase the ease of cutting. It is also essential to have sufficient space to accommodate the chips, as a bead without chip accommodation space loses

its cutting power. Otherwise, increasing the speed and, thus, the sliding distance per unit of time will not lead to more cutaway volume. Consequently, the cutting rate will not increase, and the K-factor will decrease.

It can be concluded that the speed of the diamond wire does not seem to have an impact on the K-factor, given the range of the tested cutting speeds. However, it is essential to note that based on the test results presented in Figure 4.4, no definitive conclusion can be drawn regarding speeds outside the range of tested speeds. Extrapolating the relationship between K and speed beyond this range may not be accurate, as factors such as material temperature could influence the K-factor.

4.3. Influence of normal load on K

The Archard wear equation states that the volume of material worn away is proportional to the normal load on the cut object while the K-factor remains constant. This was investigated through experiments in which the load was varied, but the general test conditions were kept constant. The results can be seen in Figure 4.5 below.

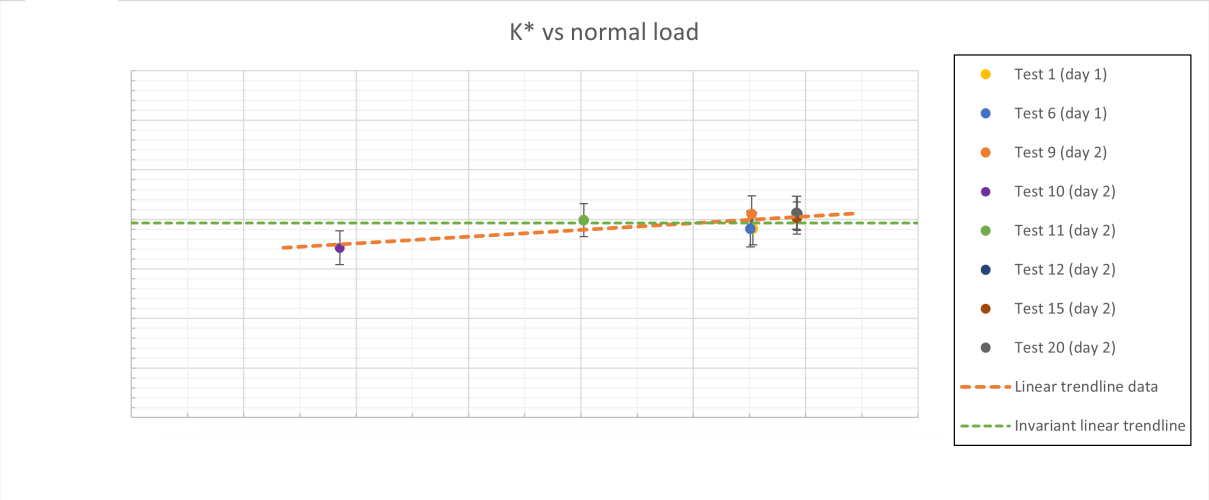

Figure 4.5: Corrected K^* factor vs varying loads (S235 (150x150x100mm) with all other parameters remaining constant)

In Figure 4.5, a linear trendline is plotted to show the relationship between K and the normal load. It can be observed that the K-factor decreases slightly at a load of about $400N$ and remains relatively constant from $800N$ and above. This suggests that the K-factor, or wear rate, remains constant and decreases below a particular load. However, due to the measurement uncertainties, it is also possible to draw a roughly horizontal line through the data points, suggesting that the K-factor is independent of the normal load, as stated by the Archard equation. In Section 4.5, the relationship will be further analyzed by examining the relationship between production $[mm^3/m]$ and load.

Modi et al. (2007) who investigated the abrasive wear response of 0.2% carbon dual phase steel, observed that the volume of material worn away increases with the normal load on the workpiece, as the penetration depth of abrasive particles also increases with the load. Additionally, Chuang et al. (2003) carried out a study that compared the sawing performance of brazed and sintered diamond wires for cutting natural stone and similarly found a linear relationship between the normal load and the material removal rate. These findings support the stated relationship that the K-factor is independent of the normal load.

Additional tests are advised to determine whether the K-factor is genuinely independent of the normal load or if it decreases from a specific value. For example, tests could be conducted at loads of $600N$ and $900N$ to understand better the gradient of the K-factor between the measured points. Repeating tests at $400N$ and $800N$ could also increase the certainty of the measured values and the course of the K-factor. Improving the measurements' accuracy would also clarify whether a roughly horizontal line is a viable representation of the data. The accuracy of the K-factor is influenced by

several factors, with the sliding distance being the most significant source of inaccuracy. Section 5.2 further discusses methods that can be used in the future to improve accuracy.

It can be concluded that based on the test results, it appears that there is a proportional relationship between load and cutaway volume. This finding is consistent with the findings of Huang and Xu (2013) and suggests that the K-factor does not depend on the load.

4.4. Influence of hardness on K

The Archard wear equation states that the volume of material worn away is inversely proportional to the hardness of the cut object, while the K-factor is independent of the hardness of the workpiece. Similarly, Williams (1999) states that the relative wear resistance is proportional to hardness, defined as the ratio of a standard material's wear volume to that of a sample material tested under the same experimental conditions.

The proposed relationship was tested by conducting experiments in which the hardness was varied while keeping all other testing conditions constant. For the 42CrMo4, the test piece geometry was round with a diameter of 120mm and a height of 120mm, due to supplier availability.

Figure 4.6: Corrected K^* factor vs varying surface hardnesses (other parameters are kept constant, except the geometry of 42CrMo4 is round d:120mm instead of a square of 150x150mm)

Figure 4.6 shows that the K-factor varies among materials. Taking S235 as a reference, it is clear that cast iron and 42CrMo4 have a significantly higher K-factor. Which in both cases contradicts the relationship suggested by Archard. Several explanations or hypotheses that could account for the non-proportionality of cutting speed and hardness include:

1. An explanation for the higher wear coefficient (K) of cast iron compared to S235
2. A hypothesis explaining why 42CrMo4 has a higher wear coefficient (K) than S235
3. The hypothesis that the wear coefficient of S235 has been underestimated and should be at the level of the coefficient of cast iron and 42Crmo4, in which case Archard's proposed correlation would apply.

These explanations and hypotheses will be further elaborated and named below starting with cast iron, followed by 42Crmo4 and finally S235.

Cast iron

The variation in the wear coefficient of cast iron can be attributed to the difference in material properties leading to brittle fracture of cast iron as described in Section 2.1.2. This difference can also be observed in the shape of the chips produced during cutting. For example, Figure 4.7 illustrates that the chips produced from cast iron are made up of small chunks, while the chips produced from ductile materials such as S235 and 42CrMo4 are longer and more ribbon-like in shape. This is due to the brittle nature

of cast iron and its lower ability to absorb energy through deformation before breaking, which leads to less energy required for cutting and thus a higher production rate, and subsequently a higher wear coefficient K, under equal testing conditions.

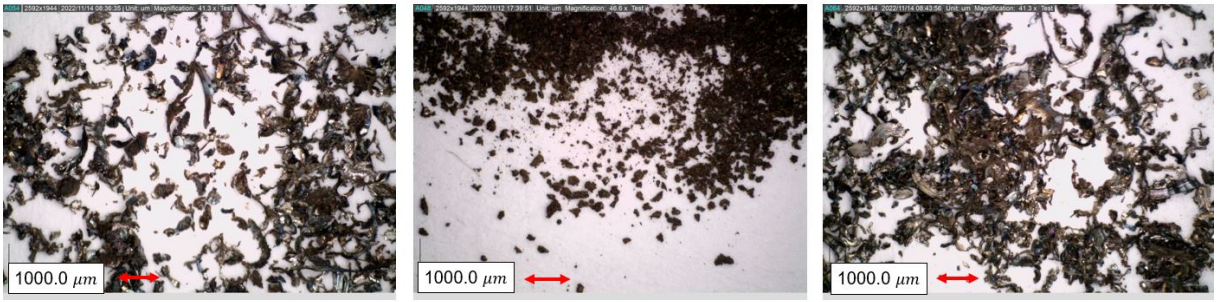

Figure 4.7: Chips produced during cutting

42CrMo4

The higher K-factor of 42CrMo4 could perhaps be attributed to the variation in the adjacent contact area/wire contact length, resulting from the difference in geometry of the round 42CrMo4 test piece. To examine this hypothesis that the higher K-factor of 42CrMo4 could perhaps be attributed to the variation in the adjacent contact area to the wire, Figure 4.8 shows the results of the tests with different geometries.

Before analyzing these results, it is important to note the following:

- These results are mutually corrected for the normal load, which varies between the different tests due to the difference in weight of the test pieces. For example, the 20x200x100mm slab was cut with the same test weight as the 150x150x100mm regular block. See Section 3.4 for more information on determining the normal load.
- In test 8, a round test piece with a diameter of 120mm and a height of 100mm was cut. Since the contact length of this piece varied during cutting, the thickness was converted to a rectangular test piece with the same area and a width of 120mm. This resulted in a test piece measuring 94mm x 120mm x 100mm for comparison.
- During test 19, the nozzles were not well targeted at the test piece, which effectively resulted in the test piece not being cooled during the test. Therefore, this result will not be included in further analysis. As lack of cooling leads to a lower cutting rate, which is discussed further in Section 4.6, no good comparison can be made between the K factors based on this measurement.

Figure 4.8: Corrected K^* factor vs varying width of the testpieces S235 (weight difference is corrected, other test parameters are constant)

Comparing the $K*$ factors in Figure 4.8, a mild correlation is seen between the $K*$ factor and the thickness of the test pieces in tests 8, 9, and 18, with $K*$ decreasing linearly as the thickness increases. This can be attributed to a reduction in the contact length between the wire and the workpiece. Leading to an increase in force per unit abrasive, which can lead to a greater degree of diamond indentation and reduced sliding of diamonds over the material. This results in a higher proportion of abrasives cutting the material instead of sliding over it, resulting in a higher cutting speed for workpieces with a smaller wire-workpiece contact length (Qiu, 2022; Tönshoff and Hillmann-Apmann, 2002)

To understand the extent to which the mild relationship between the width of the test piece and the K-factor, regardless of the cause of this relationship, shown in Figure 4.8, is responsible for the higher K of 42CrMo4. Figure 4.9 displays the K-factor at various hardnesses again. Where tests 4 and 16 are also shown after being corrected for the assumed correlation between specimen width and K-factor (indicated by an asterisk). The correction involves subtracting the supposed increase in K-factor caused by the decrease in thickness of the round test pieces. This allows seeing if the correlation between the width and K-factor is the sole reason for the higher K-factor of 42CrMo4 or if there must be other contributing factors.

Based on the data presented in Figure 4.9, it appears that the variation in the K-factor observed in Figures 4.6 and 4.9 is only slightly affected by the geometric difference.

S235

Another possibility could be that S235 was cut under less optimal conditions, resulting in a lower K value. It is generally recommended to machine harder materials at a slower speed than softer materials to minimize the build-up of heat, reduce stress on the material, and improve surface finish. However, data from Figure 4.4 suggests that increasing the sawing speed does not affect the wear coefficient (K factor) for S235, indicating that the lower K-factor for S235 is not due to a sub-optimal cutting speed according to the tested range.

In summary, the results indicated that the K-factor varied for different materials. This variation does not align with Archard's proposed relationship, in which the cutting rate is inversely proportional to hardness. There are multiple explanations and hypotheses that may explain why the cutting rate is not proportional to hardness.

First, the higher cutting rate of cast iron can be attributed to the difference in structure resulting in material loss through mechanisms such as inter- or intra-granular fracture in addition to plastic flow.

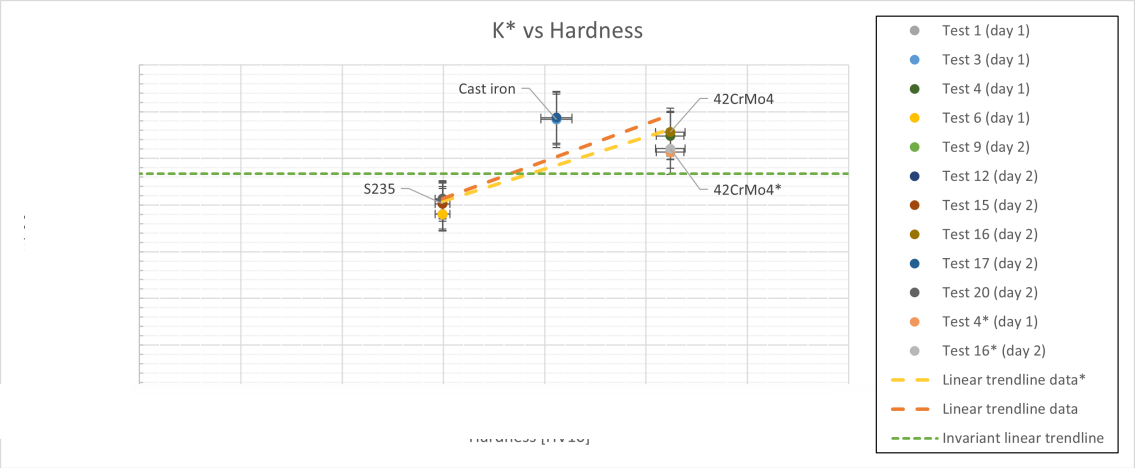

Figure 4.9: K^* vs hardness, the asterisk indicates tests that are corrected with the assumed relationship on the width of test pieces

The difference in chip formation is evident in the shape of the chips produced during cutting, which are small chunks instead of ribbon chips.

Secondly, the difference in geometry leads to an increase in force per unit abrasive if the contact length decreases, which can lead to a greater degree of diamond indentation and reduced sliding of diamonds over the material, thus leading to a higher wear coefficient K.

And third, there was a suspicion that S235 was cut under less than optimal wire speed; however, this suspicion contradicts the earlier finding that the K-factor is independent of speed.

To see to what extent the difference in geometry may have led to the deviation in K-factors, the K-factors of 42CrMo4 in Figure 4.9 are corrected for the variation in geometry. Figure 4.9 shows that considering that there is a relation between the thickness of the test piece and the cutting rate, it is not significant enough to explain the variations in the K-factors seen in Figures 4.6 and 4.9. To more conclusively establish the relationship between the hardness of a material and the K-factor, further experiments should be conducted using test pieces with similar geometries. This will enable a more accurate comparison of the results.

4.5. Production

In addition to the K^* factor, the production per meter corrected for the wear Q^* $[mm^3/m]$ (see Equations 4.2 and 4.3) can also be considered. This is calculated by dividing the total production of the test by the total sliding distance. For example, in the figures below, the production in mm^3 per meter is plotted against wire speed, normal load on the workpiece, and hardness. The same trends can be observed in these figures as with the K-factor. First of all, the production per meter does not depend on speed. This can be followed in Figure 4.10, where the trendline is almost horizontal. The trendline would be completely horizontal in an ideal situation where the results strictly follow the Archard wear equation. Secondly, in Figure 4.11, the blue trendline clearly shows that the production is proportional to the normal load on the workpiece, as stated by Archard. Finally, the blue trendline in Figure 4.12 does not show an inversely proportional relationship between hardness and production, similar to the K factor. Instead, the expected relationship that would align with the Archard wear equation is shown with the orange trendline. Figure 4.12 is particularly interesting, as it can be used as a starting point to explore potential alternative relationships that may link the results obtained for the different materials instead of hardness.

$$Q = \frac{W}{s}[\frac{mm^3}{m}] \tag{4.2}$$

$$Q^* = Q + \Delta Q \tag{4.3}$$

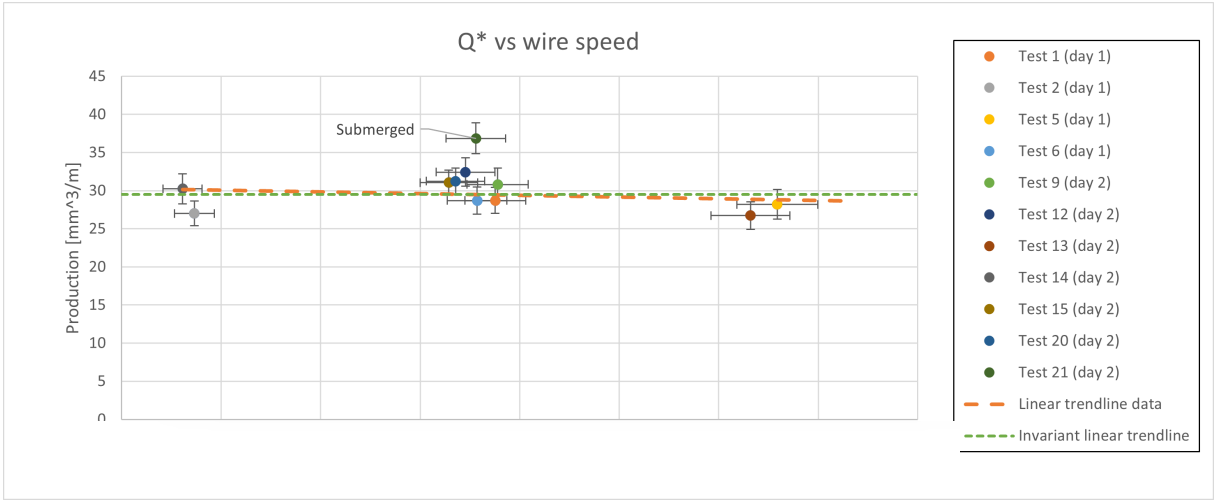

Figure 4.10: Corrected production vs varying wire speed (other parameters are kept constant)

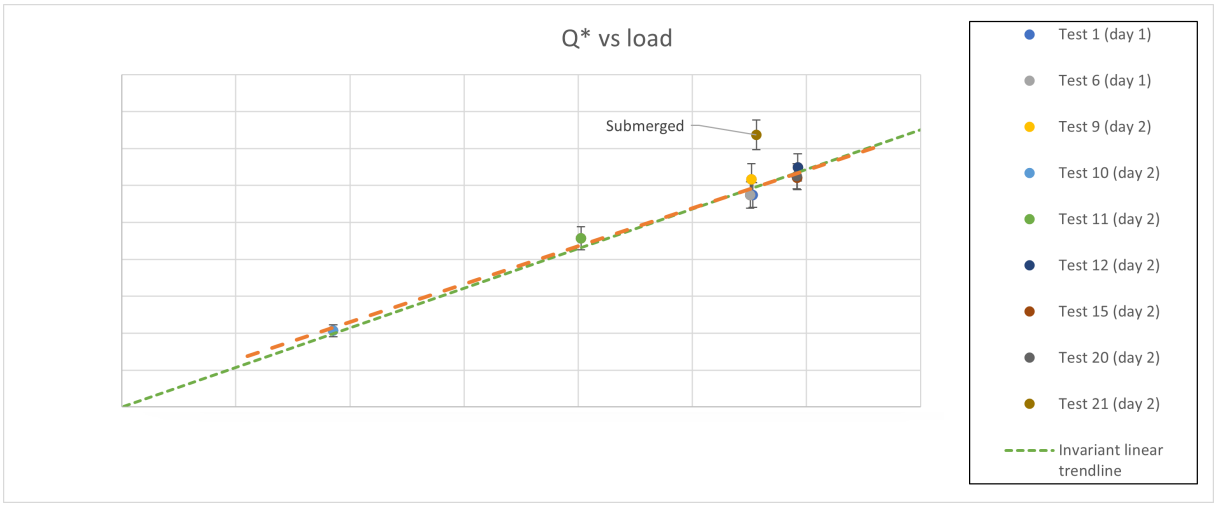

Figure 4.11: Corrected production vs varying normal load (other parameters are kept constant)

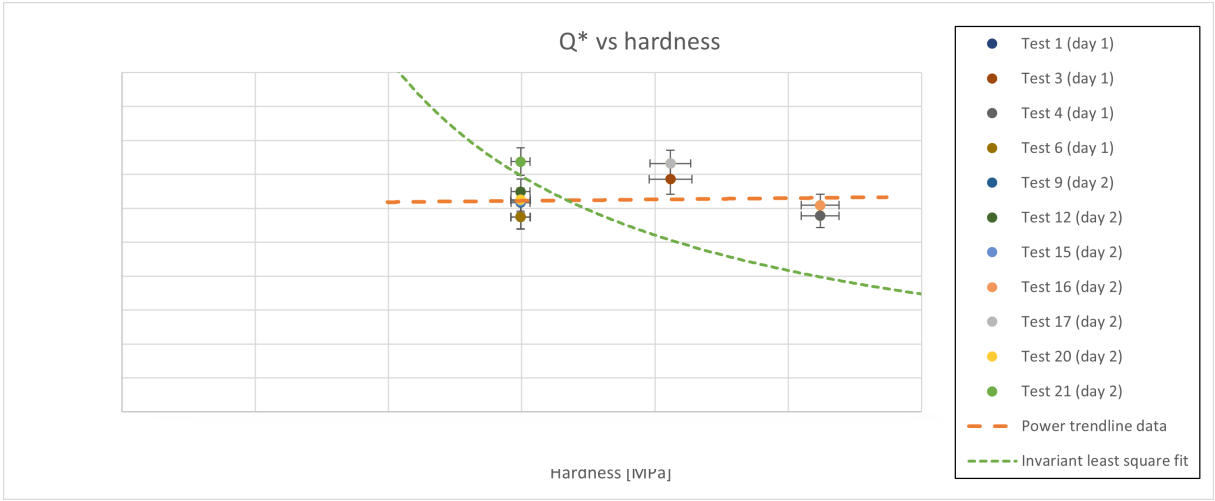

Figure 4.12: Corrected production vs varying surface hardness (other parameters are kept constant)

4.6. Test piece temperature

The temperature of the test pieces during the first day of testing was not measured, but steam was frequently observed after cutting, indicating that the temperature must have been above 100 °C. On the second day of testing, the temperature of the test pieces was measured using an infrared laser. Since the test pieces were wet at the time of measurement, the laser measurement may have been affected by the presence of water. Therefore, the temperature was also measured using a thermocouple, which can provide a more accurate measurement closer to the cut. The temperature measured by the laser and thermocouple was the same after the cutting.

The measurements revealed that when proper cooling was provided using two nozzles, the temper-ature was typically around °C and reached a maximum of °C (or °C during test 15 as shown in Figure 4.13). On the other hand, the temperature rose to °C when cooling was insufficient, according to the laser.

Figure 4.13: Thermocouple measurement test 15

As explained in Section 2.2, observing the discolouration of the test pieces after cutting is a method for determining the surface temperature of the test pieces without any measuring equipment, but this only works if the temperature was so high that discolouration had occurred. Significant discolouration is found on 5/8 of the test pieces from day 1, whereas only one test shows discolouration on day 2. Figure 4.14 depicts the typical discolouration observed on the test pieces during the first test day. The discolouration ranges from purple to grey-blue/dark grey, implying a minimum surface temperature increase of at least °C and as high as °C.

Figure 4.14: Under nominal test conditions, but with improper cooling, discolouration of the cutting surface was observed on a round S235 test piece (d: 120mm, h: 100mm)

4.6.1. Submerged in salt water

During the final test, the tank in which the experimental setup was located was filled with salt water, and a standard test piece was cut submerged in salt water using standard conditions. Limited time and the challenges of removing test pieces from the water made it possible only to conduct one test in this environment. The result of the test is shown in the figures below.

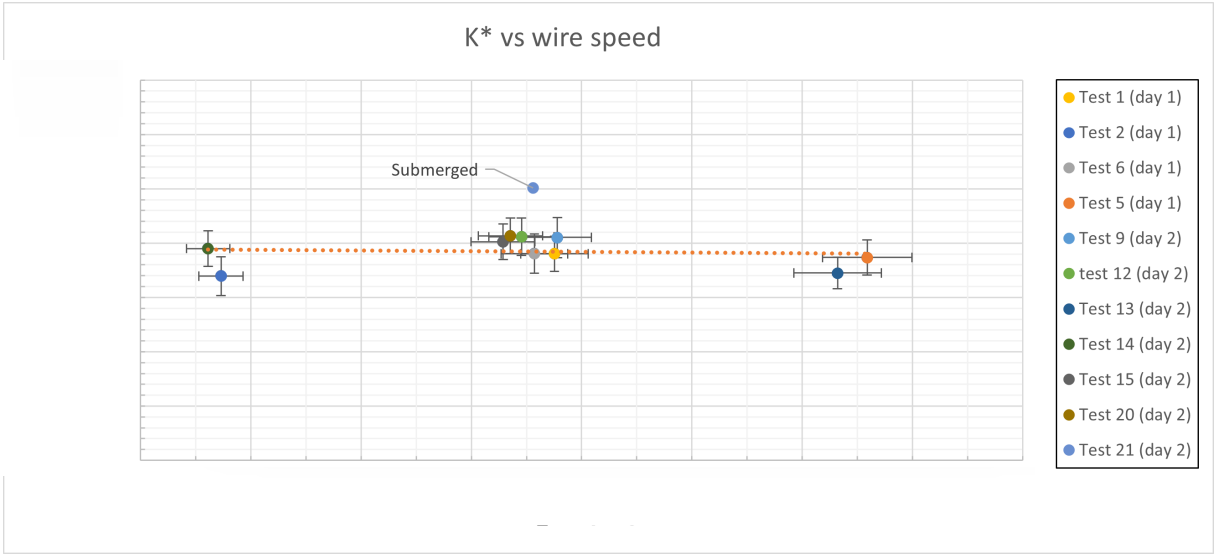

Figure 4.15: Corrected K-factor vs wire speed obtained submerged in salt water (other parameters are kept constant)

Figures 4.15, 4.16 and 4.17 show that the K-factor for the submerged test is higher than for similar tests conducted in the air with cooling via nozzles. This suggests that the cutting process was more efficient when fully submerged. It seems that the improvement in efficiency is likely the result of the wire and test piece being cooled more effectively by the surrounding water. The benefits of proper cooling are explained in detail in Section 2.1.4. But in short, it boils down to the following:

- Adequate cooling is necessary to prevent the material's properties from changing to such an extent that the material can start to adhere to the bead, covering the diamonds. This clogging of the bead results in a decrease in the wire's cutting performance.

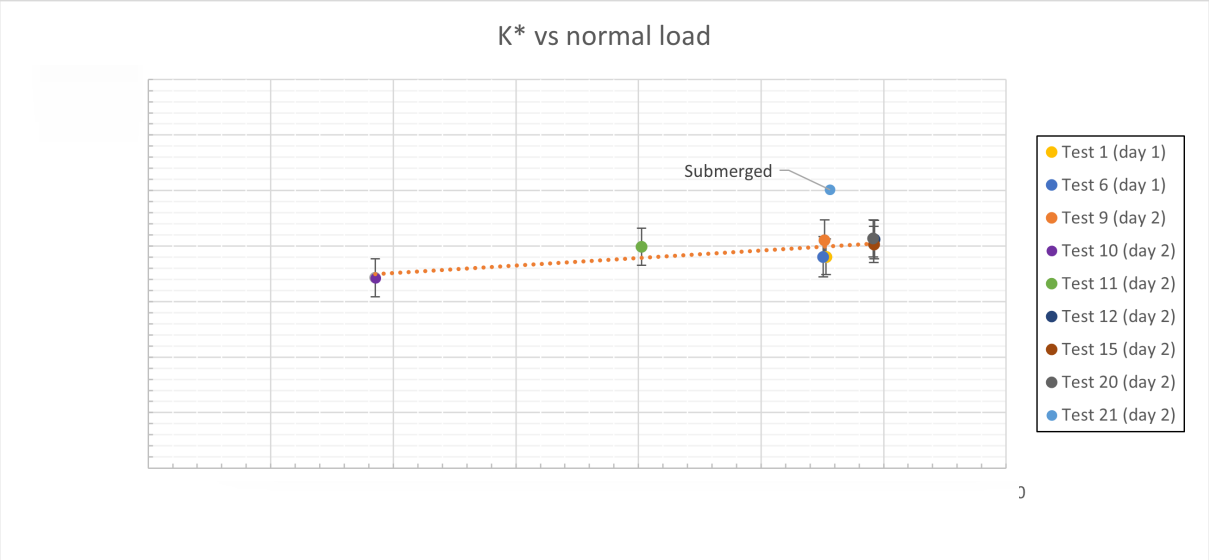

Figure 4.16: Corrected K-factor vs normal load obtained submerged in salt water (other parameters are kept constant)

Figure 4.17: Corrected K-factor vs hardness obtained submerged in salt water (other parameters are kept constant)

- Coolant aids in removing wear debris, so an increase in the coolant leads to more effective removal of chips, which improves the cutting process.

The Figures 4.18 (a) and (b) demonstrate that bead clogging is a serious problem. The photographs were taken following nominal tests, with the exception that the bead in Figure 4.18 (a) was properly cooled (nozzles position 2 in Figure 3.4) while the bead in Figure 4.18 (b) was cut without proper cooling (nozzles position 1 in Figure 3.4). It be seen that the improperly cooled bead has rusted material, i.e. material from the test piece, adhered to it (clogging of the bead).

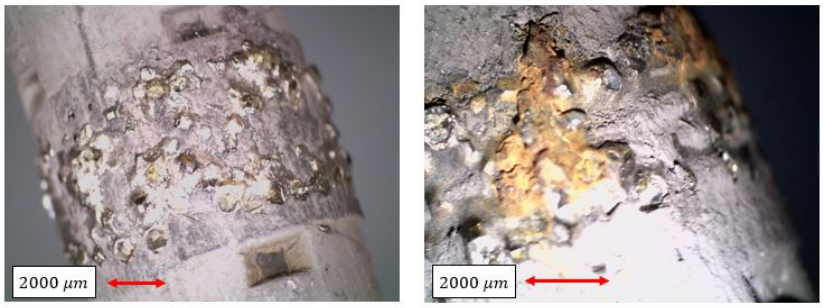

Figure 4.18: Representation of smearing the bead with steel

To summarize, properly cooling the diamond wire and workpiece is essential for reducing wire wear and optimizing the cutting process and, consequently, the cutting rate. In addition, adequate cooling prevents beads from clogging and aids in the removal of wear debris.

Due to the structure of a wreck, as depicted in Figure 2.9, it can prove challenging to properly cool a cut that is partially above the waterline if the wire is deep into the cut. This becomes particularly problematic when cuts are made from the bottom up, as water cannot be supplied to the top of the cut. These issues are not present when the wreck is entirely submerged.

4.7. Chip accommodation space

In this section, the importance of chip discharge will be investigated in relation to the filling up of the chip accommodation space (Figure 4.7 shows a schematic representation of the chip accommodation space). Because when the chip accommodation space fills up, it is no longer possible for the diamonds to come into proper contact with new workpiece material. So when the chip accommodation space fills up, from a certain point onwards, the cutting rate will decrease and the friction between the wire and the workpiece will increase as a bead 'filled' with chips is rubbing over the material instead of diamonds cutting new material away. As a result of this increase in friction between the wire and the workpiece, the temperature of the workpiece will increase, affecting the cutting process as explained in Section 2.1.4.

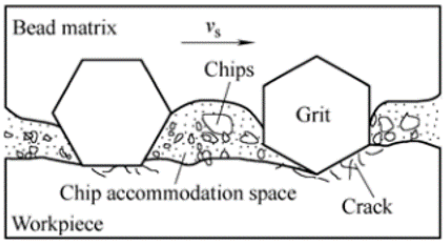

Figure 4.19: Schematic representation of the chip accommodation space (Chuang et al., 2003)

To investigate if the chip accommodation space could fill up during the experiments, the amount of available accommodation space per time unit ($Q_{accomodation,bead}$ $[mm^3/s]$) can be compared with the amount of measured wear debris per second ($Q_{produced}$ $[mm^3/s]$). Equation 4.6 estimates the amount of available accommodation space per time unit in mm^3/s. And Table 4.1 provides the required calculation parameters. The factor 0.5 in Equation 4.5 accounts for the fact that only the lower half of the bead is engaged (see Figure 4.19).

$$Q_{accomodation} = Q_{accomodation,bead} * N_{beads/s} \tag{4.4}$$

$$N_{beads/s} = N_{beads/meter,wire} * v_{wire} \tag{4.5}$$

$$Q_{produced} = Q_{accomodation,bead} * N_{beads/s} \tag{4.6}$$

Table 4.1: Calculation parameters accommodation space

Outer bead diameter $[mm]$
Inner bead diameter $[mm]$
Bead length $[mm]$
Beads per meter wire ($N_{beads/m}$)
Nominal wire speed $[m/s]$
Max reached production 150x150x100mm test piece ($Q_{produced}$) $[mm^3]$
Max reached production 20x200x100mm test piece ($Q_{produced}$) $[mm^3/s]$

Assuming 50% of the area difference between the outer and inner diameter of the bead (see Figure 4.19) is available as chip accommodation space, the amount of available accommodation space per second is equal to mm^3/s. This analysis shows that completely filling the chip accommodation space under the tested parameters is not an issue given $Q_{produced}$ of mm^3/s and mm^3/s for the plate and block, respectively. Despite this, it is recommended to utilize a coolant, as it facilitates the removal of wear debris and avoids the clustering of chips in a single location.

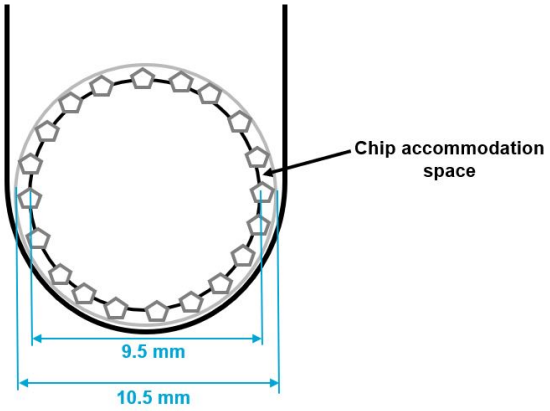

Figure 4.20: Schematic representation of chip accommodation space

4.8. Power consumption

The estimated power consumption shown in Figure 4.21 is based on the method outlined in Section 3.4. It depicts a linear increase of shaft power with speed, despite the potential non-linearity caused by factors such as pulley friction or wire drag. These non-linear contributions can be negligible compared to the power required to overcome wire abrasion against the workpiece. Therefore, a linear relationship is expected to persist at constant μ if the speed is increased while keeping the normal force F_f [N] constant, following Coulomb's law of friction. The power factor of induction motors decreases sharply in a non-linear manner below 55% load, according to Figure 3.14. Which makes extrapolating the linear relationship below this lower limit invalid. As a result, the trendline will decay non-linearly to the origin instead of decreasing linearly.

Figure 4.21 demonstrates that Cast iron requires significantly less power than S235. This can be attributed to its more brittle material structure that requires less energy to remove chips. On the other hand, 42CrMo4 has a power demand that is nearly equal to or slightly less than S235, despite having a higher yield strength. This suggests that 42CrMo4 may be more brittle. However, this is not clearly

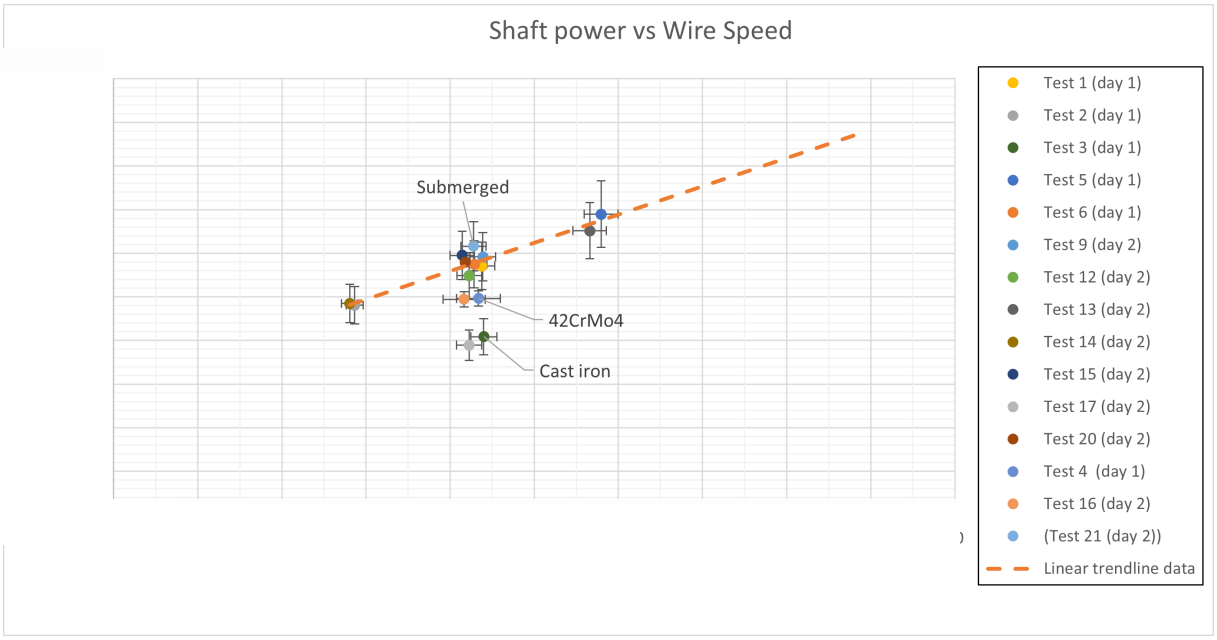

Figure 4.21: Shaft power at varying wire speeds (other parameters are kept constant unless otherwise indicated in the figure)

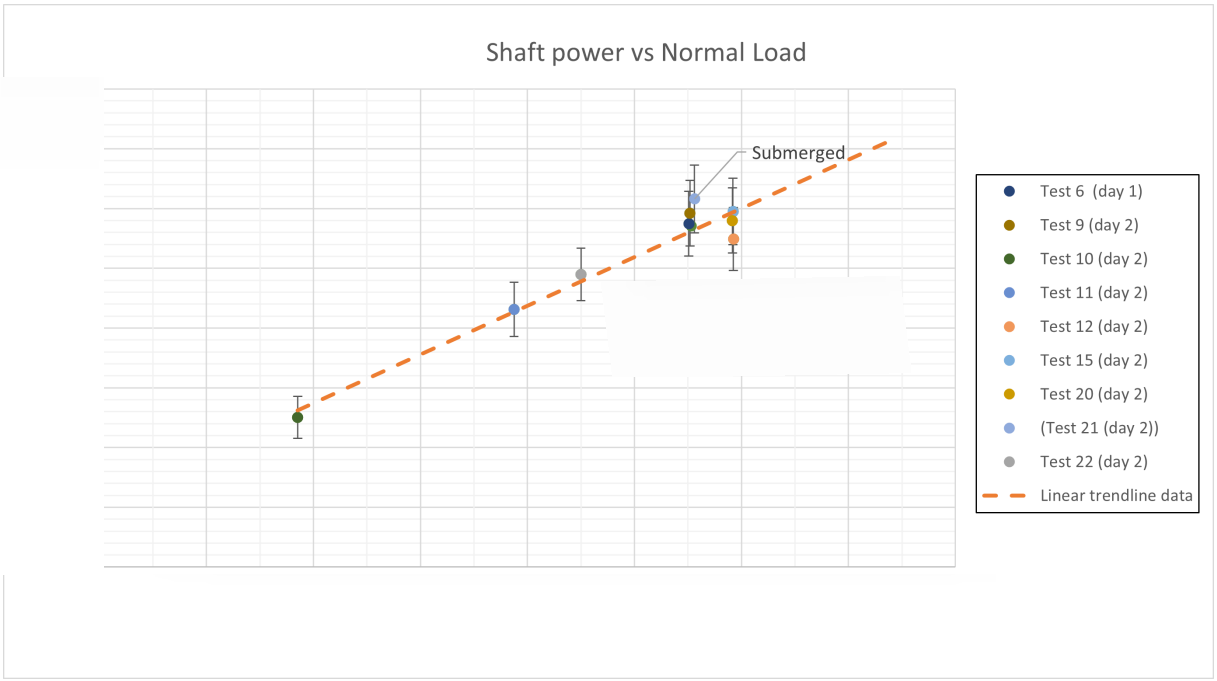

Figure 4.22: Shaft power at varying loads (other parameters are kept constant unless otherwise indicated in the figure)

evident in the chips shown in Figure 4.7, so further investigation into the material properties of 42CrMo4 is recommended.

The estimated shaft power increases linearly with normal load, as can be seen in Figure 4.22. Based on the same principles as the power - wire speed relationship, the relationship between power and increasing load is assumed to be linear if constant power factors can be assumed as explained in Section 3.4. If the coefficient of friction between the wire and workpiece is assumed to remain constant with increasing normal force and constant speed, the frictional force and thus the shaft power will increase proportionally as described by Coulomb's law of friction, shown in equation 4.7, with power Π [W], wire speed v $[m/s]$ and normal load P $[N]$.

$$\Pi = v * \mu * P \tag{4.7}$$

The average friction factor in the shaft-driven system, consisting of guide pulleys, tensioning pulleys, and the diamond wire, can be obtained by dividing the directional coefficient of the trendline shown in Figure 4.22 by the nominal cutting speed of 9 m/s used during the experiments, as shown by Equation 4.7. This results in an average friction factor of 0.91.

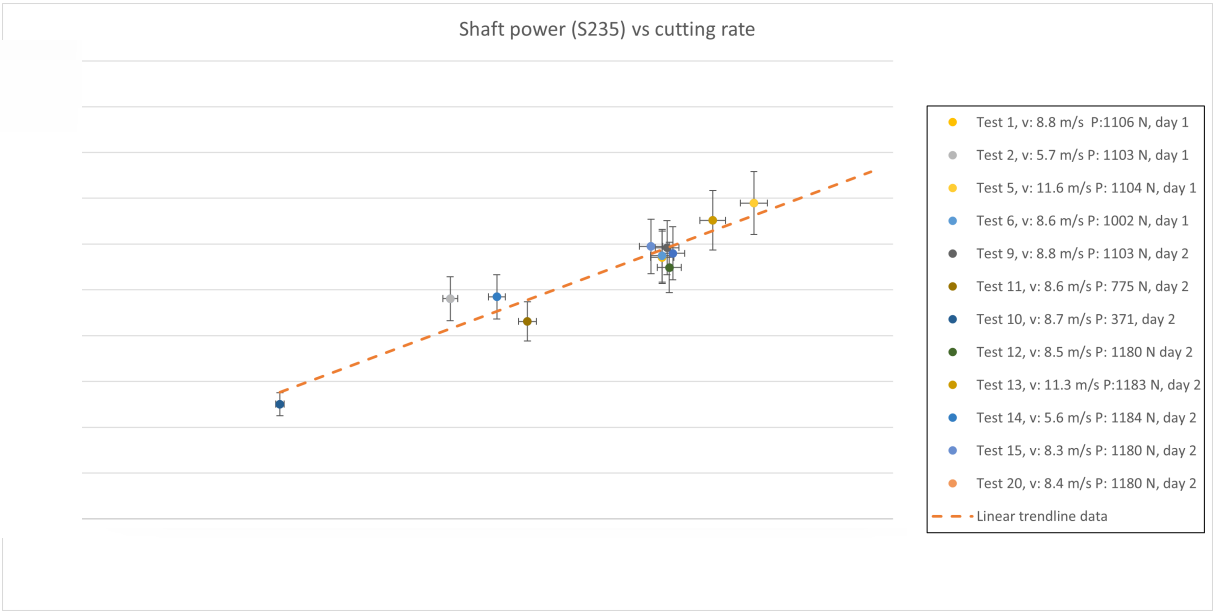

Figure 4.23: Shaft power vs wear corrected cutting rate (other parameters are kept constant unless otherwise indicated in the figure)

Cutting rate and shaft power have a linear relationship, as can be seen in Figure 4.23. The load and wire speed of the displayed measurements vary, so the relationship between cutting rate and shaft power is load and wire speed independent. Thus, within the tested range, the specific energy is independent of wire speed and normal load. Hence, it's advisable to apply the maximum normal force and load to maximise cutting speed while efficiently using power, considering the maximum pressure a diamond can endure to avoid damage. It is essential to cool the material and wire when increasing load and speed to prevent clogging of the beads and wire degradation caused by excessive heat because doing so will result in greater heat transfer of heat into the material. Additionally, it must be noted that the maximum pressure that each diamond can withstand must be taken into consideration. Otherwise, diamonds may tear out or break, reducing the bead-cutting capacity.

A derivation of the shaft power can be used to assess the linear relationship in Figure 4.23. First, the mechanical work (w [J]) is given by Equation 4.8, where ΔT $[N]$ is the change in wire tension before and after the workpiece and s $[m]$ the distance covered. With the Coulomb friction in Equation 4.9, where P $[N]$ indicates the load and μ the friction coefficient, Equation 4.10 is derived, which is then substituted into the Archard wear equation (Equation 2.10), leading to Equation 4.11.

Work equals energy, by definition. Furthermore, the time derivative of energy is equal to power, so by differentiating Equation 4.11 with respect to time and assuming K [-], μ [-], and H $[N/mm^2]$ are constant over time, Equation 4.12 is obtained. Giving the direct relationship between wear rate and power (Π $[W]$), and showing it is independent of normal load P $[N]$ and wire speed v $[m/s]$.

$$w = \Delta T * s \tag{4.8}$$

$$\Delta T = \mu * P \tag{4.9}$$

$$P * s = \frac{w}{\mu} \tag{4.10}$$

$$W = K * \frac{w}{\mu * H} \tag{4.11}$$

$$\dot{W} = K * \frac{\Pi}{\mu * H} \tag{4.12}$$

In summary, a linear relationship between power consumption and load and wire speed for cutting above water (with cooling using the nozzles) is observed during the tests. Furthermore, the relationship between cutting rate and shaft power is linear and independent of load and wire speed within the tested range. To achieve the highest cutting rate, it is therefore recommended to cut with the highest normal force and normal load, bearing in mind the maximum pressure each diamond can withstand to prevent the tearing or breaking of the diamonds. Cooling the material and wire is crucial when increasing load and speed to prevent clogging and wire deterioration due to excessive heat.

4.9. Optimal cutting parameters

It is beneficial to evaluate how different operating conditions, such as speed and load, can affect the wear of the cable to use it efficiently. Doing so makes it possible to determine the amount of wire needed under different operational conditions to cut through a wreck effectively. The optimal cutting parameters can then be identified by comparing the daily cost of cutting through a wreck with diamond wire with specific cutting parameters to the consumption cost of the wire to minimize expenses. It is also essential to consider the risks associated with higher speeds or loads, such as cable breakage and jamming, which can bring the operation to a halt and result in additional costs.

The wear of the diamond wire did not appear to be influenced by load or speed, as Figure 4.1 shows a linear decrease in the K-factor while varying load and speed during testing. However, other studies have suggested that both speed and load affect the wear rate of the wire. For example, Cao et al. (2006b) conducted a study to examine the correlation between the resistance to wear of beads on a sintered diamond wire and the cutting and feeding velocity. The study's results revealed that as the speed and feed velocity increased, there was a negative exponential relationship with the wear resistance of the beads. One possible explanation for this discrepancy may be that test conditions where higher wear can be expected, namely at higher wire speeds, were alternated with tests at lower wire speeds where lower wear is expected, which may have resulted in an averaging out of the wire wear between measuring moments.

4.10. Additional observations

The tests yielded several important practical insights for diamond wire cutting. These additional observations are discussed below.

Figure 4.24: Cut test piece consisting of a tube (120x120x100mm, thickness 16mm) containing loose round pieces

4.10.1. Data comparison

A comparison of the measured data during the experiments with the specifications provided by the diamond wire products Hilti and Husqvarna (see Appendix B.4) shows that the measured cutting rate and predicted wire lifetime while cutting steel, was below Hilti's specifications on the first day, with an average cutting rate of mm^2/s compared to the specified predicted rate of mm^2/s. And within the range on the second test day, with an average of mm^2/s. The same applies to the predicted wire lifetimes of test days 1 and 2 as shown in Table 4.2. The difference between the two days can be attributed to the difference in cooling. The measured rates and predicted lifetime were lower by a minimum of times than Husqvarna's specifications. The main difference was the cutting speed used, with Husqvarna using a cutting speed of m/s, which is to times faster than the nominal speed of used during testing. Unfortunately, the exact type of wire used to obtain the data in Table B.2 is unknown, So it cannot be reasoned whether this could have contributed to the difference in specifications.

Table 4.2: Data comparison

*Table B.3 shows how the cable's lifetimes during the test days is estimated.

5

Conclusions and Recommendations

5.1. Conclusions

The research presented in this thesis allows for several conclusions to be drawn. First, the sub-questions raised in Section 1.1 will be addressed.

1. What impact does the wire speed have on the cutting rate?

   Within the range of wire speeds tested, the cutting rate (volume per unit time) increases proportionally with the wire speed. Therefore, the factor K is independent of the wire speed, and Archard's proposed relationship, which states that the sliding distance is proportional to the wear volume, remains valid.

2. What impact does the normal load on the workpiece have on the cutting rate?

   Based on the tested range, the cutting rate increases proportionally with the normal load; thus, the K-factor is unaffected by the normal load. This aligns with Archard's wear equation.

3. How is the cutting rate affected by various materials encountered in wreck cutting?

   The cutting rate varies among different materials; however, according to the test results, it does not appear to be inversely proportional to hardness. This variation does not align with Archard's proposed relationship, which states that the cutting rate is inversely proportional to hardness. As a result, the obtained K-factor was not constant.

4. How do different geometries affect the cutting rate?

   The data suggest a mild linear correlation between specimen width and cutting speed, where cutting speed increases as specimen width decreases. This could result from reduced wire-to-specimen contact, causing an increase in force per unit abrasive. However, this effect is not substantial, and within the measurement accuracy, the cutting rate can be considered independent of specimen width and contact length. Hence, the validity of Archard's equation, stating that the K-factor is independent of contact length, remains valid.

5. How does the cutting rate vary in different environments encountered in wreck cutting?

   The test's environment differed between cutting above water with cooling using nozzles and fully submerging the test piece in salt water. It has been demonstrated that fully submerged cutting improves the cutting by about 25 % since the K-factor increases by about 25%.

6. What impact do operational parameters have on power consumption?

   The operational parameters examined are speed and normal load. The test results showed a positive linear relationship for cutting with cooling nozzles, where increasing the speed or normal load leads to increased power consumption. Furthermore, the relationship between cutting rate and shaft power is linear and independent of load and wire speed within the tested range.

Another key conclusion from the tests is the dependence of the cutting rate on the cooling of the wire and test piece. Adequate cooling prevents the test piece from overheating and causing significant changes in the material's mechanical properties, which can result in the clogging of the beads. Additionally, it promotes the discharge of chips and helps maintain the cutting process's efficiency. Moreover, cooling is vital in reducing wire wear and maintaining a higher cutting rate over an extended period.

In summary, the Archard wear equation is found to be partially valid because the negatively proportional relationship between hardness and wear volume is not valid. However, all of the other relationships are found to be valid within the range of tested variables and given accuracies. Therefore, Archard's equation can be applied to the materials from which the K-factor is determined.

Then to return to the main question:
What are the achievable cutting rates for a known diamond wire when cutting a wreck under specific conditions, and how can these rates be applied in a practical setting?

The cutting rates that can be achieved are influenced by the operational conditions and can be calculated using the Archard wear equation (Equation 5.1) and the wear coefficients from Table 5.1. As the materials used in the tests are commonly found in ships, it's likely that the materials encountered during wreck removal are similar or comparable to those tested, enabling the use of the Archard equation with the acquired K-factors to estimate the cutting rate for a given wire speed and normal force on the workpiece.

It is worth noting that based on the test results, no definitive conclusions can be drawn regarding speeds and loads outside the tested ranges. Therefore, extrapolating the relationship between K and speed or load beyond this range may not be accurate.

$$W = K\frac{Ps}{H} \tag{5.1}$$

W: wear volume $[mm^3]$
K: dimensionless wear coefficient
P: normal load on the contact $[N]$
s: sliding distance $[mm]$
H: surface hardness of the softest surface $[N/mm^2]$

Table 5.1: K factors

When using the wear coefficients to estimate cutting rates in a practical setting, it is essential to consider the importance of cooling. Proper cooling not only reduces wire wear but also improves production efficiency. For example, fully submerged cutting has been shown to perform up to 25% better, considering production per meter sliding distance. Additionally, it should be noted that the values in Table 5.1 have been corrected for wire wear, so in real-world conditions, these values will decrease over time as the wire wears down.

Additionally, the values were obtained in a set-up where the material to be cut was in good contact with the wire, the angle between the wire and the test piece was constant, and only one test piece was cut at a time. In other words, the process at the level of the entire system, while cutting through a wreck, was not considered. Therefore, further research is needed to determine the achievable rates and how the wire can be implemented at the system level when cutting through a wreck.

Practicalities
For the sake of clarity, additional practical considerations that were discussed during the thesis are listed below:

5.2. Recommendations

This section will offer suggestions for future research to address unresolved questions, as well as suggestions to enhance the confidence of the current findings and improve the current set-up.

5.2.1. Further research

- Investigate the system-level implications of how the wire will move through actual wrecks when encountering different structures. A starting point could be to experiment by cutting through a small ship with various materials.
- Examine if factors other than hardness can better predict the variations in cutting rates of different materials. For example, explore if there is a correlation between the specific energy, tensile or yield strength of the materials and the K-factor. This might allow for a better prediction of the K-factors of various materials without the need for testing. In addition, it is important to consider the strain rate relevant to the cutting process, as the strain rate significantly impacts the stress-strain curves from which the material parameters can be determined.
- Conduct an in-depth study of diamond wire wear, including the lifespan under optimal conditions, the causes of wire failure (e.g. high speed, heavy load leading to diamond breakage or detachment), and the minimum load necessary to prevent wire polishing, and maximum to prevent diamond tear out. To determine the range of operational conditions that allow for the successful use of diamond wire.
- Investigate the occurrence of wire vibrations at different speeds and spans. Analyze the impact of these vibrations on the cutting rate and explore methods to mitigate the effects, such as using conical beads.
- Conduct a study to determine the circumstances under which pinching and jamming of the wire will occur and the impact on the wire. Investigate the threshold impact load (e.g. from falling debris) and angles, in conjunction with applied force, that result in wire jamming and assess the extent of wire damage. Determine the minimum clamping force that causes pinching. Furthermore, examine the maximum force that can be applied to loosen the wire while maintaining its usability, and determine the point at which the wire becomes unusable.
- Investigate all the necessary assets for using diamond wire in an wreck removal, including an estimate of the overall cost of the assets, taking into account factors such as daily costs, consumables, and installation expenses.
- Compare the performance of various diamond wires. Measure the K values for different materials and varying wires. Additionally, investigate the impact of factors such as the number of beads, bead shape, and diamond composition on the wire's performance.

5.2.2. Improve the certainty of the current results

- Conduct additional tests at a wider range of speeds and loads to determine if the established relationships and the Archard equation hold, even under extreme conditions. It would be particularly interesting to investigate the effect of significantly higher speeds and loads, as they can potentially increase the cutting rate. Additionally, it would be valuable to investigate the optimal cutting parameters, considering the balance between cutting rate and wire wear, to determine the most cost-effective solution given the cost of the wire and potential time savings in terms of monetary gain.
- Compute additional tests with varying thicknesses while keeping the load on the workpiece constant. This will help to investigate whether the mild correlation that appeared to exist is actual or whether the width of the workpiece and, thus, the contact length of the wire has no influence on the cutting rate. Furthermore, it is also desirable to measure the temperature of the test piece during all tests to investigate the suspicion that the surface-to-volume ratio impacts the cutting rate. Placing the thermocouple closer to the cut is recommended to enhance the temperature measurements' accuracy. Additionally, it would be interesting to explore other geometries, such as comparing the cutting rate of two 20-mm plates versus one 40-mm plate.

- Conduct additional tests using materials of varying hardness while maintaining consistent geometries. Select materials where only the hardness varies while keeping other properties constant. This will allow for more accurate comparisons than the current tests, where multiple material property differences made it difficult to establish clear connections. Focusing on specific properties may make it possible to distinguish potential relationships more clearly.
- Conduct additional tests using various materials with different properties. Given the significant differences between materials, testing a range of different materials is advised. This includes investigating the impact of properties such as ductility and brittleness. To better understand the results, it is recommended only to vary one property per test. Additionally, it would be interesting to test materials listed as risks, such as materials that may adhere to the wire, such as oil, to understand how the wire performs in those conditions.
- Investigate the temperatures at which clogging of the beads occurs for various materials and determine the operational parameters (load and speed) at which these temperatures are reached, both with and without the use of cooling methods such as nozzles and complete submergence.

5.2.3. Improve the testing setup

- To improve accuracy, ensure that wire speed is continuously recorded throughout the entire measurement process, as the lack of continuous data points for wire speed is the main source of inaccuracies in the K factor and cutting rate.
- Implement a more powerful sawing machine to decrease machine downtime and thus improve data consistency. This will also enable testing at higher speeds and loads.

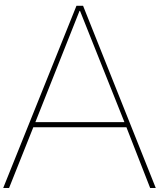

Appendix

A.1. Scientific paper

A scientific paper of this thesis is attached on the following pages.

Predicting the cutting rate of a diamond wire: Application to wreck removal

L.P.F. Pierik

***Abstract*—The process of salvaging wrecks can be costly and time-consuming, making it essential for salvagers to choose the appropriate technique(s) and accurately estimate total costs to minimize expenses and optimize efficiency. This paper focuses on developing a method to estimate the cutting rate of diamond wire when used in wreck removal. The primary aim is to fill the gap in knowledge about the cutting rates of diamond wire used in wreck removal, identified by a previously conducted literature review. The cutting rate will be predicted using the Archard wear equation with an unknown coefficient (K) that will be determined through experiments. Results from real-world experiments show that the Archard wear equation can be applied to steels and cast iron tested, but its applicability to other materials is uncertain. Additionally, results show that cooling significantly impacts both wire life and cutting rate, with fully submerging the workpiece resulting in a 25% improvement in the cutting rate compared to spraying with coolant. These results were obtained under controlled conditions, and real-world scenarios may differ, leading to deviation from the predicted cutting rates.**

***Index Terms*—Diamond wire, wreck removal, cutting rate, salvage**

I. Introduction

The transportation of goods via water is crucial for global trade, with over 80% of international trade being shipped by sea. While there have been improvements in ships' safety and operational safety, accidents involving vessels still occur and often require the assistance of marine salvors the be resolved. Accurate cost estimation is essential for salvagers to offer competitive and profitable prices for salvage projects. Typically a cost estimation of removal is made by the salvor based on their expertise, experience, and data from previous projects. Factors important in determining the feasibility of a technique include the duration of removal, the cutting/production rate, required assets and the risks associated with the technique. A model that can predict these factors could aid in evaluating a technique's potential and facilitate its application in various situations. This survey focuses on using diamond wire cutting to remove wrecks that cannot be removed as a whole. Diamond wire cutting is a material-cutting technique with much potential for use in wreck salvaging. However, a previously conducted literature review revealed a lack of sufficient information in the existing literature to accurately determine the cutting rates of diamond wire used in wreck removal, indicating a gap in current knowledge. A deeper understanding of the technique is required to assess the capability of diamond wire cutting in wreck removal by salvagers. Therefore, the primary focus of this paper is to provide a method to estimate the cutting rate of diamond wire when used in wreck removal. The effect of wire speed, normal load on the workpiece, various materials encountered in wreck cutting, different geometries, and environments on cutting rate have been investigated. Filling this knowledge gap is of particular interest to Boskalis, as they currently have limited knowledge and experience with diamond wire cutting, making it challenging to estimate costs.

The cutting rate will be predicted using the Archard wear equation, which requires an unknown constant (K) that can be determined through experiments. A real-world setup with a diamond wire was used to obtain data. The results show that for the steels and cast iron in this survey, Archard's assumption that the wear volume is inversely proportional to hardness is not supported. Consistent with Archard's equations, the wear volume has been found to be proportional to normal load and sliding distance but independent of speed within the range of tested conditions. As such, the Archard wear equation can be applied to the materials tested, but its applicability to materials that differ significantly from those tested is uncertain. Furthermore, results show that cooling significantly impacts both wire life and cutting rate. Specifically, fully submerging the workpiece resulted in a % improvement in the cutting rate as compared to spraying with coolant. It should be noted that these results were obtained under controlled conditions where normal load, wire speed, and cutting angle were kept constant, and proper cooling was possible. These operational parameters may vary in real-world scenarios, such as cutting through a shipwreck, leading to deviation from the predicted cutting rates.

A. Working principle diamond wire

The diamond wire cutting technique involves utilizing a wire with synthetic diamond beads to cut through materials such as stone, steel and other hard materials. This method was first developed in the 1960s in Italian quarries and is still widely used in the stone industry today. The process involves passing the wire around a stone block and feeding it through a wire saw using pulleys and guides. The wire saw's motor propels the wire at high speeds in a single direction along the stone block, causing the synthetic diamonds on the wire to abrade against the stone. Maintaining an appropriate level of tension on the wire is crucial in order to create the normal force required for abrasive cutting.

This method is also frequently employed in subsea applications for cutting pipes and cables, as well as for cutting through wrecks. Proper guidance of the wire is essential for ensuring the accuracy of the cut and preventing the wire from getting stuck. The wire is composed of a steel or synthetic wire core, which is strung with diamond beads (see Figures 1 and 2). These beads are made of a steel sleeve to which synthetic diamonds are bonded using various bonding techniques such as

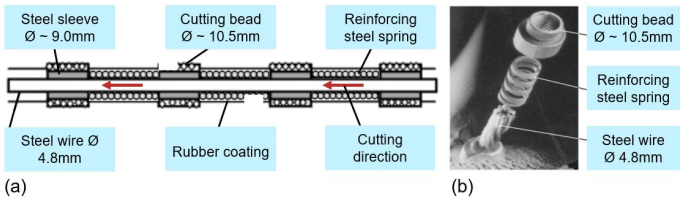

Fig. 1. **(a)** Schematic side view of the diamond wire ([1]) **(b)** Exploded view of the diamond wire ([1])

Fig. 2. Type of diamond wire used during experiments, with zoom-in on bead segment

sintering, vacuum soldering, and electroplating. Steel springs hold them in place, and finally, the wire is coated with rubber to protect it from wear and corrosion and to prevent displacements of parts. The wire can be connected into an endless loop in two ways: 'open' and 'spliced'. With 'open', a connector is used, and a 'spliced' wire is braided together at the factory.

B. Modelling cutting rate

The analysis of the diamond wire cutting can be done at different levels, including micro (at the atomic and molecular level), meso (focusing on a single abrasive particle and its effect on the material being cut), macro (analyzing multiple abrasives working together to understand the overall cutting rate and forces) and system level (looking at the implementation of diamond wire on a large scale, including equipment and personnel involved). Some analytical and numerical encountered in literature methods will be explained below.

1) Analytical modelling: The model presented by Kim et al. [2] aims to predict the theoretical sawing speed of a monocrystalline workpiece that is cut with a thin wire saw using abrasives attached directly to the wire and along its entire length, considering the wire sawing process on meso scale. The analytical model considers factors such as the indentation depth of a single (spherical) abrasive, the average force acting on it, the total number of abrasives in contact with the workpiece, and the width of the workpiece. However, it will be difficult to determine and measure the parameters required for the model in a real-world setting. Furthermore, the model assumes a thin wire with synthetic diamonds attached directly, which does not align with the wire type described above. An alternative analytical approach is to consider the cutting rate at the macro level, predicted with the help of the wear rate formula of Archard [3], which calculates the total volume of abraded material based on the total normal load, the sliding distance, the hardness of the softest material, and a factor K that must also be determined through experiments. A model can be created in a phenomenological way, combining physical and empirical methods.

2) Nummerical modelling: The studies of Zhang et al. [4] and Lan et a. [5] use numerical models, specifically finite element analysis (FEA) and response surface methods, to predict the cutting force required for machine cutting of steel considering a single diamond grit, focusing on interactions at the meso scale level. They examine the effect of different parameters on chip formation, including the cutting speed, coefficient of friction, and cutting speed of a single grain, and Lan et al. [5] found that the cutting speed, depth of cut, and density of the diamond grains all influence chip formation. However, scaling up models from the meso scale to the macro scale is difficult due to strong nonlinearities and surface uncertainties. Liu et a. [6] and Chuang et al. [7] perform FEA studies on the grinding process, focusing on the effect of different geometric and process parameters on the cutting of silicon wafers and the interaction between the grinding wheel and the workpiece, respectively, at the meso scale level.

3) Discussion: To be effective, a method or model must be simple to apply and understand, and the input parameters must be measurable in a real-world setting. In order to analyze the cutting rate at the wire level or macro level, it is preferred that the method or model is suitable for analysis at wire level. Therefore, Archard's wear equation will be utilized as the starting point for describing the cutting speed of diamond wire for wreck removal. The analytical nature of this model makes it more accessible than a finite element analysis model, and the parameters of the model align well with the variable parameters of the wire-cutting process, such as wire speed, normal load, and varying materials. The Archard equation simplifies the analysis of wire cutting by eliminating the need for scaling from the micro or meso level, providing more accurate measurements of input parameters in actual size and speed.

C. Archard's wear equation

The Archard wear equation (Equation 1) describes the relationship between the steady-state wear loss of a material, the normal load applied to it, and the hardness of the softest material. It is based on asperity contact theory, which investigates the behaviour of a single asperity (a small, raised area) in contact with a harder material. The equation can be used to estimate material wear loss and is consistent with experimental observations made by Archard [3]. It should be noted that the Archard wear equation is an empirical equation derived from several wear test data sets, and the values of the constants can vary depending on the material and tribological system under consideration, the factors and relationships that affect friction and wear. It is particularly useful for understanding abrasive wear, in which hard abrasive particles or asperities wear away the surface of a softer material. In this case, the hardness of the material, in combination with the load, controls the

penetration depth of the abrasive particles, and the wear loss can be accurately predicted using the Archard wear equation [3]; [8].

$$W = K\frac{Ps}{H} \tag{1}$$

W: wear/cutaway volume $\left[mm^3\right]$
K: dimensionless wear coefficient $\left[\frac{mm^3 N/mm^2}{mmN}\right]$
P: normal load on the contact $[N]$
s: sliding distance $[mm]$
H: surface hardness of the softest surface $\left[N/mm^2\right]$

A search for K-factors for cutting metals with diamond wire revealed a lack of available values. To the best of the author's knowledge, this represents a gap in current literature. However, Williams [8] gives a typical K value of $7*10^{-3}$ for mild steel sliding against tool steel in dry, unlubricated pin-on-disc tests in air. Furthermore, according to Thompson and Thompson [9], a typical wear coefficient by abrasive wear, the process to which diamond wire cutting can be compared, is in the order of 10^{-2} to 10^{-1}. The K-factor for diamond wire cutting is expected to be higher than Williams' value and in the range indicated by Thompson and Thompson.

The dimensionless wear coefficient K varies based on various parameters such as the environment or lubricant, temperature, and the combination of materials. Therefore, this constant must be determined through experiments under conditions as close as possible to the actual situation.

D. Test set-ups encountered in literature

To calculate the unknown wear coefficient K from Archard's wear formula, test pieces of known geometry are typically pressed against a spinning abrasive disc while being subjected to a known load. The K-factor of diamond wire cannot be tested using this method under conditions that are representative of the real world. As a result, an alternative setup must be designed for this purpose. A desirable set-up must be able to apply a constant load, allow for various geometries and materials, and simulate real-world conditions.

Set-ups used in other studies to determine wire-cutting parameters include set-ups with variations in wire types, workpiece movement, feed force vs speed regulation, parameter measurement and wire cooling. The following describes some of these setups and their variations.

1) Workpiece movement and feed force vs speed: The set-ups used in studies by Molfino and Zoppi [10] and Turchetta et al. [11] on diamond wire cutting involve moving the diamond wire against the test piece with regulated feed speed so the test piece remains stationary. On the other hand, Xu et al. [12], and Qui et al. [13] move the test piece against the wire with a regulated feed speed. Kim et al. [2], and Huang and Xu [14] also move the test piece but regulate the feed force instead of the feed speed, using a weight.

2) Parameter measurement: To assess the cutting parameters, Xu et al. [12], Turchetta et al. [11] and Huang and Xu [14] use a dynamometer. A dynamometer can measure the forces acting on a workpiece in three planes (x, y, and z) simultaneously). The biggest drawback of the dynamometer is its high cost. On the other hand, Kim et al. [2] use two individual load cells to measure the required parameters and do not measure the force in the cutting direction.

3) Wire cooling: Molfino and Zoppi [10], Qui et al. [13] and Yao et al. [15] vary in their cooling methods, with Molfino and Zoppi [10] submerging the whole set-up in a thank, Qui et al. [13] uses a small bath to submerge the workpiece, and Yao et al. [15] uses pouring liquid supply and electrostatic spraying liquid supply, but the latter method is not suitable for large-scale cutting.

4) Alternative set-up: Alternatively, Lan et al. [5], and Zang et al. [4] use a modified pin-disc friction tester to investigate the influence of cutting parameters on chip shape and residual stress. This requires a pin-disc friction tester that is able to achieve speeds and loads comparable to real-world scenarios.

II. Method

A. Experimental set-up

The experimental setup is intended to apply a contact feed force to various test pieces as they are pressed against the diamond wire. Hilit's sawing machine drives and pre-loads the diamond wire while also providing cooling via nozzles. The machine can set the wire speed to a constant speed. In addition to cooling via nozzles, the workpiece can be entirely submerged by filling the container with water, so the frame in Figure 3 is placed within the container shown in Figure 4. Figure 4 also shows the (blue) pulley system used to press the guided trolley with the attached workpiece against the diamond wire. The guided trolley is directly connected to the yellow test weight via a steel wire.

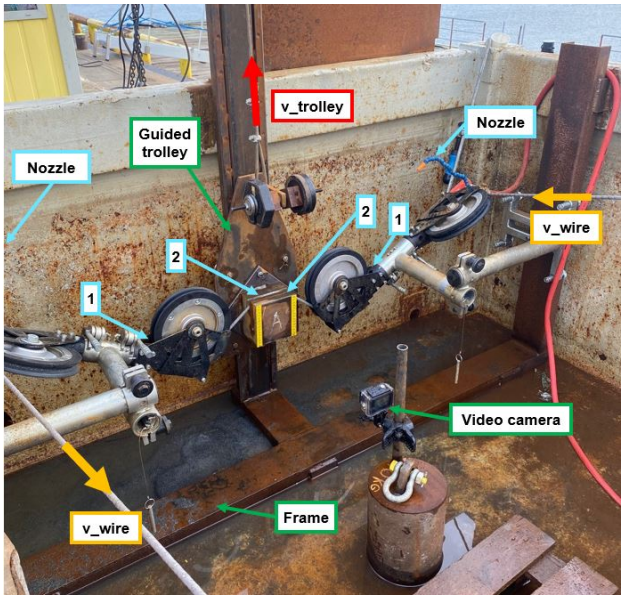

Fig. 3. Test set-up, the cooling positions of the two nozzles during test days 1 and 2 are indicated by numbers 1 and 2 accordingly

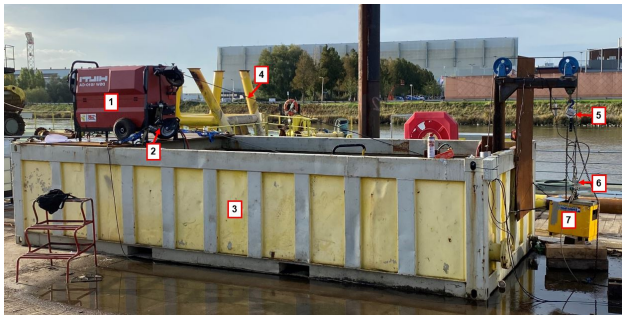

Fig. 4. Test set-up: (1):DSW 1510-CA sawing machine from Hilti (2):Tachometer (3):Steel container (4):Diamond wire (5):Hand hoist (6):Load cell (7):(variable) test weight

B. Experiments

Table I lists the parameters that will be varied during the test, considering the factors that affect the K-factor and the parameters required for the application of Archard's wear equation. The different test specimens that will be used in the experiment are outlined in Table II, with consideration given to materials commonly found in ship construction. Figure 5 shows the geometry of the test pieces from Tabel II.

Wrecks are often located at sea and either entirely or partially submerged. As a result, cutting performance is assessed below and above the waterline to account for differences in environmental conditions. It is advised to cool the wire and workpiece when cutting above the waterline; therefore, cooling via nozzles is implemented. And in order to simulate submerged cutting, the container is filled with salt water.

The cooling water will be sourced from a spur of the river IJssel, which is adjacent to the testing site and delivered through two nozzles with a flow rate of 7.5 l/min. The fully submerged conditions are simulated by dissolving NaCl in the freshwater sourced from the IJssel until it reaches a density of 1025 kg/m^3, similar to the density of seawater at 20 °C.

Tab. I
TEST PARAMETERS

Tab. II
DIFFERENT TYPES OF TEST SPECIMENS

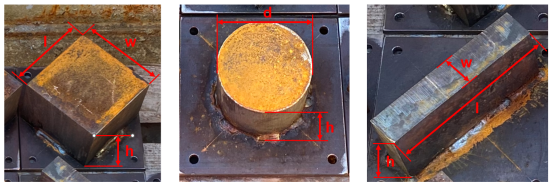

Fig. 5. Geometry of the test pieces

C. Measurement

Table I displays the parameters that will be measured during the experiments, the measuring devices and the associated uncertainties.

Tab. III
ACCURACIES MEASURED PARAMETERS

Parameter	**Device**	**Unit**	**Accuracy***
Wear volume	Submerged weighing	mm^3	± 1.79% OR
Weight	Loadcell Keli 30 kg	N	± 0.03% FS
Normal load	Load cell	N	± 0.03% FS
Speed wire	Tachoprobe A2108	m/s	± 0.5% OR
Hardness	Streuer Durascan 70	N/mm^2	± 30-70 OR
Distance	Ultrasonic sensor Honeywell	mm	± 5 mm
Pressure	Electronic pressure sensor	bar	± 0.5% OR
Temperature	Infrared laser	$°C$	± 1% OR
	Thermocouple	$°C$	± 1% OR
Water density	Hydrometer	g/ml	± 0.002

III. Results and Discussion

A. Wire wear

Two tests were conducted on the first day of testing to evaluate the wear of the diamond wire. Both tests were conducted under identical conditions, including environment, normal load, wire speed, material, and geometry of the test piece. The results showed a significant decrease in the non-dimensional wear rate between Test 1 and 6, indicating diamond wire wear. Further tests were conducted on the second day to capture the wire wear accurately. The results are depicted in Figure 6.

The second day's testing results show a linear relationship between decreasing wear coefficient (K) and increasing sliding distance (s). A linear trend is also assumed for day 1, but this relationship cannot be established with certainty based on two points. As a result, only interpolation using these data will be performed.

The results for both test days are corrected by multiplying the directional coefficient of the trendlines from Figure 6 by the total distance travelled and adding this difference in absolute form (K) to the K-factor obtained from the different tests, according to Equation 2. The effect of wire wear on the K-factor is omitted after correction to allow for comparison.

The variations in wire wear observed during test days 1 and 2 can be attributed to differences in cooling; see Figure 3. On the first day, the nozzles were positioned in a way that resulted in water flowing along the diamond wire but not being directed directly into the cut. On the second day, the nozzles were re positioned to cool the entire test piece and direct water directly into the cut and onto the wire. The data shows a strong

Fig. 6. The results of the wear tests on the diamond wire were obtained by measuring the wear coefficient K under identical test conditions, with the exception of the cooling applied during the first and second day of testing

correlation between cooling the wire and the workpiece and the wear of the wire. Cooling positively impacts wire lifetime and the cutting process by facilitating the removal of chips and small abrasive particles from the work area.

$$K^* = K + \Delta K \tag{2}$$

B. Influence of wire speed on K

Figure 7 shows that the K-factor remains relatively constant with varying speeds. The constant K-factor may be explained as the penetration depth of the abrasives remaining the same under the constant load at different speeds. The research conducted by Wei et al. [16] indicates that normal load is not influenced by the cutting speed when drilling a titanium alloy, which aligns with the finding explained above. However, it is important to ensure sufficient cooling is applied, as higher speeds can generate more heat and increase the temperature of the workpiece. It is also essential to have sufficient space to accommodate the chips, as a bead without chip accommodation space loses its cutting power.

It can be concluded that the speed of the diamond wire does not have an impact on the K-factor, given the range of the tested cutting speeds.

C. Influence of normal load on K

Figure 8 shows a linear trendline that indicates that the K-factor seems to decrease slightly at a load of about 400N and remains constant from 800N and above. However, given the measurement uncertainties, the trendline could be drawn horizontally as well, indicating that the K-factor is independent of the normal load, as stated by the Archard equation.

To further strengthen the likelihood of this correlation, Figure 9 shows proportionality between cutaway volume per meter sliding distance and the normal load, which is in line with Archard.

In addition, Modi et al. [17] investigated the abrasive wear response of 0.2% carbon dual phase steel, and observed that

Fig. 7. Corrected K^* factor vs varying wire speeds (other parameters are kept constant)

Fig. 8. Corrected K^* factor vs normal load (other parameters are kept constant)

the volume of material worn away increases with the normal load on the workpiece, as the penetration depth of abrasive particles also increases with the load. Additionally, Chuang et al. [7], who carried out a study that compared the sawing performance of brazed and sintered diamond wires for cutting natural stone, found a linear relationship between the normal load and the material removal rate as well. These findings are in line with the stated relationship that the K-factor is independent of the normal load.

D. Influence of hardness on K

Figure 11 shows that the K-factor varies among materials. This variation does not align with Archard's proposed relationship, in which the cutting rate is inversely proportional to hardness and independent of wear coefficient K. Taking S235 as a reference, it is clear that cast iron and 42CrMo4 have a higher K-factor. Figure 12 shows the wear-corrected production compared to the hardness. Indicating the trendline based on the data point (orange) and least square fit following Archard's wear equation (green). The material structure and

Fig. 9. Wear corrected production Q^* vs normal load (other parameters are kept constant)

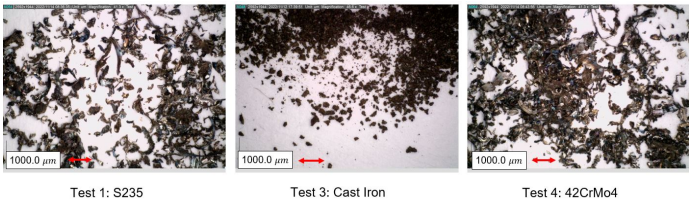

Fig. 10. Chips produced during cutting with identical wire speed, load and cooling method

variation in contact are explanations/hypotheses for the non-proportionality of cutting speed and hardness discussed below.

1) Material structure: The variation in the wear coefficient of cast iron can be attributed to the difference in material properties leading to brittle fracture of cast iron. This difference can also be observed in the shape of the chips produced during cutting. For example, Figure 10 illustrates that the chips produced from cast iron are made up of small chunks, while the chips produced from ductile materials such as S235 and 42CrMo4 are longer and more ribbon-like in shape. This is due to cast iron's brittle nature and lower ability to absorb energy through deformation before breaking, which results in less energy required for cutting and thus a higher production rate, and thus a higher wear coefficient K under equal testing conditions. Furthermore, compared to ductile materials, brittle materials can experience additional mechanisms of material loss via inter- or intra-granular factor Williams [8].

2) Variation in contact length: The geometry of 42CrMo4 varies, resulting in less contact area between the wire and the workpiece. This reduction in contact length between the wire and the workpiece increases the force per unit abrasive, which can result in more diamond indentation and less diamond sliding over the material. This causes a higher proportion of abrasives to cut the material rather than slide over it, resulting in a higher wear coefficient for workpieces with a shorter wire-workpiece contact length [13], [1].

Fig. 11. K^* factor vs surface hardnesses (other parameters are kept constant, except the geometry of 42CrMo4 is round d:120mm instead of a square of 150x150mm)

Fig. 12. Wear corrected production Q^* vs surface hardnesses (other parameters are kept constant, except the geometry of 42CrMo4 is round d:120mm instead of a square of 150x150mm)

E. Test piece temperature

The temperature of the test pieces during the first day of testing was not measured, but steam was frequently observed after cutting, indicating that the temperature must have been above °C. On the second day of testing, the temperature of the test pieces was measured using an infrared laser and verified by thermocouple measurements.

The measurements revealed that when proper cooling was provided using two nozzles, the temperature was typically around °C and reached a maximum of degrees°C.

Observing the discolouration of the test pieces after cutting is a method for determining the surface temperature of the test pieces without any measuring equipment, but this only works if the temperature was so high that discolouration had occurred. Significant discolouration is found on of the test pieces from day 1, whereas only one test shows discolouration on day 2. Figure 13 depicts the typical discolouration observed on the

Fig. 13. Discolouration of cutting surface of a test piece due to improper cooling (test 8)

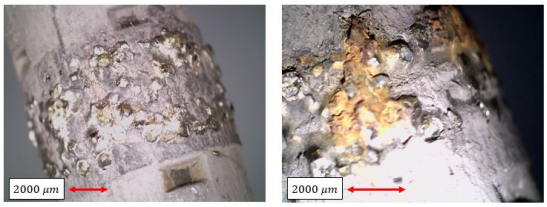

Fig. 14. Comparison of (a) properly cooled bead and (b) improperly cooled bead, with adhered material (clogging)

Fig. 15. Shaft power vs wire speed (other parameters are kept constant unless otherwise indicated in the figure)

test pieces during the first test day. The discolouration ranges from purple to grey-blue/dark grey, implying a minimum surface temperature increase of at least °C and as high as °C.

It is important to avoid high material temperatures as they can negatively impact wire wear and cutting rate. Proper cooling has several benefits such as preventing the material from adhering to the bead and covering the diamonds subsequently, which decreases their cutting performance. Additionally, coolant helps in removing wear debris to allow for proper contact of diamonds with new uncut material. The clogging of the beads is a significant concern, as Figure 14, shows that poor cooling can lead to material sticking to the bead. Analysis of the beads revealed that there was clogged material on every bead of the wire used during the first test day, in contrast to an average of 4 out of 44 beads per meter on the second test day.

Furthermore, the results of the fully submersed test, in which the container was filled with water from the IJsel river to which NaCl was added to attain a density of 1025 kg/m^3, comparable to seawater, showed that better cooling resulted in a % increase in the K-factor, which has a direct correlation with cutting speed.

F. Power consumption

The estimated total power on the drive shafts of the drive pulleys (P_{shaft} [W]) shown in Figure 15 is estimated using Equation 3 and depicts a linear increase of shaft power with wire speed. Power consumption (I [A]) is measured using an ampere clamp (FLUKE i310s), the Line-to-Line Voltage (V_{L-L} [V]) is displayed by the sawing machine, which was approximately constant at 390V throughout the measurements. The non-linear factors, such as pulley friction or wire drag, are negligible compared to the power required to overcome wire abrasion against the workpiece. Therefore, a linear relationship is expected to persist at constant μ if the speed is increased while keeping the normal force F_f [N] constant, following Coulomb's law of friction. The power factor of induction motors generally is constant above 55% load. An overload error during testing indicated that the induction motors operated above this limit during the tests; therefore, the power factors PF_{motor} and $PF_{transformer}$ are taken as constants of 0.89 and 0.97, respectively. The power factor of induction motors decreases sharply in a non-linear manner below 55% load, making extrapolating the linear relationship below this lower limit invalid. As a result, instead of decreasing linearly, the trendline will decay non-linearly toward the origin as the power factor goes to zero [18], [19].

$$P_{shaft} = \sqrt{3} * PF_{motor} * I * V_{L-L} * PF_{transformer} \quad (3)$$

In Figure 16, it can be observed that power consumption increases proportionally with the normal load P [N] on the workpiece. Equation 4 shows that assuming the friction coefficient between the wire and workpiece remains constant, the friction force and power will increase proportionally with the increase in normal force, with power Π [W], wire speed v $[m/s]$ and normal load P $[N]$.

Furthermore, Figure 16 depicts a lower power consumption than S235 for Cast iron due to the brittle material structure of cast iron that requires less energy to remove chips. 42CrMo4 requires nearly the same or slightly less power than S235 despite having a higher yield strength, implying it may be more brittle, but this is not confirmed by the chips shown in Figure 10. Further investigation of 42CrMo4's material properties is recommended.

The average friction factor in the shaft-driven system, consisting of guide pulleys, tensioning pulleys, and the diamond wire, can be obtained by dividing the directional coefficient of the trendline [N] shown in Figure 16 by the nominal cutting speed of 9 m/s used during the experiments, as shown by Equation 4. This results in an average friction factor of 0.91.

Fig. 16. Shaft power vs normal load (other parameters are kept constant unless otherwise indicated in the figure)

Fig. 17. Shaft power vs wear corrected cutting rate (other parameters are kept constant unless otherwise indicated in the figure)

$$\Pi = v * \mu * P \tag{4}$$

Figure 17 shows that the relationship between cutting rate and shaft power is linear and independent of load and wire speed within a tested range. The load and wire speed of the displayed measurements vary, so the relationship between cutting rate and shaft power is load and wire speed independent. Thus, within the tested range, the specific energy is independent of wire speed and normal load. Therefore, in order to achieve the highest cutting rate whilst remaining efficient use of power, it is recommended to cut with the highest normal force and normal load possible, bearing in mind the maximum pressure that each diamond can withstand to prevent tearing or breaking. Cooling the material and wire is crucial when increasing load and speed to prevent clogging and wire deterioration due to excessive heat.

G. Additional observations

The tests yielded several important practical insights for diamond wire cutting. These additional observations are discussed below.

- The alignment of the wire proved to be a crucial aspect. On the first day of testing, wire jamming occurred due to misalignment. This misalignment was caused because the pre-cuts were made with lower wire tension than the actual test cuts. This increased tension caused the pulleys to move, resulting in wire misalignment and jamming, which caused the machine to shut down. Once the wire became jammed, it was challenging to remove it manually, and a hammer had to be used.
- The test of cutting through a tube filled with loose parts was conducted by placing round steel pieces into a steel tube, resembling a loose piece in a wreck. The test showed that the wire could cut through the tube when the loose pieces were pressed against the side of the tube, overcoming the initial problems with rotating parts.

IV. Conclusions and recommendation

A. Conclusion

In this paper, the cutting speed of diamond wire for application in wreck removal has been evaluated using Archard's wear equation. Considering the influence of wire speed, normal load on the workpiece, different materials typically encountered in wreck removal, different geometries and environments on the cutting speed, respectively, the following conclusions can be drawn:

1) The cutting rate increases proportionally with the wire speed, and the factor K is independent of the wire speed, supporting Archard's proposed relationship that the sliding distance is proportional to the wear volume.
2) The cutting rate increases proportionally with the normal load, and the K factor is not affected by the normal load, supporting Archard's wear equation.
3) The cutting rate varies among different materials and does not appear to be inversely proportional to hardness, which does not align with Archard's proposed relationship. As a result, the obtained K-factor was not constant.
4) A mild correlation was found between the width of the workpiece and the K-factor. However given the accuracies associated with the measured data, Archard's wear equation is not rejected and remains valid within the tested range because the width appears only of minor influence. This implies that the geometry has no significant effect on the cutting rate.
5) The test's environment differed between cutting above water with cooling using nozzles and fully submerging the test piece. It has been demonstrated that fully sub-merged cutting improves the cutting rate by about %since the K-factor increases by about %
6) The test results show a positive linear correlation between speed and normal load with shaft power consumption for cutting with cooling nozzles. Furthermore, the relationship between cutting rate and shaft power is

Tab. IV
WEAR COEFFICIENTS K OF TESTED MATERIALS

linear and independent of load and wire speed within the tested range.

7) The tests have shown that the cutting rate strongly depends on the cooling of the wire and test piece. Adequate cooling prevents overheating of the workpiece and clogging of beads and helps to maintain the cutting process's efficiency. It also reduces wire wear, helping to maintain a higher cutting rate over an extended period.

In summary, the Archard wear equation is found to be partially valid because the negatively proportional relationship between hardness and wear volume is not valid. However, all of the other relationships are found to be valid, within the range of tested variables and given accuracies. Therefore, Archard's equation can be applied to the materials from which the K-factor is obtained. Furthermore, these materials were chosen to be commonly found in ships or similar to materials commonly found in ships. Thus, it is likely that the materials in a wreck removal will match or closely resemble the materials tested, allowing the Archard equation in combination with K-factors obtained to be used to estimate the cutting rate.

.

When using the above factors to estimate cutting rates in a practical setting, it is important to consider the importance of cooling. Proper cooling not only reduces wire wear but also improves production efficiency. For example, fully submerged cutting has been shown to perform up to % better, considering production per meter sliding distance. Additionally, it should be noted that the values in Table IV have been corrected for wire wear, so in real-world conditions, these values will decrease over time as the wire wears down. Furthermore, the values were obtained in a set-up where the material to be cut was in good contact with the wire, the angle between the wire and the test piece was constant, and only one test piece was cut at a time. Thus, the process at the level of the entire system while cutting through a wreck was not considered and further research is required to determine the achievable rates and how the wire can be implemented at the system level when cutting through a wreck.

B. Recommendations

The following topics are recommended for further research:

- Examine the system-level implication of the wire, and how the wire will move through actual wrecks when encountering different structures. A starting point could be to experiment by cutting through a small ship with various materials.
- Examine an alternative to a hardness that can be used to predict the variations in cutting rates of different materials more accurately. The goal is to have better predictions of K-factors without the need for testing.
- Examine the circumstances under which pinching and jamming of the wire occur and the impact on the wire. Investigate the threshold impact load (e.g. from falling debris) and angles, in conjunction with applied force, that result in wire jamming and assess the extent of wire damage. Determine the minimum clamping force that causes pinching. Furthermore, examine the maximum force that can be applied to loosen the wire while maintaining its usability, and determine the point at which the wire becomes unusable.
- Conduct an in-depth study of diamond wire wear, including lifespan, causes of wire failure and determine the range of operational conditions that allow for the successful use of diamond wire.
- Investigate the occurrence of wire vibrations at different speeds and spans, analyzing their impact on the cutting rate and methods to mitigate them.
- Investigate the necessary assets for using diamond wire in a wreck removal, including an estimate of the overall cost of the assets, taking into account factors such as daily costs, consumables, and installation expenses.
- Examine the performance and wear of various diamond wires, such as a sintered wire versus an electroplated wire. Measure the K values for different materials and varying wires. Additionally, investigate the impact of factors such as the number of beads, bead shape, and diamond composition on the wire's performance.
- Examine the power consumption resulting from cutting different materials under different conditions.

To further investigate the effect of different operational parameters on the cutting rate and wire wear, the following additional tests are recommended:

- Conducting tests at extreme speeds and loads to determine if the Archard wear equation holds under these conditions.
- Conducting tests with varying thicknesses while keeping the load on the workpiece constant to investigate the correlation between the width of the workpiece and the cutting rate.
- Conducting tests using materials of varying hardness while maintaining consistent geometries.
- Conducting tests using various materials with different material properties to understand the impact of different properties, such as ductility and brittleness, on the cutting rate.
- Investigating the temperatures at which clogging of the beads occurs for various materials and determining the operational parameters (load and speed) at which these temperatures are reached.

And finally, to improve the testing setup, it is recommended to:

- Ensure that wire speed is continuously recorded throughout the entire measurement process to improve accuracy.
- Implement a more powerful sawing machine to decrease machine downtime, improve data consistency, and enable

testing at higher speeds and loads.

REFERENCES

[1] H. Tönshoff and H. Hillmann-Apmann, "Diamond tools for wire sawing metal components," *Diamond and Related Materials*, vol. 11, no. 3-6, pp. 742–748, 2002.

[2] D. Kim, H. Kim, S. Lee, T. Lee, and H. Jeong, "Characterization of diamond wire-cutting performance for lifetime estimation and process optimization," *Journal of Mechanical Science and Technology*, vol. 30, no. 2, pp. 847–852, 2016. DOI: 10.1007/s12206-016-0139-0.

[3] J. F. Archard, "Contact and rubbing of flat surfaces," *Journal of Applied Physics*, vol. 24, no. 8, pp. 981–988, 1953. DOI: 10.1063/1.1721448.

[4] L. Zhang, X. Sha, M. Liu, L. Wang, and Y. Pang, "Cutting force prediction models by fea and rsm when machining x56 steel with single diamond grit," *Micromachines*, vol. 12, no. 3, p. 326, 2021. DOI: 10.3390/mi12030326.

[5] Z. Lan, S. Yongquan, L. Ming, L. Ming, and W. Liquan, "Research on the influence of cutting parameters on chips in the process of diamond bead cutting pipeline steel," *Diamond and Related Materials*, vol. 111, p. 108 220, 2020. DOI: 10.1016/j.diamond.2020.108220.

[6] W. Liu, Z. Pei, and X. Xin, "Finite element analysis for grinding and lapping of wire-sawn silicon wafers," *Journal of Materials Processing Technology*, vol. 129, no. 1-3, pp. 2–9, 2002. DOI: https://doi.org/10.1016/S0924-0136(02)00565-4.

[7] T.-j. Chuang, S. Jahanmir, and H. C. Tang, "Finite element simulation of straight plunge grinding for advanced ceramics," *Journal of the European Ceramic Society*, vol. 23, no. 10, pp. 1723–1733, 2003.

[8] J. a. A. Williams, "Wear modelling: Analytical, computational and mapping: A continuum mechanics approach," *Wear*, vol. 225, pp. 1–17, 1999.

[9] J. M. Thompson and M. K. Thompson, "A proposal for the calculation of wear," in *Proceedings of the 2006 international ansys users conference & exhibition, Pittsburgh, Pa*, 2006.

[10] R. M. Molfino and M. Zoppi, "A robotic system for underwater eco-sustainable wire-cutting," *Automation in Construction*, vol. 24, pp. 213–223, 2012.

[11] S. Turchetta, L. Sorrentino, and C. Bellini, "A method to optimize the diamond wire cutting process," *Diamond and Related Materials*, vol. 71, pp. 90–97, 2017. DOI: https://doi.org/10.1016/j.diamond.2016.11.016.

[12] Z. Xu, H. Huang, and C. Cui, "Measurement and simulation calculation of wire bow angle during the diamond wire saw process," *The International Journal of Advanced Manufacturing Technology*, vol. 120, no. 11-12, pp. 7197–7204, 2022.

[13] J. Qiu, "Fundamental research on machining performance of diamond wire sawing and diamond wire electrical discharge sawing quartz glass," *Ceramics International*, vol. 48, no. 17, pp. 24 332–24 345, 2022.

[14] G. Huang and X. Xu, "Sawing performance comparison of brazed and sintered diamond wires," *Chinese journal of mechanical engineering*, vol. 26, no. 2, pp. 393–399, 2013.

[15] C. Y. Yao, Z. L. Zheng, and D. D. Chen, "Effect of voltage on cutting quality of electrostatic spray diamond wire saw," *J. Huazhong Univ. Sci. Technol. (Nat. Sci.)*, vol. 48, no. 04, p. 73, 2020.

[16] Y. Wei, Q. An, W. Ming, and M. Chen, "Effect of drilling parameters and tool geometry on drilling performance in drilling carbon fiber–reinforced plastic/titanium alloy stacks," *Advances in Mechanical Engineering*, vol. 8, no. 9, p. 1 687 814 016 670 281, 2016.

[17] O. Modi, P. Pandit, D. Mondal, B. Prasad, A. Yegneswaran, and A. Chrysanthou, "High-stress abrasive wear response of 0.2% carbon dual phase steel: Effects of microstructural features and experimental conditions," *Materials Science and Engineering: A*, vol. 458, no. 1-2, pp. 303–311, 2007.

[18] Natural Resources Canada, "Office of Energy Efficiency technicalfact sheet—Premium-efficiency motors," Tech. Rep. M144-21/2003E, 2004.

[19] E. I. Amoiralis, M. A. Tsili, P. S. Georgilakis, and A. G. Kladas, "Energy efficient transformer selection implementing life cycle costs and environmental externalities," in *2007 9th International Conference on Electrical Power Quality and Utilisation*, IEEE, 2007, pp. 1–6.

B

Appendix

B.1. Accuracies

Test	Test piece	K factor	Accuracy +-	%	Run time [s]	Accuracy +-	%	Volume cut [mm^3]	Accuracy +-	%	Hardness [N/mm^2]	Accuracy +-	%	Normal load [N]	Accuracy +-	%	Wire speed [m/s]	Accuracy +-	%
9	B	3.29E-04	2.82E-05	8.56	538.60	2.40	0.45	1.12E+05	2010.76	1.79	150.00	3.56	2.37	1106.18	3.70	0.33	8.75	0.31	3.50
10	C	2.66E-04	2.839E-05	10.69	659.80	2.40	0.36	6.90E+04	1234.84	1.79	150.00	3.56	2.37	1103.23	3.70	0.34	5.73	0.20	3.50
12	E	4.91E-04	5.11E-05	10.40	437.10	0.60	0.14	9.91E+04	1773.87	1.79	206.00	7.70	3.74	1106.00	3.70	0.33	8.80	0.31	3.50
13	F	4.32E-04	3.986E-05	9.23	455.80	0.60	0.13	7.45E+04	1333.28	1.79	262.00	6.75	2.58	1165.63	3.70	0.32	8.68	0.30	3.50
19	Z	2.06E-04	1.8E-05	8.72	654.90	0.60	0.09	1.13E+05	2030.54	1.79	150.00	3.56	2.37	1104.41	3.70	0.34	11.59	0.41	3.50
14	G	1.80E-04	1.73E-05	9.63	683.40	1.80	0.26	7.66E+04	1370.51	1.79	150.00	3.56	2.37	1101.61	3.70	0.34	8.57	0.30	3.50
16	D	2.46E-04	2.201E-05	8.94	480.70	1.20	0.25	8.14E+04	1457.20	1.79	149.00	3.56	2.39	1179.18	3.70	0.31	8.55	0.30	3.50
20	R	4.13E-04	3.719E-05	9.01	513.70	3.00	0.58	1.26E+05	2260.68	1.79	150.00	3.56	2.37	1103.79	3.70	0.34	8.78	0.31	3.50
21	S	3.02E-04	3.095E-05	10.26	1082.10	0.60	0.06	6.87E+04	1230.52	1.79	150.00	3.56	2.37	370.62	3.70	1.00	8.67	0.30	3.50
22	A	3.62E-04	3.08E-05	8.51	632.11	0.60	0.09	9.96E+04	1782.28	1.79	150.00	3.56	2.37	775.11	3.70	0.48	8.57	0.30	3.50
23	B	3.45E-04	2.934E-05	8.51	709.10	1.80	0.25	1.48E+05	2643.90	1.79	150.00	3.56	2.37	1184.90	3.70	0.31	8.45	0.30	3.50
24	C	2.46E-04	2.058E-05	8.35	554.20	1.20	0.22	1.17E+05	2091.46	1.79	150.00	3.56	2.37	1182.68	3.70	0.31	11.32	0.40	3.50
25	Z	2.78E-04	2.357E-05	8.49	936.60	2.40	0.26	1.03E+05	1843.02	1.79	150.00	3.56	2.37	1183.88	3.70	0.31	5.61	0.20	3.50
26	BZN	2.71E-04	2.215E-05	8.17	768.60	2.40	0.31	1.27E+05	2271.17	1.79	150.00	3.56	2.37	1184.09	3.70	0.31	8.29	0.29	3.50
32	F	4.14E-04	3.383E-05	8.17	625.40	0.60	0.10	1.00E+05	1797.19	1.79	262.00	6.75	2.58	1244.05	3.70	0.30	8.33	0.29	3.50
33	E	4.26E-04	3.984E-05	9.35	735.17	0.60	0.08	1.49E+05	2666.99	1.79	206.00	7.70	3.74	1185.63	3.70	0.31	8.45	0.30	3.50
34	J	3.87E-04	3.073E-05	7.94	116.44	0.60	0.52	3.18E+04	570.03	1.79	151.00	3.56	2.36	1303.87	3.70	0.28	8.34	0.29	3.50
35	K	2.30E-04	1.828E-05	7.96	379.55	1.20	0.32	6.02E+04	1077.54	1.79	151.00	3.56	2.36	1275.10	3.70	0.29	8.35	0.29	3.50
36	R	2.12E-04	1.719E-05	8.10	637.80	1.20	0.19	8.65E+04	1548.03	1.79	150.00	3.56	2.37	1183.17	3.70	0.31	8.35	0.29	3.50
37	G	2.88E-04	2.361E-05	8.20	571.49	1.80	0.31	1.03E+05	1838.51	1.79	150.00	3.56	2.37	1112.35	3.70	0.33	8.56	0.30	3.50

Test	Test piece	Sliding distance [mm]	Accuracy +-	%	Due to model	Moddeled %	Production [mm^3/s]	Accuracy +-	%	Press [bar]	Accuracy +-	%	Wire speed [m/s]	Accuracy +-	%
9	B	4.70E+06	191.15	4.06	26.50	0.02	208.56	4.66	2.24	3.20	0.02	0.50	8.75	0.31	3.50
10	C	3.59E+06	222.30	6.19	96.59	0.44	104.56	2.25	2.15	3.20	0.02	0.50	5.73	0.20	3.50
12	E	3.83E+06	173.65	4.54	39.70	0.31	226.72	4.37	1.93	3.20	0.02	0.50	8.80	0.31	3.50
13	F	3.95E+06	179.87	4.55	41.48	0.31	163.42	3.14	1.92	3.20	0.02	0.50	8.68	0.30	3.50
19	Z	7.59E+06	320.24	4.22	54.61	0.30	173.21	3.26	1.88	3.20	0.02	0.50	11.59	0.41	3.50
14	G	5.90E+06	302.46	5.13	95.98	0.46	112.04	2.30	2.05	3.20	0.02	0.50	8.57	0.30	3.50
16	D	4.26E+06	189.55	4.45	40.40	0.24	169.35	3.45	2.04	3.20	0.02	0.50	8.55	0.30	3.50
20	R	4.23E+06	190.42	4.51	42.50	0.10	245.85	5.84	2.37	3.20	0.02	0.50	8.78	0.31	3.50
21	S	9.38E+06	693.39	5.10	217.17	0.78	63.53	1.17	1.85	3.20	0.02	0.50	8.67	0.30	3.50
22	A	5.41E+06	781.76	3.87	74.01	0.43	157.52	2.97	1.88	3.20	0.02	0.50	8.57	0.30	3.50
23	B	5.52E+06	1039.08	4.04	138.21	0.68	208.30	4.26	2.04	0.00	0.00	-	8.45	0.30	-
24	C	6.12E+06	1344.75	3.88	130.60	0.86	210.83	4.23	2.01	0.00	0.00	-	11.32	0.40	-
25	Z	4.78E+06	1582.52	4.01	201.16	0.76	109.93	2.25	2.05	3.20	0.02	0.50	5.61	0.20	3.50
26	BZN	6.03E+06	1681.44	3.70	88.95	0.34	165.08	3.47	2.10	3.20	0.02	0.50	8.29	0.29	3.50
32	F	5.21E+06	1780.88	3.51	6.00	0.00	160.54	3.03	1.89	3.20	0.02	0.50	8.33	0.29	3.50
33	E	6.19E+06	1997.50	3.51	6.00	0.00	202.66	3.79	1.87	3.20	0.02	0.50	8.45	0.30	3.50
34	J	9.71E+05	2031.49	3.51	6.00	0.00	273.50	6.31	2.31	3.20	0.02	0.50	8.34	0.29	3.50
35	K	3.16E+06	2148.10	3.52	12.00	0.00	158.60	3.34	2.11	3.20	0.02	0.50	8.35	0.29	3.50
36	R	5.25E+06	2429.51	3.62	79.85	0.43	135.59	2.68	1.98	3.20	0.02	0.50	8.35	0.29	3.50
37	G	4.89E+06	2666.02	3.70	145.14	0.89	179.72	3.78	2.10	3.20	0.02	0.50	8.56	0.30	3.50

Parameter	Device	Accuracy	Reading error	Value	Variation	Total deviation
RMP	A2108 Multimeter Tachoprobe	+/- 0.50 %				+/- 0.50 %
r_pulley	Measure tape	+/- 1 mm	+/- 1 mm	120 mm		
h_drop	Hogetex digital capliper	+/- 0.1 mm	+/- 1 mm	15 mm		
r_wire	Hogetex digital capliper	+/- 0.1 mm	+/- 0.1 mm	9.5 mm	+/- 0.25 mm	
r_total	r_pulley - h_drop + r_wire/2	+/- 1.2 mm	+/- 2.1 mm	109.5 mm*		+/- 3.0 %
					Total	**+/- 3.5%**

Cause	Device/explenation	Deviation	Reading error	Total error		
Model	Max devation found (compared to real data)	+- 0.2 m/s				
Model	speed jumps"	+- 0.05 m/s		+/- 0.25	m/s	
Selection	Human error of +/- 6 measurements per 'cut', worst case is 5 'cuts'		+/- 6m	+/- 6	m/stop	
Speed measurement	Summation of speed errors			+/- 3.5%		

Parameter	Device/explenation	Accuracy	FS	Variation	'Reading' error	Total deviation
Load	SCAIME 500kg loadcell	0.03 %FS	3000 N	+/- 0.9 N	+/- 0.1 N	+/- 1 N
W_testpiece	SCAIME 150kg loadcell	0.03 %FS	250 N	+/- 0.075 N	+/- 0.265 N	+/- 0.34 N
W_balance	SCAIME 150kg loadcell	0.03 %FS	250 N	+/- 0.075 N	+/- 0.265 N	+/- 0.34 N
F_friction	500kg loadcell + 3x 150 kg			+/- 1.125 N	+/- 0.895N	+/- 2.02 N
Normal load	Load - W_test - W_balance - F_friction				**Total error**	**+/- 3.70 N**

Parameter	Device	Accuracy		Reading error	Worst case	Total error
ro_water	Hydrometer	+/- 0.0005 gr/ml	+/- 0.001 gr/ml	+/- 0.0015 gr/cm^3	998 kg/m^3	+/- 0.2%
Weighing dry	Digital scale	+/- 0.1 gr			236 gr	+/- 0.04 %
Weighing wet	Digital scale	+/- 0.1 gr			205 gr	+/- 0.05 %
ro_testpiece	Wet / dry weighing				**Total error**	**+- 0.29%**

Parameter	Device	Accuracy	'reading' error		Worst case	
Load	SCAIME 150kg loadcell	+/- 0.075 N	+/- 0.135 N	+/- 0.21 N	170 N	+/- 0.12 %
Density piece	Wet / dry weighing					+/- 0.29 %
Density water	Hydrometer	+/- 0.0005 gr/ml	*+/- 0.0015 gr/ml	+/- 0.002 gr/ml	1002 kg/m^3	+/- 0.2 %
Load	Filth on workpiece	+/- 2 N			170 N	+/- 1.18 %
Volume	2x load measurement + ro_water + ro_piece				**Total error**	**+/- 1.79%**
		*+/- 0.001gr/ml + 0.0005 for temp differnce				

Parameter	Device	Hardness [HV]	Error [HV}	Reading 'error'	Total error [HV]
Hardness	Durascan 70 Struers			+/- 1 HV	
	Load accurate, micro meter deviation	150	2.6		+- 3.6
		200	4.1		+- 5.1
		260	5.7		+- 6.7

Wear volume

The error of the wear volume is a sum of the inaccuracies in weighing, determining the density of the test pieces, determining the density of the water and the reading.

Normal load

The error is a sum of the error margin obtained when measuring: the load caused by the test weight, the trolley, the test pieces, the balance weights and measuring the friction and reading errors.

Wire-speed

The error is the sum of the error due to the tachometer (given by the manufacturer), the errors from measuring the radius of the pulley on which the tachometer is mounted and reading errors.

Hardness

The error in the measurement was determined by estimating the margin of error of the diagonal indention length at 3 μm and supposing that the chosen load is accurate.

Distance

The error of the distance meter is only based on its own error (given by the manufacturer).

Pressure

The error of the pressure sensors is based only on their error (given by the manufacturer).

Temperature workpiece

The error of the thermocouple and the laser in both cases is only based on their own error.

Water density

The error of the hydrometer is based only on its own error (given by the manufacturer) as well as a reading error.

K factor

The total error of the K factor is equal to the sum of the errors of all parameters required to determine the factor. Namely: the cutaway/wear volume, the normal load, the sliding distance and the hardness.

B.2. Detailed test procedure

A list of tasks that are performed during each test is provided below: 1. Hoist-guided trolley
2. Secure the test piece on the guided trolley
3. Lower guide trolley with test piece into the container (has to pass by the wire, so wire must be loose)
4. Pre-tension the wire to desired tension (with Hilti machine)
5. Attach desired weight pieces to the cable at the correct height (approx. 5 cm above the ground); the wire will press against the workpiece
6. Start camera
7. Start data logging
8. Distance yourself
9. Set desired speed on the controller
10. Cut the test piece until the cut is fully developed
11. Stop cutting; loosen the wire
12. Detach the weight
13. Hoist-guided trolley
14. Detach the test piece and weigh the pre-cut test piece using the weighing set-up (submerged)
15. Re-install the test piece and lower the guided trolley with the test piece into the container (it has to pass by the wire, so the wire must be loose)
16. Pre-tension the wire to desired tension (with Hilti machine
17. Attach the selected weight to the steel cable connected to the guided troller. The workpiece will press against the wire
18. Distance yourself and do a safety check
19. Set desired speed on the controller and start the machine
20. Cut the test piece up to 3-5 cm from the end
21. Stop cutting, loosen the wire
22. Stop camera + data logging
23. Detach the weight
24. Hoist guided trolley
25. Detach the work piece

B.3. Data gaps

To fill the data gaps, the following steps were taken:
First, all the data sets' wire speed courses were reviewed. A modest decrease in wire speed over time was observed for all measurements.

Several reasons could cause the drop in speed. First of all, it could be due to the sensor. Tests have shown that it is not due to a fault in the Tachometer. Secondly, slip between the wire and drive pulley could be the reason. The wire speed is controlled based on rpm and not with feedback on the basis of the actual wire speed. Thus, slip between the drive pulley may increase as the diamond wire carries water and dirt during the cutting process while the speed of the drive pulley remains the same. At a constant speed with increasing slip, the wire speed will decrease. However, with a lot of slip, it is to be expected that pulleys will wear out quickly as the diamond beads then rub the surface of the rubber pulley. Thirdly, it could be because the electric motor heats up. This increases the resistance in the motor, which also increases the slip between the stator and rotor. This then leads to a decrease in the speed of the drive pulley. Given the short duration of the experiments, it is not very likely that this is the cause.

Furthermore, results showed that when the wire tension remained constant, the speed decline was also constant. But if the wire tension dropped during a start/stop, the speed could be seen to start again at its 'old' level and then decrease again. The reason for this is unknown, but it has been observed.

To fill the data gaps in the wire speed measurements, the trendline of the speed was examined for both complete and incomplete measurements. This consistently revealed an almost linearly decreasing trendline. Looking at the possible causes, an exponential trendline would probably make more sense. After all, the slip in both cases does not increase infinitely and reaches a steady state over time. Based on complete data, it was found that the difference between linear and exponential trendlines was less than 1 per cent. Hence a linear trendline was used for convenience. Ultimately, the following steps were followed for each incomplete test to fill in the speed gaps:

- Obtain the trendline of the wire speed based on measured data
- Extrapolate trendline formula according to running time (read from oscillation in load)
- Determine the start value of each section (continue trend if pressure is kept constant, 'start' with original speed if the pressure has dropped in between)
- Integrate trendline sections to obtain the sliding distance
- Correct the sliding distance for start/stops during the measurement. Because the data showed that the machine takes 2 seconds to get from 0 to v_max and, when stopped, drops from v_max to 0 again in 1 second, Equation B.1 can be used to account for a start/stops. For simplification, a linear progression from 0 to v_max and back was assumed during this trajectory.

$$s_{correction\ start/stops} = 0.5 * v_{average} * N_{start/stops} \tag{B.1}$$

Accuracy

The total error for the computed sling distance is estimated at 0.25 m/s, plus +- 2 meters per start/stop.

- Deviation from data selection is estimated at max 5 measurements incorrectly, resulting in an estimated error of +- 2 m sliding distance per start/stop
- Furthermore, the method to fill the data gaps were also applied to complete sets to check the accuracy of data filling. This revealed a maximum deviation of 0.25 m/s.

B.4. Data Hilti and Husqvarna

Table B.2 and Table B.1 Hilti give rough estimations on diamond wire cutting rates and wire lifetime. Hilti's table provides data specific to the wire, but not for different materials. Husqvarna's table provides material-specific information but does not specify the wire used, nor if they used the same wire for the different materials. The tables only present theoretical results under ideal conditions; therefore, actual results may vary based on factors such as wire speed, normal force, and cooling type.

Table B.1: Life time and speed prediction for wet cutting of solid steel metal of standard steel grade (J. Vos, personal communication, August 8)

Table B.2: Wire life time and cutting rate predictions from Husqvarna (D. Demey, personal communication, June 23)

	Wet	Dry

Table B.3: Lifetime estimation test day 1 and 2

B.5. Steel discolouration temperatures

Table B.4: Steel colouring due to temperature (Cotoco et al., 2017)

Steel color	Temperature [°C]
Light yellow	220
Dark straw	240
Brown yellow	260
Brown purple	270
Dark purple	285
Full blue	290
Dark blue	300
Very dark blue	315
Greyish blue	330
Dark grey	427
Brown red	600
Blood red	650
Full cherry red	815
Orange	930
White	1200

C

Appendix: Raw data

Figure C.1: Raw data test 1

Figure C.2: Raw data test 2

Figure C.3: Raw data test 3

Figure C.4: Raw data test 4

Figure C.5: Raw data test 5

Figure C.6: Raw data test 6

Figure C.7: Raw data test 7

Figure C.8: Raw data test 8

Figure C.9: Raw data test 9

Figure C.10: Raw data test 10

Figure C.11: Raw data test 11

Figure C.12: Raw data test 12

Figure C.13: Raw data test 13

Figure C.14: Raw data test 14

Figure C.15: Raw data test 15

Figure C.16: Raw data test 16

Figure C.17: Raw data test 17

Figure C.18: Raw data test 18

Figure C.19: Raw data test 19

Figure C.20: Raw data test 20

Figure C.21: Raw data test 21

Bibliography

Amoiralis, E. I., Tsili, M. A., Georgilakis, P. S., & Kladas, A. G. (2007). Energy efficient transformer selection implementing life cycle costs and environmental externalities. *2007 9th International Conference on Electrical Power Quality and Utilisation*, 1–6.

Archard, J. F. (1953). Contact and rubbing of flat surfaces. *Journal of Applied Physics*, *24*(8), 981–988. https://doi.org/10.1063/1.1721448

Ashtead Technology. (2022). *Cutting equipment* [Photograph]. https://www.ashtead-technology.com/equipment/cutting/

Atkins. (2009). Types of chip: Load fluctuations, scaling and deformation transitions. In *The science and engineering of cutting*. Elsevier Ltd. https://doi.org/10.1016/C2009-0-17178-7

BBC News. (2021, August 20). *Ever given: Cargo ship returns through suez canal it blocked*. https://www.bbc.com/news/world-middle-east-58288512

Bureau Veritas. (2021). *Rules for the Classification of Steel Ships: Part B - Hull and Stability* (tech. rep. NR 467.B1 DT R13 E). https://marine-offshore.bureauveritas.com/bv-rules

Cao, L., Meng, Q., Wang, L., & Tong, W. (2006a). Research on underwater diamond wire saw. *2006 International Conference on Mechatronics and Automation*, 1695–1700. https://doi.org/10.1109/icma.2006.257452

Cao, L., Meng, Q., Wang, L., & Tong, W. (2006b). Research on underwater diamond wire saw. *2006 International Conference on Mechatronics and Automation*, 1695–1700.

Chuang, T.-j., Jahanmir, S., & Tang, H. C. (2003). Finite element simulation of straight plunge grinding for advanced ceramics. *Journal of the European Ceramic Society*, *23*(10), 1723–1733.

Cotoco, E. K. A., Lindo, D. E. G., Baldovino, R. G., & Dadios, E. P. (2017). Tempering color classification via artificial neural network (ann): An intelligent system approach to steel thermography. *2017 International Conference on Electrical, Electronics and System Engineering (ICEESE)*, 84–88.

Cutting Undewater Technologies. (2019). *Ship wrecks dwcm* [Illustration]. https://www.cut-group.com/special-dwcms/wreck-dwcm/

Denkena, B., Krödel, A., & Ellersiek, L. (2022). Influence of metal working fluid on chip formation and mechanical loads in orthogonal cutting. *The International Journal of Advanced Manufacturing Technology*, *118*(9), 3005–3013.

Deshpande, S., & Deshpande, Y. (2019). A review on cooling systems used in machining processes. *Materials Today: Proceedings*, *18*, 5019–5031.

Ertingshausen, W. (1985). *Zerspanung von granit mit diamant-trennschleifscheiben* (Doctoral dissertation). Universität Hannover.

Heuer, W. (1992). *Außenrundschleifen mit kleinen keramisch gebundenen cbn-schleifscheiben*. VDI-Verlag.

Hilti. (2022). *Single-pair pulley dsw-spp* [Photograph]. https://www.hilti.com/c/CLS_POWER_TOOLS_7124/CLS_DIAMOND_WIRE_WALL_SAWS_7124/CLS_ACCESSORIES_FOR_WIRES_SAWS_7124/2205152

Hu, Q., Zhang, F., Li, X., & Chen, J. (2018). Overview on the prediction models for sheet metal forming failure: Necking and ductile fracture. *Acta Mechanica Solida Sinica*, *31*(3), 259–289. https://doi.org/https://doi.org/10.1007/s10338-018-0026-6

Huang, G., & Xu, X. (2013). Sawing performance comparison of brazed and sintered diamond wires. *Chinese journal of mechanical engineering*, *26*(2), 393–399.

Kim, D., Kim, H., Lee, S., Lee, T., & Jeong, H. (2016). Characterization of diamond wire-cutting performance for lifetime estimation and process optimization. *Journal of Mechanical Science and Technology*, *30*(2), 847–852. https://doi.org/10.1007/s12206-016-0139-0

Kulbiej, E., & Wołejsza, P. (2016). An analysis of possibilities how the collision between m/v" baltic ace" and m/v" corvus j" could have been avoided. *Annual of Navigation*.

Lan, Z., Yongquan, S., Ming, L., Ming, L., & Liquan, W. (2020). Research on the influence of cutting parameters on chips in the process of diamond bead cutting pipeline steel. *Diamond and Related Materials*, *111*, 108220. https://doi.org/10.1016/j.diamond.2020.108220

Liu, W., Pei, Z., & Xin, X. (2002). Finite element analysis for grinding and lapping of wire-sawn silicon wafers. *Journal of Materials Processing Technology*, *129*(1-3), 2–9. https://doi.org/https://doi.org/10.1016/S0924-0136(02)00565-4

Modi, O., Pandit, P., Mondal, D., Prasad, B., Yegneswaran, A., & Chrysanthou, A. (2007). High-stress abrasive wear response of 0.2% carbon dual phase steel: Effects of microstructural features and experimental conditions. *Materials Science and Engineering: A*, *458*(1-2), 303–311.

Molfino, R. M., & Zoppi, M. (2012). A robotic system for underwater eco-sustainable wire-cutting. *Automation in Construction*, *24*, 213–223.

Muller. (2020). *International salvage union opinion for fairplay*. https://www.marine-salvage.com/overview/wreck-removal/#:%7E:text=The%20majority%20of%20coastal%20states,is%20a%20hazard%20to%20navigation

Natural Resources Canada. (2004). *Office of Energy Efficiency technicalfact sheet—Premium-efficiency motors* (tech. rep. M144-21/2003E). Office of Energy Efficiency, Energy Innovators Initiative,Ottawa.

Qiang, X., Bijlaard, F. S., & Kolstein, H. (2012). Deterioration of mechanical properties of high strength structural steel s460n under steady state fire condition. *Materials & Design (1980-2015)*, *36*, 438–442.

Qiu, J. (2022). Fundamental research on machining performance of diamond wire sawing and diamond wire electrical discharge sawing quartz glass. *Ceramics International*, *48*(17), 24332–24345.

Thompson, J. M., & Thompson, M. K. (2006). A proposal for the calculation of wear. *Proceedings of the 2006 international ansys users conference & exhibition, Pittsburgh, Pa*.

Tikannen. (2017, March 21). *Costa concordia disaster: Collision, rescue, salvage, facts*. https://www.britannica.com/event/Costa-Concordia-disaster

Tönshoff, H., & Hillmann-Apmann, H. (2002). Diamond tools for wire sawing metal components. *Diamond and Related Materials*, *11*(3-6), 742–748.

Tu, L., & Shi, W. (2019). Establish using fem method of constitutive model for chip formation in the cutting process of gray cast iron. *Metals*, *10*(1), 33.

Turchetta, S., Sorrentino, L., & Bellini, C. (2017). A method to optimize the diamond wire cutting process. *Diamond and Related Materials*, *71*, 90–97. https://doi.org/https://doi.org/10.1016/j.diamond.2016.11.016

United Nations. (2021). *Review of maritime transport 2021 - overview*. https://unctad.org/system/files/official-document/rmt2021summary_en.pdf

Wei, Y., An, Q., Ming, W., & Chen, M. (2016). Effect of drilling parameters and tool geometry on drilling performance in drilling carbon fiber–reinforced plastic/titanium alloy stacks. *Advances in Mechanical Engineering*, *8*(9), 1687814016670281.

Williams, J. a. A. (1999). Wear modelling: Analytical, computational and mapping: A continuum mechanics approach. *Wear*, *225*, 1–17.

Xu, Z., Huang, H., & Cui, C. (2022). Measurement and simulation calculation of wire bow angle during the diamond wire saw process. *The International Journal of Advanced Manufacturing Technology*, *120*(11-12), 7197–7204.

Yao, C. Y., Zheng, Z. L., & Chen, D. D. (2020). Effect of voltage on cutting quality of electrostatic spray diamond wire saw. *J. Huazhong Univ. Sci. Technol. (Nat. Sci.)*, *48*(04), 73.

Zhang, L., Sha, X., Liu, M., Wang, L., & Pang, Y. (2021). Cutting force prediction models by fea and rsm when machining x56 steel with single diamond grit. *Micromachines*, *12*(3), 326. https://doi.org/10.3390/mi12030326